Aus dem Institut für Kardiovaskuläre Physiologie und Pathophysiologie
(im Walter-Brendel-Zentrum für Experimentelle Medizin, WBex)
der Ludwig-Maximilians-Universität München
Direktor: Prof. Dr. Markus Sperandio

Role of Coronin 1B on the regulation of endothelial cell function and angiogenesis

Dissertation

zum Erwerb des Doktorgrades der Naturwissenschaften

an der Medizinischen Fakultät der

Ludwig-Maximilians-Universität München

vorgelegt von

Ann-Cathrin Werner

aus Kassel

Jahr

2021

Mit Genehmigung der Medizinischen Fakultät
der Universität München

Betreuer:	Prof. Dr. Jörg Renkawitz
Zweitgutachterin:	Prof. Dr. Hanna Mannell
Dekan:	Prof. Dr. Thomas Gudermann
Tag der mündlichen Prüfung:	12.05.2022

Table of contents

Abstract

Coronin (Coro) 1B, an actin-binding protein of the family of type I coronins, is a key regulator of actin polymerization at the leading edge of lamellipodia. The endothelium expresses the type I coronins Coro1B and Coro1C but their roles in endothelial cell (EC) behavior and vessel function are poorly understood. In the present study, the role of Coro1B on the regulation of EC function and angiogenesis was investigated. The data showed that Coro1B was present at leading edges of lamellipodia and Coro1B was identified as a new member of the endothelial cell-cell junction. At the cell-cell junction, Coro1B was localized at two specific structures: (1) Junction-associated intermittent lamellipodia (JAIL) and (2) reticular adherens junctions (AJs). JAIL regulate vascular endothelial cadherin (VEcad) dynamics and thereby AJ integrity. Using confocal microscopy Coro1B was found to be enriched at the leading edge of JAIL and localized at sites of actin polymerization in reticular AJs suggesting that Coro1B controls VEcad dynamics at the cell-cell junction by regulating actin rearrangement and JAIL formation. Pharmacological manipulation of the actin cytoskeleton by affecting the RhoA / ROCK signaling pathway indicated that Coro1B localized at cell-cell junctions in an actin-dependent manner. To analyze the function of Coro1B for the regulation of EC behavior, Coro1B was downregulated in ECs using specific siRNA and adhesion, migration, monolayer formation and *in vitro* angiogenesis was analyzed. The findings revealed that Coro1B was required for proper tube formation of tube-like structures although it was dispensable for cell migration, morphology, spreading and monolayer integrity. Whereas initial formation of tube-like structures was not affected by the absence of Coro1B, stability of tube-like structures was Coro1B-dependent. However, this was not due to impaired proliferation and survival of Coro1B knockdown cells. In order to understand the molecular mechanism by which Coro1B regulates angiogenesis *in vitro*, the Coro1B interactome in ECs consisting of 215 proteins was defined. Apart from the known interacting partners of Coro1B including cofilin and actin related protein (Arp) 2/3 complex, mass spectrometry analysis identified novel interacting partners involved in cell adhesion and angiogenesis. One of the selected proteins was integrin-linked kinase (ILK), which was shown to be critical for endothelial function and vessel formation. Finally, a Coro1B knockout in zebrafish using CRISPR / Cas9 technology was generated. The zebrafish represents a new powerful model to analyze the physiological functions of Coro1B. Taken together, these findings suggest that Coro1B is necessary for EC function during *in vitro* tube formation.

Zusammenfassung

Coronin (Coro) 1B ist ein Aktin-bindendes Protein aus der Familie der Typ I Coronine. An der Vorderkante von Lamellipodia spielt es eine wichtige Rolle bei der Regulation der Aktin-Polymerisation. Endothelzellen exprimieren sowohl Coro1B als auch Coro1C, jedoch ist ihre genaue Funktion in Endothelzellen und während der Gefäßbildung nicht bekannt. In der folgenden Arbeit wurde die Rolle des Proteins Coro1B im Endothel untersucht. Dabei konnte gezeigt werden, dass Coro1B an der Vorderkante von Lamellipodia sowie an Zell-Zellkontakten lokalisiert ist. Insbesondere war Coro1B an zwei speziellen Strukturen der Zell-Zellkontakte zu finden: (1) Zellkontakt-assoziierte intermittierende Lamellipodia (JAIL) und (2) retikuläre Adhäsionsverbindungen. JAIL regulieren die Dynamik des Proteins vaskulär endotheliales Cadherin (VEcad) und damit die Integrität der Zellkontakte. In dieser Arbeit konnte mit Hilfe von Zellaufnahmen in Echtzeit gezeigt werden, dass Coro1B sich an der Vorderkante von JAIL anreichert. Darüber hinaus konnte herausgestellt werden, dass Coro1B in Bereichen der Aktin-Polymerisation in retikulären Adhäsionsverbindungen lokalisiert ist. Pharmakologische Inhibition oder Aktivierung der Actomyosin-Kontraktion lassen auf eine Aktin-abhängige Lokalisation von Coro1B an den Zell-Zellkontakten schließen. Coro1B kontrolliert somit möglicherweise die Dynamik von VEcad, indem es die Reorganisation von Aktin sowie die Entstehung von JAIL reguliert. Um die Rolle von Coro1B in der Regulation von Endothelzellen zu untersuchen, wurde die Proteinexpression von Coro1B mit spezifischer siRNA herabreguliert und der Einfluss von Coro1B auf Adhäsion, Migration und Angiogenese *in vitro* untersucht. Unsere Ergebnisse zeigen, dass Coro1B keinen Einfluss auf die Zellmigration hat. Außerdem wiesen Endothelzellen mit herabreguliertem Coro1B keine abweichende Morphologie auf. Darüber hinaus konnte dargestellt werden, dass Zellen mit verminderter Coro1B-Expression weiterhin in der Lage sind sich auszubreiten und auch die Integrität an Zell-Zellkontakten nicht gemindert ist. Jedoch konnte in dieser Studie gezeigt werden, dass in Endothelzellen mit herabreguliertem Coro1B die Bildung von gefäßartigen Strukturen beeinträchtigt ist. Dabei hatte Coro1B keinen Einfluss auf die Entstehung der gefäßartigen Strukturen, sondern vielmehr auf ihre Stabilität. Weiterführende Experimente konnten nachweisen, dass dies nicht aus einem veränderten Proliferations- oder Apoptose-Verhalten der Zellen resultiert. Um zu verstehen, wie Coro1B auf molekularer Ebene an der Regulation der Angiogenese *in vitro* beteiligt ist, wurde das gesamte Interaktom von Coro1B in Endothelzellen untersucht. Insgesamt wurden 215 Proteine als Interaktionspartner von

Coro1B ermittelt. Neben den bekannten Interaktionspartnern von Coro1B, wie Cofilin oder dem Arp 2/3-Komplex, wurden zusätzlich Proteine, die an der Zelladhäsion und in der Angiogenese beteiligt sind, als neue Interaktionspartner von Coro1B identifiziert. Unter anderem konnte eine Interaktion von Coro1B und dem Protein Integrin-linked Kinase (ILK), welches eine wichtige Rolle bei der endothelialen Zellfunktion sowie bei der Gefäßentstehung spielt, aufgezeigt werden. Darüber hinaus wurde die Relevanz von Coro1B während der Gefäßentwicklung *in vivo* untersucht. Dazu wurde mit Hilfe der CRISPR / Cas9 Technologie ein Coro1B-defizienter Fisch generiert. Zusammenfassend weisen diese Ergebnisse darauf hin, dass Coro1B für die Funktion von Endothelzellen während der Bildung von Blutgefäßen von Relevanz ist.

Table of figures and tables

Abbreviations

ACTR3	actin related protein 3
ADP	adenosine diphosphate
AJ	adherens junction
AmpR	ampicillin resistance
APS	ammonium persulfate
Arp2/3	actin related protein 2/3
ARPC3	actin related protein 2/3 complex subunit 3
ARPC4	actin related protein 2/3 complex subunit 4
ARPC5L	actin related protein 2/3 complex subunit 5-like protein
ATP	adenosine triphosphate
bp	base pairs
BSA	bovine serum albumin
Cas9	CRISPR-associated 9
CMV	cytomegalovirus
CRIP2	cysteine-rich intestinal protein 2
CRISPR	Clustered Regularly Interspaced Short Palindromic Repeats
C-terminal	carboxy-terminal
DA	dorsal aorta
DAPI	4’,6-diamidino-2-phenylindole
DFP	diisopropyl phosphofluoridate
DII4	ligand delta-like 4
DLAV	dorsal longitudinal anastomotic vessel
DMEM	Dulbecco's modified eagle's medium
dpf	days post fertilization
DTT	dithiothreitol
EC	endothelial cell
ECGM	endothelial cell growth medium
ECM	extracellular matrix
EDTA	ethylenediaminetetraacetic acid
EPLIN	epithelial protein lost in neoplasm
FA	focal adhesion
F-actin	filamentous actin
FAK	focal adhesion kinase
FB	fibrillar adhesion

FCS	fetal calf serum
flk1	fetal liver kinase 1
FN	fibronectin
FOV	field of view
FX	focal complex
GAP	GTPase-activating protein
GAPDH	glyceraldehyde-3-phosphate dehydrogenase
GDP	guanosine diphosphate
GEF	guanine-nucleotide-exchange factor
gRNA	guide RNA
GTP	guanosine triphosphate
HEK-293T	human embryonic kidney cells
HMEC-1	human microvascular endothelial cells
hpf	hours post fertilization
HUVEC	human umbilical vein endothelial cells
ILK	integrin-linked kinase
IP	immunoprecipitation
IPP complex	ILK / PINCH / parvin complex
IRES	internal ribosomal entry site
ISA	intersegmental artery
JAAF	junction-associated actin filaments
JAIL	junction-associated intermittent lamellipodia
KanR	kanamycin resistance
LB	luria broth
MATra	magnet assisted transfection
MCS	multiple cloning site
mECs	mouse endothelial cells
MLC	myosin light chain
MMP	matrix metalloprotease
MYPT-1	myosin phosphatase target subunit 1
NCoR	nuclear co-repressor
NICD	notch intracellular domain
NPF	nucleation-promoting factors
N-terminal	amino-terminal
P / S	penicillin / streptomycin

PBS	phosphate buffered saline
PCR	polymerase chain reaction
PCV	posterior cardinal vein
PDGF	platelet-derived growth factor
PE	pericytes
pHH3	phospho-Histone H3
PINCH	particularly interesting Cys-His-rich protein
PURO	puromycin
RFLP	restriction fragment length polymorphism
ROCK	Rho-serine / threonine kinase
RPMI	Roswell Park Memorial Institute
SDS	sodium dodecyl sulphate
ser2	serine 2
siRNA	small interfering RNA
SSHL1	slingshot
TBS-T	tris buffered saline with Tween20
TEER	transendothelial electrical resistance
TEMED	tetramethylethylenediamine
TJ	tight junction
TMOD3	tropomodulin-3
tris	Trizma base
VEcad	vascular endothelial cadherin
VEGFR 2	vascular endothelial growth factor receptor 2
VE-PTP	vascular endothelial protein tyrosine phosphatase
vs	versus
vSMC	vascular smooth muscle cells
WASP	Wiskott-Aldrich syndrome protein

1. Introduction

1.1 The vascular system

The vascular system is one of the most important in the body of mammals. It consists of two hierarchically branched networks: the blood and the lymphatic vasculature[1]. The main function of the blood vasculature is to supply all tissues of the body with gases, fluids, nutrients, hormones and metabolites[2-4]. Thus, blood vessel function is important for tissue growth and organ function in embryonic development and in the adult organism, under physiological and pathological conditions[5]. Interstitial fluid, immune cells, and macromolecules are carried by lymphatic vessels to the lymph nodes and from these back into the blood circulation as the lymphatic vessels are connected to the blood vasculature[1,6]. Thereby, it maintains tissue fluid homeostasis and is important for immune cell trafficking and uptake of dietary fats[6]. In contrast to the lymphatic system, which is blind-ended and unidirectional, the blood vasculature is a circulatory system[1]. It consists of an organized network of blood vessels including arteries, veins and vessels with a small diameter such as arterioles, capillaries and venules[1]. In the vascular system the oxygenated blood that returned from the lung, flows from the left ventricle of the heart through the aorta into numerous smaller arteries that branch off into smaller and smaller ones[1,7]. The smallest arteries and veins, named arterioles and venules, are linked by capillaries, which enable the exchange of metabolic products between the blood and the tissue of the organs[7]. The blood flows via venules into the venous system where it proceeds through veins with increasing diameter before it returns through the pulmonary veins back to the right atrium of the heart[7]. Blood vessels have a distinct architecture that consists of an inner layer of endothelial cells (ECs) surrounded by mural cells that provide stability to the vessel[8]. Mural cells include two cell types, namely vascular smooth muscle cells (vSMC), which are found in veins and arteries, and pericytes (PE) present in veins and arteries but also in small diameter vessels such as arterioles, capillaries and venules[8]. Dysfunction or pathological structural changes of the vascular system are associated with numerous diseases such as cancer, arthritis, diabetic retinopathy, psoriasis and neurodegenerative disorders[9,10]. Thus, a better comprehension of the mechanisms that regulate blood vessel function, could pave the way for the development of novel treatment strategies.

The development of the vascular system can be differentiated into two processes: (1) Vasculogenesis, which is the formation of a primary vascular network and (2) angiogenesis, the formation of new blood vessels from pre-existing ones[11,12]. During embryonic vasculogenesis, vessels form *de novo* from mesoderm-derived endothelial precursors, named angioblasts[11]. Hypoxic signals then trigger the expansion of the primary vascular plexus via angiogenesis[13].

1.2 Angiogenesis

Angiogenesis involves EC adhesion, migration and proliferation. There are two types of angiogenesis known: Sprouting angiogenesis and intussusceptive angiogenesis[11]. During sprouting angiogenesis, a new vessel sprouts or elongates from an already existing one, during intussusceptive angiogenesis, new vessels are formed by remodeling of existing vessels via internal division in the capillary plexus[11]. Sprouting angiogenesis is induced during tissue growth, tissue regeneration and during development when supply with oxygen and nutrients is insufficient[9,14]. It is initiated by the activation of ECs sensing proangiogenic factors for example the vascular endothelial growth factor A (VEGF-A)[13]. Matrix metalloproteases (MMPs)-dependent proteolytic degradation of the extracellular matrix (ECM) allows migration of activated ECs out of a quiescent vessel[9]. ECs themselves can generate podosomes that form cell–matrix contacts allowing locally degradation of the ECM[15]. VEGF and Notch signaling pathways trigger the specification of tip cells and stalk cells (figure 1)[9]. Tip cells are highly polarized ECs, which develop filopodia that detect directional cues in the environment and show a migratory behavior guided by a VEGF gradient[12]. Following tip cells, stalk cells lengthen the sprout by proliferation[9]. Expression of vascular endothelial growth factor receptor 2 (VEGFR2) results in highly motile behavior and filopodia activity. Tip cells arise from ECs with a high VEGFR2 expression or a locally high VEGF environment[13]. Stalk cells develop from ECs, which are laterally inhibited via Notch signaling. Leading tip cells express high levels of the Notch ligand delta-like 4 (DII4)[16,17]. The binding of this ligand to Notch receptors on adjacent cells results in the release of Notch intracellular domain (NICD) inducing the downregulation of VEGFR2 expression in these cells[5,18-20]. Once tip cells anastomose with neighboring sprouts, stalk cells form adherent and tight junctions to facilitate stability of the novel sprout to establish a vascular lumen[5,9]. The components of

the basement membrane were secreted by stalk cells and form the lumen of the vessel[9]. Mural cells are then transferred to the nascent vessels for stabilization[9]. Subsequently, the new vessel switches into a quiescent state until reactivation by new stimuli[9].

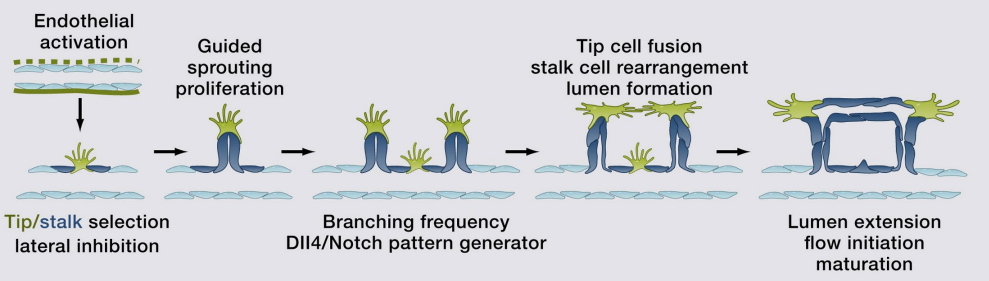

Figure 1. Schematic overview of vessel formation
After endothelial tip / stalk cell formation initiation, tip cells guide, and stalk cells elongate the sprout by proliferation. Branching frequency coordinates this process. Tip cells anastomose with neighboring sprouts before stalk cells form the lumen. Afterwards the lumen extends and the vessel matures (modified from Potente et al.[9]).

1.2.1 Models of angiogenesis

To approach scientific questions regarding processes in angiogenesis, conclusive systems are needed. The matrigel-assay is one of the most common *in vitro* angiogenesis models applied in basic research. The matrigel is a reconstituted basement membrane derived from Engelbreth-Holm-Swarm mouse sarcoma and is rich of ECM proteins such as its major component laminin, soluble growth factors, hormones and other molecules with which ECs interact in an *in vivo* environment[21,22]. In order to simulate a basement membrane, the matrigel matrix imitates the *in vivo* situation and stimulates the attachment, migration and differentiation of ECs into tubular structures forming a branched 3D network[21,23,24]. Using live-cell imaging, all steps of sprouting angiogenesis can be examined. A drawback of this *in vitro* model is the lack of blood flow[23].

To study angiogenesis *in vivo*, a common model is the vascularization of the retina in the postnatal mouse[25]. The mouse retina model has the benefit that retinal vessels extend beyond the superficial layer of the retina from the center to the periphery and form a flat two-dimensional network[25]. This allows making whole flat preparations that can be used for imaging with a confocal microscope[26,27]. Additionally, sprouts and tip cells differentiation can be observed, as vessels at the growing edges of the retina are less mature than the central

ones[27]. This spatial separation allows the observation of different aspects of vascular development[27]. Another *in vivo* angiogenesis model is the vascularization of the murine hindbrain. Preparation and imaging of the hindbrain vascular network with spinning disc confocal microscopy allows for example the study of sprouting defects in embryonic lethal mutants[28]. Both *in vivo* models exhibit the disadvantage that imaging is only possible at a certain time point of angiogenesis[28]. To analyze blood vessel formation over a period of time, the developing zebrafish offers another *in vivo* angiogenesis model[28].

1.2.2 Development of the zebrafish vasculature

The zebrafish is a prominent model to examine angiogenesis and vascular development[28]. Zebrafish are easy to manipulate, their development is fast and due to their optical transparency, it is possible to image and analyze the development of organs and tissues[28,29]. The first vessels in the zebrafish are formed by vasculogenesis[29]. Initially, single angioblasts migrate towards the embryonic midline and contribute to the formation of the dorsal aorta (DA) and posterior cardinal vein (PCV) by condensing together[30-32]. During this process, two consecutive waves of angioblast migration occur[31]. Angioblasts of the first wave give rise to the DA while those of the second wave contribute to the PCV[31,32]. Once the first longitudinal trunk axial vessel is formed, the vasculature extends by sprouting of the already existing vessel. Intersegmental arteries (ISAs) start to form 22 hours post fertilization (hpf) (figure 2). Interconnection of neighboring ISAs 32 hpf leads to the formation of the dorsal longitudinal anastomotic vessel (DLAV). Concurrent, sprouts arise from PCV and develop into intersegmental veins. The fetal liver kinase 1 (flk1) is a VEGF receptor, which is selectively expressed in vascular endothelium[33]. Using the red fluorescent protein mCherry, the vasculature can be displayed during development in flk1:mCherry expressing zebrafish (figure 2). Similar to the human embryonic development, the sprouting of the ISAs in zebrafish is VEGF / Notch signaling-dependent[34,35]. In developing ISAs, Notch signaling antagonizes VEGF signaling, which regulates sprouting behavior of tip cells[35].

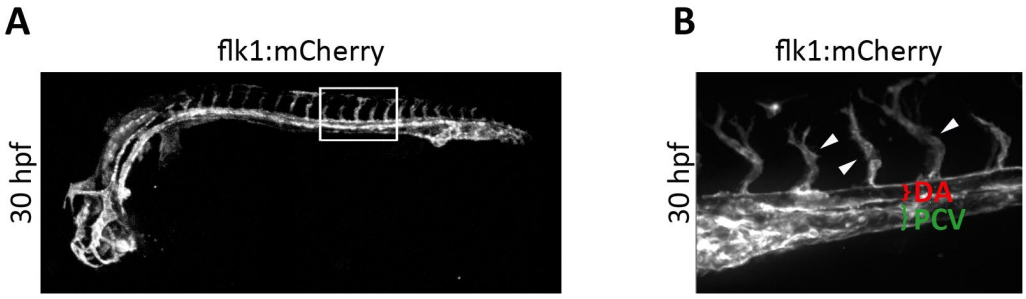

Figure 2. Overview of the vasculature in flk1:mCherry expressing zebrafish 30 hpf
30 hpf old zebrafish expressing selectively flk1:mCherry in the vascular endothelium. (A) Overview of the vasculature of a whole zebrafish. Rectangle highlights section of interest. (B) Magnification of the developing zebrafish vasculature. The DA is marked in red, whereas the PCV is marked in green. Arrowheads point to ISAs.

1.3 EC-ECM adhesion

1.3.1 Integrin-mediated adhesion

In the process of angiogenesis EC need to adhere to ECM for their proliferation, survival and migration[36]. The assembly of EC-ECM adhesion sites is initiated at F-actin rich protrusions at the cell periphery[37]. These contain high levels of integrins, which are the main ECM adhesion receptors[37-39]. This integrin-mediated adhesion of EC to the ECM is essential for angiogenesis and proper function of vessels[38,40]. Integrins contain an α- and a β-subunit classifying them as heterodimeric transmembrane receptors[41]. In mammals 24 different integrins are described of which nine were reported to be expressed on ECs[38,42]. Integrins own a large extracellular domain, a single transmembrane helix and a smaller cytoplasmic domain and can shift between an active and inactive conformation[41,43]. When being inactive, integrins have a bent conformation E(-) with a closed headpiece H(-) and a low affinity for extracellular ligand binding[43-45]. Integrin activation is triggered by intracellular signals inducing conformational changes, which leads to increased extracellular ligand binding[46]. This process is called “Inside-out” signaling[46]. Activation results in conformational changes into a partially activated integrin with intermediate affinity characterized by a closed headpiece H(-) and an extended conformation E(+) and further to the full activation of the integrin with a high ligand binding affinity characterized by an open head domain H(+) and the extended conformation E(+)[44,47,48]. On the other hand, integrins can transduce signals from the outside to the inside by activating intracellular pathways after extracellular ligand binding[49]. This process is termed as „Outside-in” signaling[49]. Thereby, integrins control several intracellular signaling pathways that are crucial for cell migration, differentiation,

proliferation and survival[43]. The bi-directional signaling is essential for a rapid response of the cell to environmental changes[46]. Upon binding to ligands, integrins recruit cytoplasmic proteins to their cytoplasmic domain to generate focal adhesions (FAs), through which signals from the outside of the cell are transported into the cell[14].

In migrating but also in quiescent ECs, adhesion to the ECM is initiated at protruding cell edges[37]. Lamellipodia form sheet-like protrusions, whereas filopodia generate finger-like protrusions that branch out from lamellipodia[39]. EC-ECM adhesion is mediated by integrin clustering into nascent adhesion and focal complexes (FXs) within lamellipodia or filopodia[14,39]. The maturation of a couple of FX results in the formation of FA (figure 3)[14,39,43]. FA proteins include intracellular signaling and adaptor molecules like the integrin-linked kinase focal adhesion kinase (FAK) and Paxillin[14]. Through integrins FAs connect the actin cytoskeleton to the ECM[43,50]. Stress fibers are contractile actomyosin bundles, which are important for cell adhesion and changes in cell morphology during cell migration[51]. The continuous assembly and disassembly of stress fibers allows modifications in response to force[51,52]. A subset of FAs develops into fibrillar adhesions (FBs) that are primarily located at the cell center and characterized by their association to thin actin cables which bind to fibronectin (FN)[53]. FBs are particularly found in fibroblasts where they mediate the adherence to the FN matrix[54].

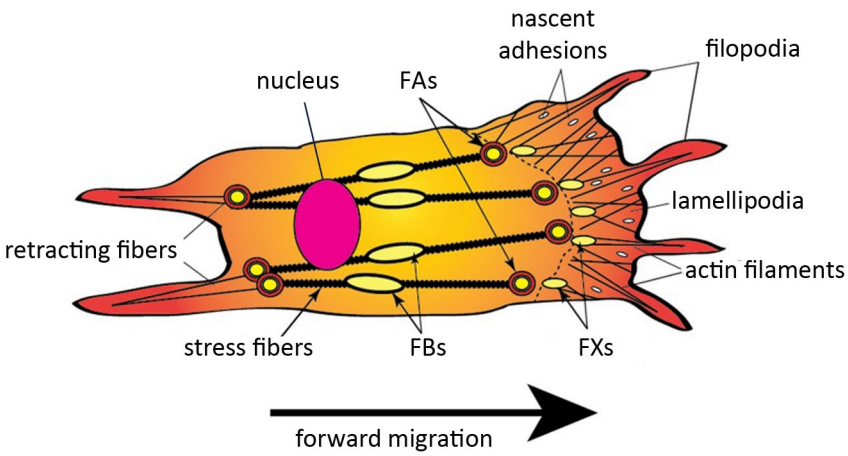

Figure 3. Overview of cell-adhesion structures

Cell-matrix adhesion structures include nascent adhesions, FXs, FAs, FBs and stress fibers (modified from Anderson et al.[39]).

Migrating ECs have two additional types of F-actin based adhesive structures that are missing in quiescent ECs. These are named podosome or invadopodium. Both have a larger diameter than lamellipodia or filopodia and are usually found on the ventral cell surface behind the leading edge (podosomes) or under the nucleus (invadopodia)[39]. They allow attachment to the ECM and are involved in recruitment and activation of multiple pericellular proteases[55]. Thereby, podsomes or invadopodia facilitate the degradation of the ECM and subsequently the cell migration through tissue microenvironments[55]. Many proteins, which are found in FAs, are also present in podosomes such as talin, vinculin and paxillin[56]. Podosomes are typical for the monocytic immune cell lineage but are also present in migrating ECs[57,58]. Invadopodia have morphological and functional similarities to podosomes and are found in malignant cell types[59].

1.3.2 ILK / PINCH / parvin (IPP) complex

To link integrins with the actin cytoskeleton at FXs and FAs, adaptor proteins are needed. One group of adaptor proteins that centered to FXs and FAs are parvins. The family of parvins consists of α-parvin, β-parvin and γ-parvin. ECs express α-parvin and β-parvin, whereas γ-parvin is only expressed in hematopoietic cells[43,60]. In a ternary protein complex they promote the interaction of integrins with the actin cytoskeleton[43]. In this complex, ILK interacts with the particularly interesting Cys-His-rich protein (PINCH) and parvin[61]. It is therefore named the ILK / PINCH / parvin (IPP) complex. PINCH couples integrin signaling with receptor tyrosine kinase signaling pathways, whereas parvin is responsible for the interaction of the IPP complex with the actin cytoskeleton (figure 4)[62].

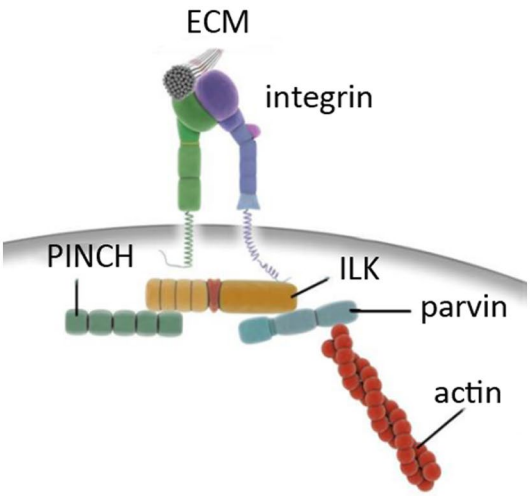

Figure 4. Components of the IPP complex
The IPP complex consists of ILK, PINCH and parvin. ILK is the central component by binding to PINCH and parvin. ILK also facilitates the interaction with integrins at the ECM, whereas parvin interacts with actin (modified from Wickstrom et al.[63]).

Thus, the IPP complex regulates signaling pathways, is a main regulator of integrin signaling and vascular development and connects the ECM with the actin cytoskeleton by facilitating the interaction with integrins[43,61,62].

1.3.3 Actin filaments

The actin cytoskeleton facilitates cellular dynamics such as EC adhesion to the ECM, cell migration and cell-cell junction formation and maintenance[64]. To fulfill these functions, actin filaments have to be highly dynamic. The continuous cycle of polymerization and depolymerization is regulated by actin bindings proteins compromising the activated actin related protein 2/3 (Arp2/3) complex and cofilin[64]. In ECs, actin filaments are part of the cytoskeleton, which can form filament bundles including stress fibers or junction-associated actin filaments (JAAFs), which are crucial for the formation of cell protrusions namely lamellipodia and filopodia. Lamellipodia are membrane protrusions at the leading edge of migrating and spreading cells, which include a highly branched actin network[43]. Lamellipodia are initiated by the Arp2/3 complex inducing actin nucleation. By regulating actin dynamics of ECs, the Arp2/3 complex is essential for angiogenesis[65,66]. Filopodia consist of thin bundles of filamentous actin (F-actin)[67]. Filopodia as well as lamellipodia sense the environment for attracting or repellent guidance cues resulting in either F-actin polymerization or

depolymerization, which induces filopodia extension or retraction respectively[68]. A main regulator of lamellipodia and filopodia formation is the family of small Rho GTPases[66,69]. Rho proteins can switch between an active guanosine triphosphate (GTP) and an inactive guanosine diphosphate (GDP) bound form[70]. Their activation is regulated by guanine-nucleotide-exchange factors (GEFs) and GTPase-activating proteins (GAPs). To activate Rho proteins, GAPs enhance GTPase activity favoring the inactive states while GEFs exchange GDP with GTP[71]. Activated Rho GTPases are able to bind to effector proteins resulting in a direct or indirect assembly or disassembly of F-actin[72]. Rho GTPases are thereby critically involved in regulating cytoskeletal changes, which are important for contraction, cell motility and cell shape[73]. Approximately 20 small GTPases are identified in humans of which Cdc42, Rac1 and RhoA are most comprehensively studied[69]. While Cdc42 is involved in filopodia formation, Rac1 and RhoA antagonize each other and control migration behavior and lamellipodia formation[74,75]. Rac1 stimulates actin polymerization and thereby controls lamellipodia projection, whereas high levels of RhoA inhibit migration by inducing retraction of lamellipodia[76,77]. RhoA is also involved in the formation of FA and activation of RhoA enhances contractility by forming stress fibers, which are actin bundles associated with nonmuscle myosin II[78-80]. Accordingly, activated RhoA induces the phosphorylation of the myosin light chain (MLC) through its downstream effectors Rho-serine / threonine kinase (ROCK) and myosin light chain kinase (MLCK)[73]. The phosphorylation of MLC allows myosin to change its conformation, which enable the interaction with actin and to slide along actin filaments resulting in contractility and the formation of stress fibers. Upon MLC phosphorylation induced by several permeability-increasing mediators such as thrombin, histamine or tumor necrosis factor α (TNF-α), F-actin starts to form stress fibers[78].

1.4 Cell-cell junctions

In the vascular endothelium, ECs are linked via cell junctions. They build the vascular barrier between the blood stream and the interstitial tissue, which is highly dynamic and regulates the exchange of water and solutes[81]. Endothelial cell-cell junctions consist of adherens junctions (AJs), tight junctions (TJs) and gap junctions. Whereas AJs and TJs are important for the barrier function, gap junctions are responsible for cell-cell communication[82]. TJs regulate the flow of ions and solutes and restrict the passage of lipids and proteins between the

apical and the basolateral cell surface[83]. Claudins are the main component of TJs[84]. Adhesion of AJs is mediated by calcium-dependent cadherins[85]. The predominant proteins in endothelial AJs are the vascular endothelial cadherin (VEcad) and N-cadherin[86]. An overview of the organization of AJs is illustrated in figure 5. Since ECs line the entire vascular system from the heart to the microvasculature of all tissues, vascular ECs vary between organs and blood vessel types (aterial, capillary or venous)[87]. VEcad - a transmembrane protein of the family of type II cadherin, which consists of an intracellular domain and an extracellular domain – is expressed in all types of vascular ECs[88]. In the VEcad-catenin complex, VEcad is linked through its cytosplasmic domain to p120-catenin, β-catenin and γ-catenin[89]. While p120 prevents the endocytosis of VEcad, β- and γ-catenin bind to α-catenin linking the VEcad-catenin complex to actin filaments[86,90]. The binding of α-catenin to the VEcad-catenin complex has a negative impact on actin polymerization[91]. The actin cytoskeleton can also be regulated via other actin binding proteins like epithelial protein lost in neoplasm (EPLIN), Vinculin and α-actinin. In AJs the organization of the actin cytoskeleton is modulated through small Rho GTPases[92]. Furthermore, AJs are regulated by the phosphorylation of VEcad, which is mediated by permeability increasing factors such as VEGF, TNF-α, platelet-activating factor, histamine, bradykinin and thrombin[93]. Phosphorylation induces VEcad internalization and reduces the amount of VEcad at AJs leading to an opening of the junction[86,93]. To this end, VEcad controls cell permeability[86]. VEcad also mediates adhesion between cells in a Ca^{2+}-dependent manner by establishing interactions of neighboring ECs[81,86]. When ECs come in contact, they inhibit their growth and establish cell-cell junctions[84]. VEcad expression and clustering at AJs blocks the proliferative response of the cell to growth factors by modulation of their downstream signaling[86,94,95]. VEcad interacts with vascular endothelial protein tyrosine phosphatase (VE-PTP) that supresses VEGFR2 activity resulting in the inhibition of VEGF-induced cell proliferation[94,95]. Thereby, VE-PTP regulates junctional stability[95].

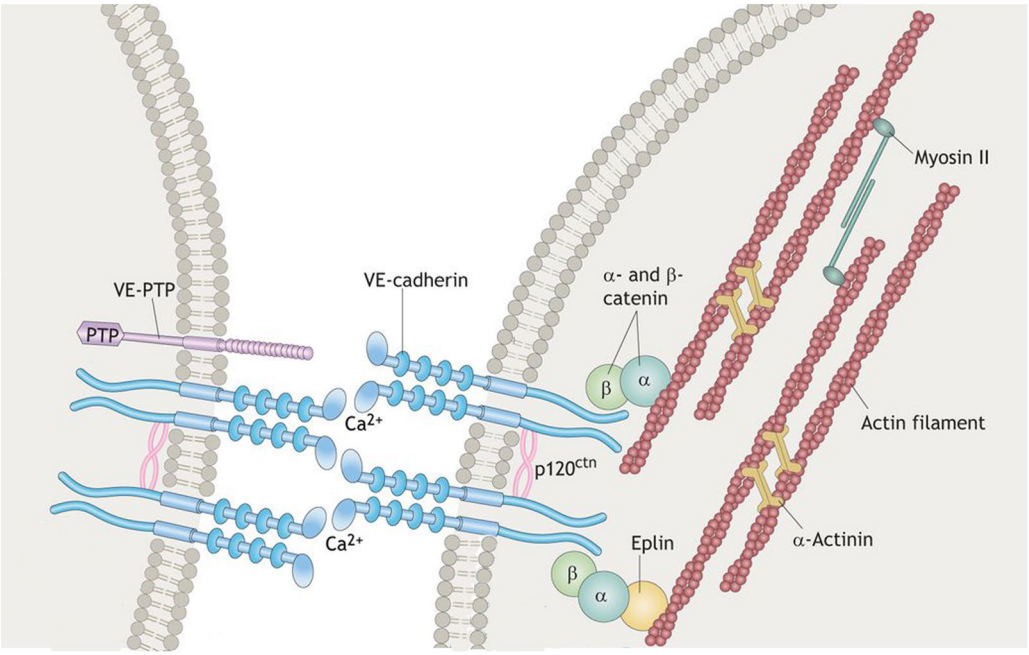

Figure 5. Organization of AJs in ECs
The VEcad-catenin complex is the basis of the AJ. The cytoplasmic domain of VEcad binds to p120, β-catenin-α-catenin and to β-catenin-α-catenin-EPLIN, which connects VEcad to the actin cytoskeleton. A modulator for stabilization and signaling is VE-PTP (modified from Cao and Schnittler [81]).

Whereas N-cadherin is important for cell migration and vascular elongation, VEcad has the opposite effect and limits cell movement by controlling growth factor signaling[86]. Thereby, the interplay of the VEcad-catenin complex and actin is important for cell adhesion, barrier function, cell migration and angiogenesis. Importantly, AJs are not static and their organization and disorganization are regulated by a complex network of intracellular signaling pathways and by the actin cytoskeleton, which is crucial for physiological and pathophysiological processes[86].

1.4.1 Dynamics of AJs

AJs are highly dynamic structures and their connection to the actin cytoskeleton allows a fast remodeling of the junction increasing the local permeability to small molecules and cells from the bloodstream. This is important for tissue homeostasis and the inflammatory response[96]. The vascular changes are important for leukocyte extravasation from the circulation to the injury site to demolish pathogens, remove debris and the process of tissue reparation[97]. AJs can be differentiated into linear and discontinuous AJs. Linear AJs are orientated to cortical F-actin, whereas discontinuous AJ are attached to the end of stress

fibers[96]. Acute inflammatory stimuli activate the RhoA / ROCK signaling pathway. Its activation consequently stimulates the actomyosin contractility and increases the permeability of the endothelial cell-cell junction[86,98,99].

Additionally, ECs have reticular AJs, which are characterized by a polygonal distribution of VEcad[100]. These are found in quiescent ECs and are restricted to primary ECs. Reticular AJs are localized in areas with low actomyosin-mediated tension where neighboring cells overlap. AJ proteins, like p120-catenin, α-catenin and β-catenin from both overlapping cells are involved in the formation of reticular AJs[98]. In contrast to linear or discontinuous AJs, which are always associated with F-actin, reticular AJs do not require direct interaction with F-actin. For that reason, F-actin is not enriched within reticular AJs but localizes at their edges and thereby surrounds them[101]. The physiological relevance of reticular AJs is unknown to date.

1.4.2 Junction-associated intermittent lamellipodia (JAIL)

Recently, Arp2/3 complex-dependent lamellipodia at cell-cell junctions, which develop at VEcad free spaces, were discovered[102]. These structures, named junction-associated intermittent lamellipodia (JAIL), regulate local VEcad dynamics. Arp2/3 complex activity supports VEcad dynamics and junctional plasticity. Inhibition of the Arp2/3 complex in subconfluent cells results in a discontinuous VEcad pattern with locally reduced VEcad. At these VEcad free spots, branched actin filaments form JAIL, which protrude across a small part of the apical membrane of the neighboring cell[81,102]. VEcad plaques arise as a result of trans-interactions between VEcad molecules in the region that overlaps[102,103]. When the Arp2/3 complex dissociates from actin filaments, the formation of JAIL is finished. Following Actin disassembly, the clustered VEcad molecules are moving out of the plaque into the junction by which a novel VEcad adhesion site is formed in order to establish a new AJ[81,103].

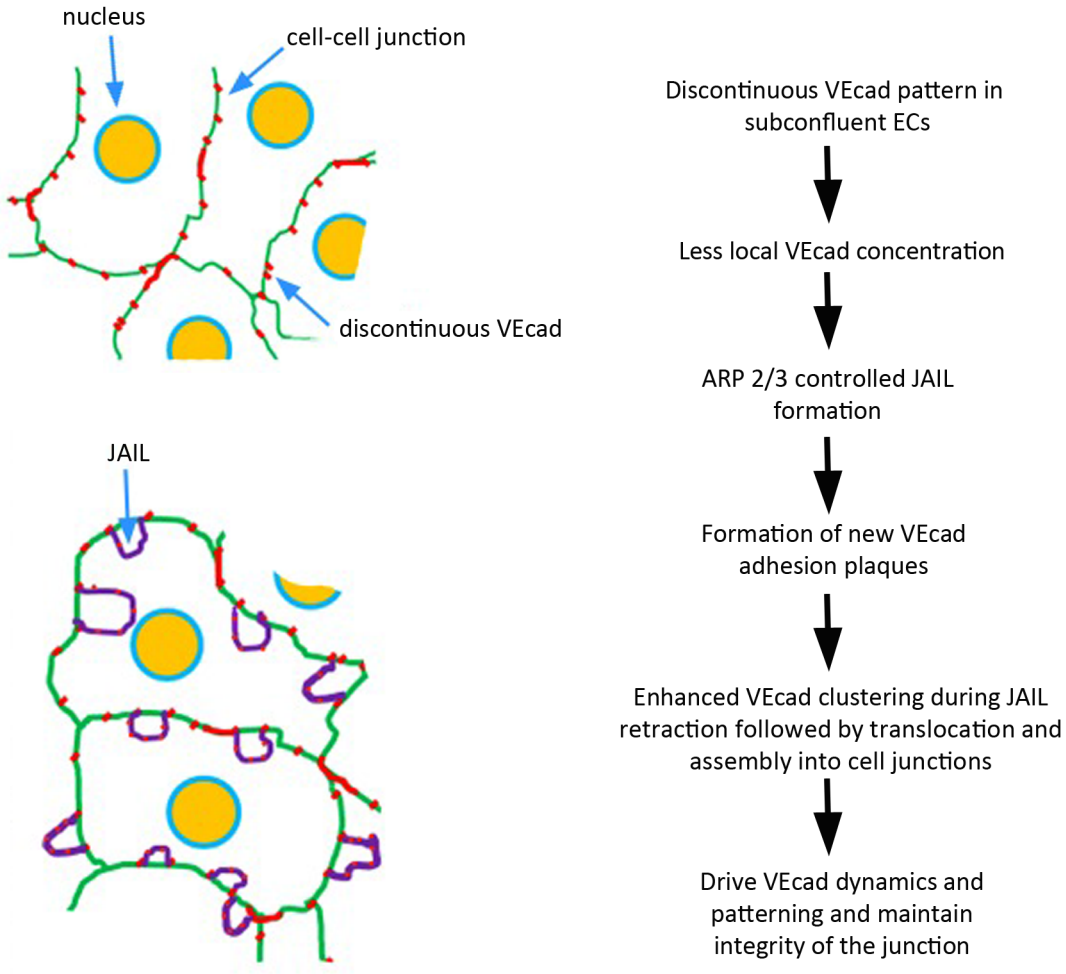

Figure 6. JAIL formation in subconfluent cells
A local reduction of VEcad leads to an Arp2/3-controlled JAIL formation. JAIL drive VEcad dynamics and maintain the integrity of the junction (modified from Taha et al.[102]).

Integration of signal transduction and cytoskeletal modification of the junction is the basis of EC cell-junction dynamics[81]. JAIL are involved in the regulation of cell–cell junctions by inducing new VEcad adhesion sites[103,104]. Their formation is controlled by several actin-binding proteins including EPLIN or α-parvin, which localize to JAIL[14,105]. By regulating local VEcad dynamics, JAIL are important in controlling endothelial permeability. To this end, they are critical for monolayer integrity[102]. Moreover, clustering of large JAIL at the cell poles drives forward-directed migration, whereby small JAIL at lateral cell junctions grant the relative movement of adjacent cells[106]. As such, JAIL are essential for sprouting angiogenesis and vessel function[106].

1.5 Coronins

Coronins are grouped to the family of actin-binding proteins expressed in most eukaryotes. The name coronin has its origin in the localization to crown-like structures[107]. Coronins - discovered in *Dictyostelium discoideum* - localize at the leading edges of migrating cells and in crown-shaped extensions of the dorsal cell surface[108-110]. The family of coronins compromises three isoforms, type I, type II and type III. In the mammalian genome seven coronin genes are present, of which three coronins belong to the group of isoform type I namely coronin 1A, 1B and 1C. Coronin 6 exhibits a similar structure as type I coronins but does not belong to one of the three isoforms. Type I coronins are known to coordinate actin filaments assembly via the Arp2/3 complex and its disassembly is promoted by cofilin[107]. The characteristic structure of the type I coronin is the WD40-repeats containing β-propeller (figure 7). Besides the five WD40 repeats, the β-propeller contains an amino (N)-terminal region flanked by a carboxy (C)-terminal extension. The C-terminal extension consists of a conserved and a unique region stabilizing the β-propeller[111]. Moreover, the C-terminal extension connects the β-propeller to a coiled-coil domain, which is required for multimerization[112]. Phosphorylation at a threonine in the coiled-coil domain leads to monomerization by interrupting coiled-coiled interactions[113]. A charged patch on the top surface area of the β-propeller is critical to bind F-actin[107]. Specifically, the surface-exposed conserved arginine residue at position 30 (R30) was identified as the responsible domain for coronin type I to bind F-actin (figure 7)[113,114]. In contrast to this specific binding site in type I coronins, type II coronins lack this conserved residue. However, type II coronins comprise various other blocks of conserved residues in the β-propeller. Additionally, the unique regions in type II coronins differ from those of type I coronins[107]. Type III coronins exhibit a C-terminal acidic region instead of the coiled-coil domain and have two β-propellers, which are both linked with C-terminal and N-terminal extensions[115]. The β-propellers are connected by a sequence that links the unique region of the C-terminal extension of one β-propeller to the N-terminal extension of the other one[107].

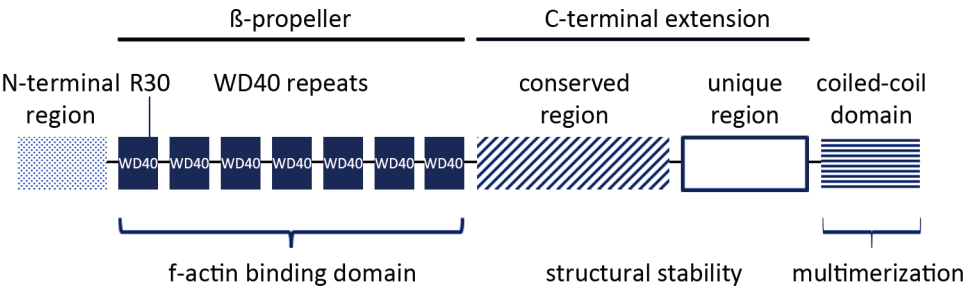

Figure 7. Schematic structure of type I coronin
Coro1B consists of a β-propeller, which is surrounded by an N-terminal region and a C-terminal extension. Whereas the β-propeller facilitates F-actin binding, the C-terminal extension provides structural stability. The coiled-coil domain is relevant for multimerization that give them their dimeric or trimeric form.

The latest identified coronin (Coro6) is expressed in the adult muscle. Coro6 is enriched in neuromuscular junctions where it regulates acetylcholine receptors clustering[116]. Coronin2A (Coro2A) and coronin2B (Coro2B) represent the family of type II coronins[107]. In contrast to type I coronins, the members of type II coronins localize mainly to stress fibers and FAs[108]. It was shown that Coro2A regulates cofilin activity at FAs[117]. In addition, Coro2A was classified as a component of the nuclear co-repressor complex in the nucleus of hematopoietic cells where it regulates actin-dependent de-repression of genes involved in inflammatory response[118]. Coro2B is enriched in the nervous system. Co-immunoprecipitation with the FA protein vinculin indicated its localization to FAs[108]. Coronin 7 (Coro7) belongs to the family of type III coronin. It localizes at the membrane of the Golgi apparatus and is important for the organization of intracellular membrane compartments and vesicular trafficking[119].

1.5.1 Type I coronins

Whereas Coronin1A (Coro1A) is only expressed in hematopoietic cells, Coronin 1B (Coro1B) and Coronin1C (Coro1C) are ubiquitously expressed[107]. Coro1A was identified as a novel regulator of β_2 integrins controlling leukocyte adhesion in innate immunity[120]. Coro1A-deficient mice exhibit an immunodeficiency by impaired chemokine-mediated migration of T lymphocytes, which results from a defect actin regulation in T lymphocytes[121]. In the absence of Coro1A and Coro1B, mast cell degranulation in mice is impaired[122]. Coro1B and Coro1C localize at lamellipodia together with the Arp2/3 complex and cofilin[123-126]. Coro1B has been identified to negatively regulate cell migration by binding to and inhibiting Arp2/3

complex activities at the leading edge of migrating cells[124,127]. Coro1C was found to be relevant for the regulation of FA dynamics and cell migration in epithelial cells[123].

1.5.2 Coronin 1B

Coro1B is highly expressed in vascular cells and ECs. Coro1B is localized at the periphery of ECs under confluent conditions[128,129]. However, the role of Coro1B in ECs and blood vessel formation is widely unknown. It has been shown that Coro1B is also expressed in fibroblasts. Specifically, it colocalizes with the Arp2/3 complex at the leading edges of migrating fibroblasts where it negatively regulates migration[124,130]. For the formation and maintenance of lamellipodia at the leading edge of migrating cells, actin nucleation is crucial. Cortactin or other nucleation-promoting factors (NPFs) like Wiskott-Aldrich syndrome protein (WASP) and SCAR/WAVE proteins such as myosin 1 and Pan1 activate the Arp2/3 complex promoting its binding to actin filaments. Coro1B is able to inhibit cortactin-mediated activation of the Arp2/3 complex, thereby impeding Arp2/3-mediated actin filament nucleation and promoting debranching in fibroblasts[131]. In epithelial cells, Coro1B interacts with slingshot (SSH1L) phosphatase. This protein binds in a complex with Waf1 Cip1 stabilizing protein 39 (WISp39) to Coro1B. This interaction results in dephosphorylation of Coro1B, which then enables Coro1B to bind to the Arp2/3 complex[127]. However, phosphorylation of Coro1B at the serine 2 (ser2) residue leads to dissociation from the Arp2/3 complex and subsequently to an attenuated inhibition of the Arp2/3 complex. This phosphorylation of Coro1B at ser2 residue occurs after stimulation with VEGF in ECs[128]. Activated p38α directly binds to and phosphorylates Coro1B at ser2. The dissociation of Coro1B from the Arp2/3 complex leads to in an increased cell motility and a translocation of Coro1B to the leading edge of lamellipodia[128]. The same effect has been observed in VSMC where platelet-derived growth factor (PDGF) is able to phosphorylate Coro1B at ser2 resulting in its dissociation from the Arp2/3 complex and induction of migration[132]. Additionally, Coro1B regulates cofilin activity through SSH1L in fibroblasts[124]. Coro1B directs SSHL1 to lamellipodia where SSHL1 dephosphorylates and hence activates cofilin[124]. The dephosphorylation of cofilin enhances its F-actin binding and activates depolymerization[133]. A surface-exposed conserved arginine residue at position 30 (R30) in the β-propeller of Coro1B was identified as the interaction site of Coro1B with actin[114]. Coro1B binds to adenosine triphosphate (ATP) F-actin with high

affinity and to adenosine diphosphate (ADP) F-actin with lower affinity. As result of this binding, cofilin is disabled to induce actin filament depolymerization (figure 8). Cofilin enhances depolymerization by binding to freshly polymerized actin filaments and induces conformational changes in filament structures[134]. A mutation in the R30 region of Coro1B inhibits its binding to F-actin and results in an inefficient localization of Coro1B to the leading edge[114].

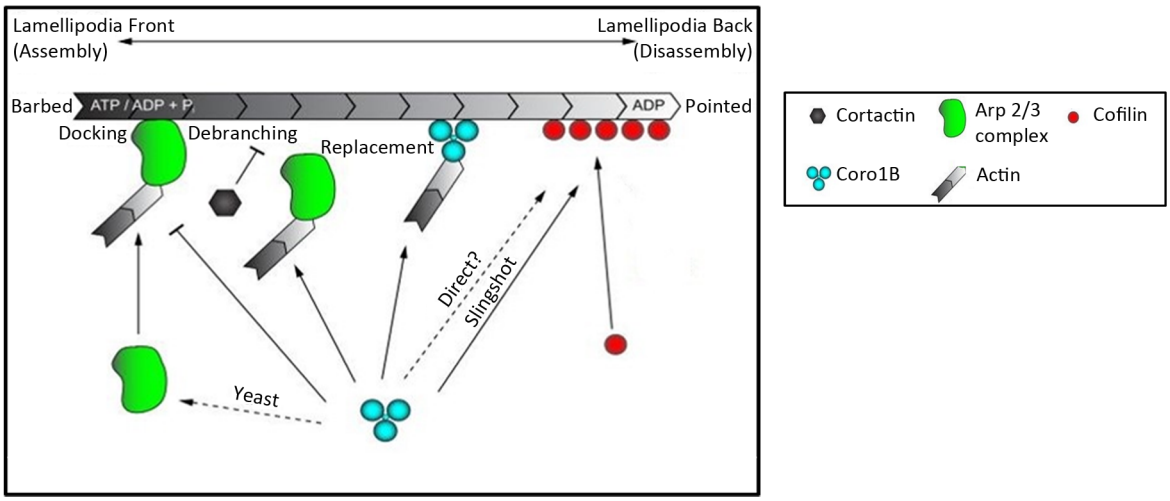

Figure 8. Schematic overview of Coro1B function
Coro1B inhibits cortactin activation of the Arp2/3 complex and thereby promotes debranching. In addition, Coro1B hinders the binding of cofilin to freshly polymerized actin filaments (modified from Chan et al.[107]).

In epithelial cells, Coro1B regulates the reorganization of non-aligned F-actin into aligned bundles through RhoA signaling[135,136]. Coro1B maintains the junctional pool of non-muscle myosin II by inhibiting ROCK signaling through SSH1L and is thereby crucial for myosin accumulation and the stability of the junction[136,137]. Myosin contraction is promoted by phosphorylation and activation of MLC. This process is facilitated when Myosin phosphatase target subunit 1 (MYPT-1) gets inactivated by phosphorylation[138]. Coro1B negatively impacts ROCK signaling via recruiting SSH1L, which reduces phosphorylation levels of MYPT-1[137]. Thereby Coro1B modulates myosin activity, which is crucial for cell motility[137]. Whether Coro1B is also involved in regulating endothelial cell-cell junctions is currently unknown.

2. Aim of the study

Coro1B is an actin-binding protein, which is highly expressed in ECs. However, its impact on EC function is not fully understood. The aim of this PhD project was to analyze the role of Coro1B for EC function.

For this purpose, the first aim of the study was to characterize the role of Coro1B for EC adhesion, migration and monolayer formation using Coro1B knockdown ECs. Additionally, these cells in combination with *in vitro* angiogenic models were used to determine the role of Coro1B in angiogenesis. Furthermore, pulldown experiments using stably expressing Coro1B-EGFP ECs followed by mass spectrometry analysis were performed to identify potential Coro1B binding partners. The second aim of this study was to investigate the impact of Coro1B on angiogenesis *in vivo*. To address this point, a Coro1B knockout zebrafish line was generated to study the vascular development.

In summary, this study was aimed at shedding light on the involvement of Coro1B in the regulation of cell-cell junctions, angiogenesis and vessel permeability, which provides new insights into endothelial cell function.

3. Materials

3.1 Antibodies and fluorescently labelled peptides

Antigen	Dye	Reactivity	Clone	Company
ARP2/3 complex		mouse anti-human	13C9	Merck Millipore, USA
α-parvin		rabbit anti-human		Cell Signaling, USA
β-actin		mouse anti-human	C4	Santa Cruz Biotechnology, USA
CD144		mouse anti-human	16B1	eBioscience Thermo Fisher Scientific, Germany
Coronin 1A		mouse anti-human	14.1	Santa Cruz Biotechnology, USA
Coro1B		rabbit anti-human	polyclonal	Sigma-Aldrich, Germany
Coro1C		rabbit anti-human	polyclonal	Sigma-Aldrich, Germany
ILK1		rabbit anti-human	polyclonal	Cell Signaling, USA
Glyceraldehyde-3-Phosphate Dehydrogenase (GAPDH)		mouse anti-human	6C5	Merck Millipore, USA
Paxillin		mouse anti-human	349	BD Bioscience, USA
Phalloidin	Alexa Fluor 546			Invitrogen, Germany
Phalloidin	Alexa Fluor 633			Invitrogen, Germany
Phospho-Histone H3 (Ser10)		rabbit anti-human	polyclonal	Merck Millipore, USA
secondary antibody	Alexa Fluor 488	donkey anti-rabbit		Thermo Fisher Scientific, Germany
secondary antibody	Alexa Fluor 488	goat anti-rabbit		Invitrogen, Germany
secondary antibody	Alexa Fluor 488	goat anti-mouse		Thermo Fisher Scientific, Germany

Antigen	Dye	Reactivity	Clone	Company
secondary antibody	Alexa Fluor 546	donkey anti-rabbit		Invitrogen, Germany
secondary antibody	Alexa Fluor 546	donkey anti-mouse		Invitrogen, Germany
secondary infrared	680 RD	donkey anti-mouse		Li-Cor Biotechnology, USA
secondary infrared	680 RD	donkey anti-rabbit		Li-Cor Biotechnology, USA
secondary infrared	800 CW	donkey anti-mouse		Li-Cor Biotechnology, USA
secondary infrared	800 CW	donkey anti-rabbit		Li-Cor Biotechnology, USA

3.2 Cell lines

Name	Description	Source
HEK-293T	human embryonic kidney cells	American Type Culture Collection, CRL-11268™, USA
HUVEC	primary human umbilical vein endothelial cells	Pelobiotech, PB-CH-190-8013, Germany
HMEC-1	immortalized human microvascular endothelial cells	American Type Culture Collection, CRL-3243™, USA
fibroblasts	mouse embryonic fibroblasts	generation described in Montanez et al.[139]

3.3 Chemicals

Name	Company
acrylamide 4K-solution (30%)	AppliChem, Germany
agarose	Genaxxon bioscience, Germany
ammonium persulfate (APS)	AppliChem, Germany
albumin fraction V	AppliChem, Germany
bromophenol blue	Thermo Fisher Scientific, Germany
calcium chloride ($CaCl_2$)	AppliChem, Germany

Name	Company
collagenase 2	CellSystems, Germany
collagenase 4	CellSystems, Germany
complete protease inhibitor	Roche, Switzerland
desoxyribonuclease 1	CellSystems, Germany
DH5α competent cells	Thermo Fisher Scientific, Germany
diisopropyl phosphofluoridate (DFP)	Sigma-Aldrich, Germany
dimethyl sulfoxide (DMSO)	AppliChem, Germany
dithiothreitol (DTT)	AppliChem, Germany
Dulbecco's phosphate buffered saline (PBS)	Thermo Fisher Scientific, Germany
Dulbecco's modified eagle medium (DMEM)	Thermo Fisher Scientific, Germany
dynabeads sheep anti-rat	Thermo Fisher Scientific, Germany
endothelial cell growth medium (ECGM)	PromoCell, Germany
ethylenediaminetetraacetic acid (EDTA)	AppliChem, Germany
formaldehyde 37%, pure	Waldeck, Germany
fetal calf serum (FCS)	Biochrom, Germany
Fluoromount-G	Southern Biotech, USA
gelatine	Sigma-Aldrich, Germany
GeneRuler™ 1 kb DNA ladder	Nippon Genetics, Japan
GeneRuler™ 100 bp DNA ladder	Nippon Genetics, Japan
GFP-Trap agarose	ChromoTek, Germany
glycerol	AppliChem, Germany
glycine	AppliChem, Germany
GoTaq G2 polymerase	Promega, USA
kanamycin	Sigma-Aldrich, Germany

Name	Company
Lipofectamine® 2000	Thermo Fisher Scientific, Germany
magnesium sulfate ($MgSO_4$)	Sigma-Aldrich, Germany
magnet assisted transfection (MATra)-si reagent	PromoCell, Germany
matrigel matrix	Corning, USA
2-mercaptoethanol	Sigma-Aldrich, Germany
midori green	Nippon Genetics, Japan
Odyssey® blocking buffer	Li-Cor Biotechnology, USA
modified eagle's minimum essential medium (Opti-MEM)	Thermo Fisher Scientific, Germany
PageRuler™ prestained protein ladder	Thermo Fisher Scientific, Germany
penicillin / streptomycin (P / S)	Biochrom, Germany
sodium acetate	Sigma-Aldrich, Germany
sodium fluoride (NaF)	Sigma-Aldrich, Germany
Phusion DNA polymerase	New England Biolabs, Germany
potassium chloride (KCl)	AppliChem, Germany
protease inhibitor mix B	Sigma-Aldrich, Germany
proteinase K	Roche, Switzerland
pronase	Roche, Switzerland
puromycin	Sigma-Aldrich, Germany
Roswell Park Memorial Institute 1640 (RPMI)	Biochrom, Germany
stellar competent cells	Clontech - Takara Bio Company, USA
sodium acetate	AppliChem, Germany
sodium dodecyl sulphate (SDS) 10% solution	AppliChem, Germany
sodium chloride (NaCl)	AppliChem, Germany

Name	Company
sodium deoxycholate	AppliChem, Germany
sodium orthovanadate (Na_3VO_4)	Sigma-Aldrich, Germany
T4 DNA ligase	New England Biolabs, Germany
tetramethylethylenediamine (TEMED)	AppliChem, Germany
thrombin from human plasma	Sigma-Aldrich, Germany
Trans-Blot Turbo ™ 5x transfer buffer	Bio-Rad Laboratories, USA
tricaine	Sigma-Aldrich, Germany
Triton X 100	AppliChem, Germany
Trizma base (tris)	AppliChem, Germany
tris-hydrochloride (tris-HCl)	AppliChem, Germany
tryptone	Chemsolute, Germany
Y-27632	Merck Millipore, USA
Tween 20	Sigma-Aldrich, Germany
yeast extract	AppliChem, Germany

3.4 Disposables / Consumables

Name	Company
cell culture dishes	Greiner Bio-One, Germany
cell culture plates (12 well / 24 well)	Sarstedt, Germany
coverslips 24 x 24 mm	Carl Roth & Co KG, Germany
cryopure tube	Sarstedt, Germany
E-Plate insert 16	ACEA Biosciences Inc., USA
NALGENE™ cryo 1 °C freezing container	Thermo Fisher Scientific, Germany
tissue culture plate (12 well / 24 well)	Sarstedt, Germany
universal magnet plate	PromoCell, Germany

3.5 Equipment

Name	Company
dyna magnet	Thermo Fisher Scientific, Germany
sonicator	Hielscher Ultrasonics, Germany
XCelligence system	Roche, Switzerland

3.6 Restriction enzymes

Name	Company
AgeI	New England Biolabs, Germany
BtsCI	New England Biolabs, Germany
HindIII	New England Biolabs, Germany
MluI	New England Biolabs, Germany
SacII	New England Biolabs, Germany

3.7 Kits

Name	Company
APO-BrdU™ TUNEL assay kit	Thermo Fisher Scientific, Germany
In-Fusion® cloning HD kit	Clontech - Takara Bio Company, USA
iST sample preparation kit	PreOmics**,** Germany
MEGAshortscript T7 Transcription Kit	Thermo Fisher Scientific, Germany
PureYield™ plasmid miniprep system	Promega, USA
QIAGEN plasmid maxi kit	Qiagen, Germany
QIAquick gel extraction kit	Qiagen, Germany
Qubit™ protein assay kit	Thermo Fisher Scientific, Germany

3.8 Primers

Name	Oligonucleotide 5’ – 3’	Melting temperature (Tm) [°C]	Supplier
Coro1B forward	GCATAAGCTTATGTCCTTCCG	56.8	Metabion, Germany
Coro1B reverse	GTGAAAGGAAGGCCCATGA	57.3	Metabion, Germany
Coro1B-EGFP In-Fusion® cloning forward	TCGGCGCGCCACGCGTATGTCCT TCCGCAAAGTGG	51.1	Metabion, Germany
Coro1B-EGFP In-Fusion® cloning reverse	AATGTTAACGACCGTTTACTTTAC TTGTACAGCTCGTCCAT	50.5	Metabion, Germany
EGFP In-Fusion® cloning forward	TCGGCGCGCCACGCGTATGGTGA GCAAGGGCGAGGAGC	86	Metabion, Germany
EGFP In-Fusion® cloning reverse	CGGCATGGACGAGCTGTACAAG TAAACCGGTCGTTAACATT	79	Metabion, Germany
Coro1B #6 forward	AGAGCACATGACAGAGGACTCA	62	Metabion, Germany
Coro1B #6 reverse	CTGCACTGTCAAGGTCAGTTTC	62	Metabion, Germany

3.9 siRNA

siRNA ID	siRNA type	Sequence start	Supplier
SASI_Hs01_00084499	Rosetta Predictions	342	Sigma-Aldrich, Germany
SASI_Hs01_00084500	Rosetta Predictions	547	Sigma-Aldrich, Germany
SIC001	Mission siRNA Universal negative Control #1		Sigma-Aldrich, Germany

3.10 guideRNA

Name	Oligonucleotide 5’ – 3’	Melting temperature (Tm) [°C]	Supplier
Coro1B #6	CGCCAGTGCTGGATGTGCAG	63.5	Metabion, Germany

3.11 Plasmids

Name	Company
coro1B_pMK-RQ (15AB3P2P)	Invitrogen, Germany
pEGFP-N1 (6085-1)	Clontech, USA
pCMV-VSV-G (plasmid 8454)	Addgene, USA
pCMV-ΔR8.91	Addgene, USA

3.12 Software

Name	Company
Adobe Photoshop, Illustrator, Acrobat X Pro	Adobe, USA
EndNote X7.7	Clarivate Analytics, USA
Fiji / ImageJ	NIH, USA
Image Studio Lite V5.2	Li-Cor Biotechnology, USA
Prism 6	GraphPad, USA
RTCA Software 2.0	ACEA Biosciences Inc., USA
Slidebook 6.0.8	3i Intelligent Imaging Innovations, USA

3.13 Buffers and solutions

Name	Ingredients
dilution buffer	H_2O_{dest} + 25 nM tris-HCl (pH 7.5) + 150 nM NaCl + 0.5 EDTA + 1 mM DTT
digestion solution	PBS + 2.5 mg / ml collagenase 2 + 2.5 mg / ml collagenase 4

Name	Ingredients
	+ 1 mg / ml desoxyribonuclease 1
	+ 10% FCS
E3 medium	H_2O_{dest}
	+ 5 mM NaCl
	+ 0.17 mM KCl
	+ 0.33 mM $CaCl_2$
	+ 0.33 mM $MgSO_4$
2x Lämmli-buffer	H_2O_{dest}
	+ 125 mM tris-HCl pH 6.8
	+ 4% SDS 10% solution
	+ 20% glycerol
	+ 10% 2-mercaptoethanol
	+ 0.002% bromophenol blue
luria broth medium	H_2O_{dest}
	+ 0.01% tryptone
	+ 0.005% yeast extract
	+ 0.01% NaCl
	pH 7.0
lysis buffer Berton II	H_2O_{dest}
	+ 25 mM tris-HCl (pH 7.5)
	+ 150 mM NaCl
	+ 0.5 mM EDTA
	+ 1% Triton X 100
	+ 1% sodium deoxycholate
	+ 1 mM DTT
PCR mix	36.3 ml H_2O_{dest}
	+ 60 µl dATP 100 mM
	+ 60 µl dTTP 100 mM
	+ 60 µl dGTP 100 mM

Name	Ingredients
	+ 60 µl dCTP 100 mM
	+ 6 ml 10x PCR buffer
10x PCR buffer	38.5 ml H_2O_{dest}
	+ 10 ml 1M tris-HCl (pH 8.3)
	+ 50 ml 1M KCl
	+ 1.5 ml 1M MgCl
	+ 0.1 g gelatine
RIPA lysis buffer	H_2O_{dest}
	+ 50 mM tris-HCl (pH 8.0)
	+ 150 mM NaCl
	+ 0.1% Triton X 100
	+ 0.1% sodium deoxycholate
	+ 0.1% SDS 10% solution
	+ 5 mM EDTA
SDS-PAGE running buffer	H_2O_{dest}
	+ 200 mM glycine
	+ 25 mM tris
	+ 0.1% SDS 10% solution
50x TAE buffer	H_2O_{dest}
	+ 2 M tris
	+ 1 M sodium acetate
	+ 62.5 mM EDTA
	pH 8.5
TBS-T	H_2O_{dest}
	+ 20 mM tris
	+ 137.2 mM NaCl
	+ 0.1% Tween 20
	pH 7.6

Name	Ingredients
tris-EDTA buffer	H_2O_{dest} + 10 mM tris + 1 mM EDTA pH 8.0
tricaine stock solution	H_2O_{dest} + 20 mM tris (pH 9.0) + 0.004 g / ml tricaine pH 7.0
western blot 10% separating gel	5.9 ml H_2O_{dest} + 5.0 ml acrylamide 4K-solution (30%) + 3.8 ml 1.5 M tris (pH 8.8) + 150 µl SDS 10% solution + 150 µl APS + 10 µl TEMED
western blot 12% separating gel	4.9 ml H_2O_{dest} + 6.0 ml acrylamide 4K-solution (30%) + 3.8 ml 1.5M tris (pH 8.8) + 150 µl SDS 10% solution + 150 µl APS + 10 µl TEMED
western blot 4% stacking gel	2.7 ml H_2O_{dest} + 670 µl acrylamide 4K-solution (30%) + 500 µl 1 M tris (pH 6.8) + 40 µl SDS 10% solution + 40 µl APS + 10 µl TEMED

4. Methods

4.1 Generation of a Coro1B-EGFP construct

Coro1B cDNA was purchased as coro1B_pMK-RQ plasmid from Invitrogen. First, the sequences encoding for Coro1B was amplified out of the coro1B_pMK-RQ plasmid by PCR. The PCR protocol revealed an initial denaturation step at 98 °C for 30 seconds, followed by 30 cycles each of 10 seconds at 98 °C (denaturation), 30 seconds at 62 °C the annealing temperature of the primers (hybridization), 30 seconds at 72 °C (extension) and a final extension step of 10 minutes at 72 °C.

Table 1. PCR components to amplify Coro1B

Components	**Final concentration**
Phusion DNA polymerase	0.5 µl
5x Phusion HF buffer	10 µl
Coro1B forward primer (10 µm)	2.5 µl
Coro1B reverse primer (10 µm)	2.5 µl
dNTPs (10 mM)	1 µl
H_2O_{dest}	33 µl
template DNA	0.5 µl

With the use of specifically designed Coro1B forward and Coro1B reverse primers for PCR, overlapping ends containing binding sites for the restriction enzymes SacII and HindIII were generated. To clone Coro1B into the pEGFP-N1 vector (provided by Prof. Dr. Barbara Walzog, Ludwig Maximilian University of Munich), the PCR product and the pEGFP-N1 vector were digested with the restriction enzymes SacII and HindIII (figure 9). Ligation of insert (Coro1B) and vector (pEGFP-N1) was performed with T4 DNA ligase. The necessary amount of insert was calculated as follows:

$$ng_{\text{ of insert}} = (ng_{\text{ of vector}} \times \text{kb size}_{\text{ of insert}} / \text{kb size}_{\text{ of vector}}) \times \text{molar ratio (insert / vector)}$$

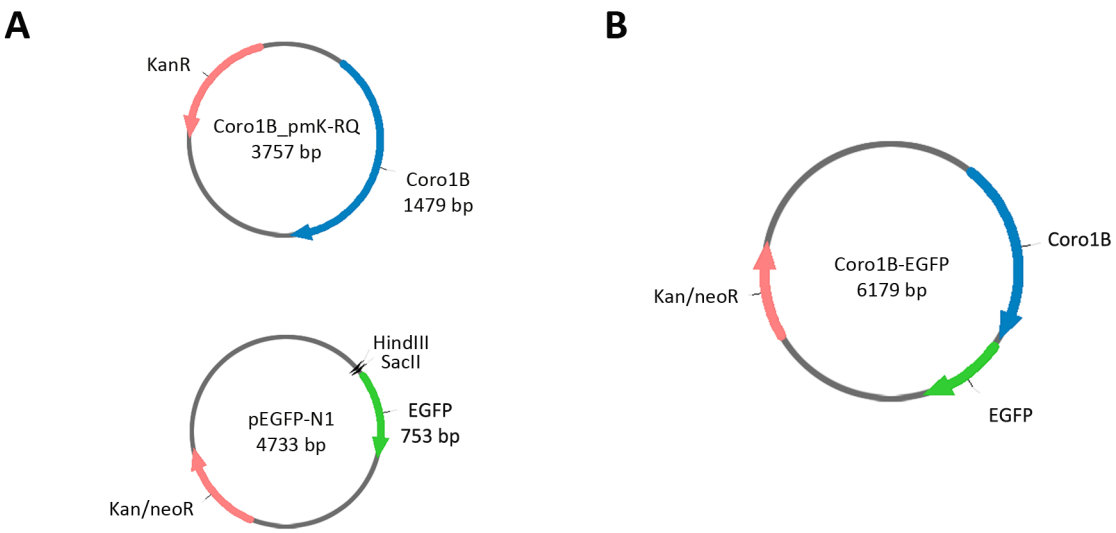

Figure 9. Generation of a Coro1B-EGFP construct
(A) Structure of initial Coro1B_pmK-RQ and pEGFP-N1 plasmid. The Coro1B_pmK-RQ plasmid containing the sequence for Coro1B and a kanamycin resistance (KanR). Structure of the initial used vector pEGFP-N1 containing the sequence for EGFP, recognition sites for the restriction enzymes HindIII and SacII and a kanamycin / neomycin resistance (Kan / neoR). (B) Structure of the generated Coro1B-EGFP construct containing the sequence for Coro1B-EGFP and for Kan / neoR resistance.

After ligation, the circular vector was transformed into competent DH5α *E. coli* cells, plated on LB-agar plates with kanamycin resistance and incubated at 37 °C overnight. Raised clones were picked and plasmid DNA from overnight cultures was isolated using PureYield™ plasmid miniprep system[103].

4.2 Agarose gel electrophoresis

To verify successful cloning, a control digest with SacII and HindIII was performed and gel electrophoresis in 1.5% agarose gel in TAE buffer was conducted. Here, separation of DNA fragments occurred according to their size visualized with midori green and UV light. The DNA ladder was used to determine band size. Clones containing the expected band size were selected and plasmid DNA of Coro1B-EGFP was purified with QIAquick gel extraction kit and plasmid DNA was isolated from overnight cultures using QIAGEN plasmid maxi kit.

4.3 Cell culture

Cells were cultivated under sterile conditions at 37 °C, 5% CO_2 and 95% air humidity to guarantee conditions for optimal growth. To store cells long-time, cells were centrifuged at

300 g for 5 minutes and suspended in 80% culture medium with 10% FCS and 10% DMSO. A NALGENE™ cryo 1 °C freezing container allowed freezing of cells at constant rate of approximately -1 °C per minute. Cells were stored at -80 °C overnight before storing at -196 °C in liquid nitrogen. For cultivation frozen cell line stocks in cryotubes were quickly thawed in a water bath at 37 °C and suspended in fresh culture medium.
HEK-293T cells were cultured in RPMI containing 10% FCS and 1% P / S. HUVECs and mouse endothelial cells (mECs) were cultured in ECGM. HMEC-1 and fibroblasts were cultured in DMEM containing 10% FCS, 10% ECGM and 1% P / S.

4.4 Isolation of mECs

Tissue from mouse embryos was used for endothelial cell (EC) isolation. Therefore, embryos were cut in 5 mm pieces and transferred to digestion solution after washing with PBS. Samples were placed in a shaker and incubated at 37 °C for 1 hour. Samples were filtered through a 40 µm cell strainer with isolation medium (DMEM + 10% FCS) and subsequently centrifuged two times at 160 g for 5 minutes and suspended in PBS (containing 1% P / S and 1% FCS). Dynabeads solution was prepared by washing 6 µl dynabeads per embryo five times in PBS (containing 1% P / S and 1% FCS) with the dyna magnet. Next, dynabeads were incubated with 1.25 µl VEcad antibody per embryo for 2 hours (protected from light). After three cycles of washing, dynabeads were suspended in 100 µl PBS containing 1% P / S and 1% FCS before 100 µl VEcad-coated dynabeads solution was added to one sample and incubated for 30 minutes (protected from light). VEcad-positive cells were purified with Dyna magnets. Cells were cultured on glass coverslips coated with 0.15% gelatine and used in passage one.

4.5 Transfection of the Coro1B-EGFP construct

To check for proper localization of Coro1B, 7 x 10^4 cells per ml were seeded in a 24-well plate on coverslips coated with 0.15% gelatine. Lipofectamine® 2000 and the generated Coro1B-EGFP construct encoding for Coro1B-EGFP were diluted in serum reduced medium (Opti-MEM medium) and incubated for 30 minutes. Cells were treated with the transfection mixture diluted 1:4 in culture medium. After 6 hours a medium change with fresh medium was performed. HUVECs, HMEC-1 and fibroblasts were transfected with the generated

Coro1B-EGFP plasmid, cultured for 48 hours and fixed with 4% formaldehyde (in PBS) for 10 minutes. Cells were stained for Coro1B (staining protocol see section 4.15).

4.6 Generation of Coro1B-EGFP expressing HMEC-1

HMEC-1 stably expressing Coro1B-EGFP were generated using lentiviral gene transfer. To this end, the sequence encoding for Coro1B-EGFP was cloned into the lentiviral backbone pLV-CMV-MCS-IRES-PURO-SIN (provided by Dr. Stephan Huveneers, University of Amsterdam) using the In-Fusion® HD cloning kit (base is the homologous recombination)[140]. PCR amplification of the insert using specific designed forward and reverse primers generates 15 base pairs (bp) homologous overlapping ends to the target vector. During the In-Fusion® reaction the overlapping ends of the insert become annealed to complementary sites of the before linearized vector. In this work, the vector containing pLV-CMV-MCS-PURO-IRES-SIN was linearized with the restriction enzymes MluI and AgeI. The sequence encoding for Coro1B-EGFP was cloned out of the Coro1B-EGFP plasmid (generation described in chapter 4.1) and amplified using Coro1B-EGFP In-Fusion® cloning forward primer and Coro1B-EGFP In-Fusion® cloning reverse primer[103].

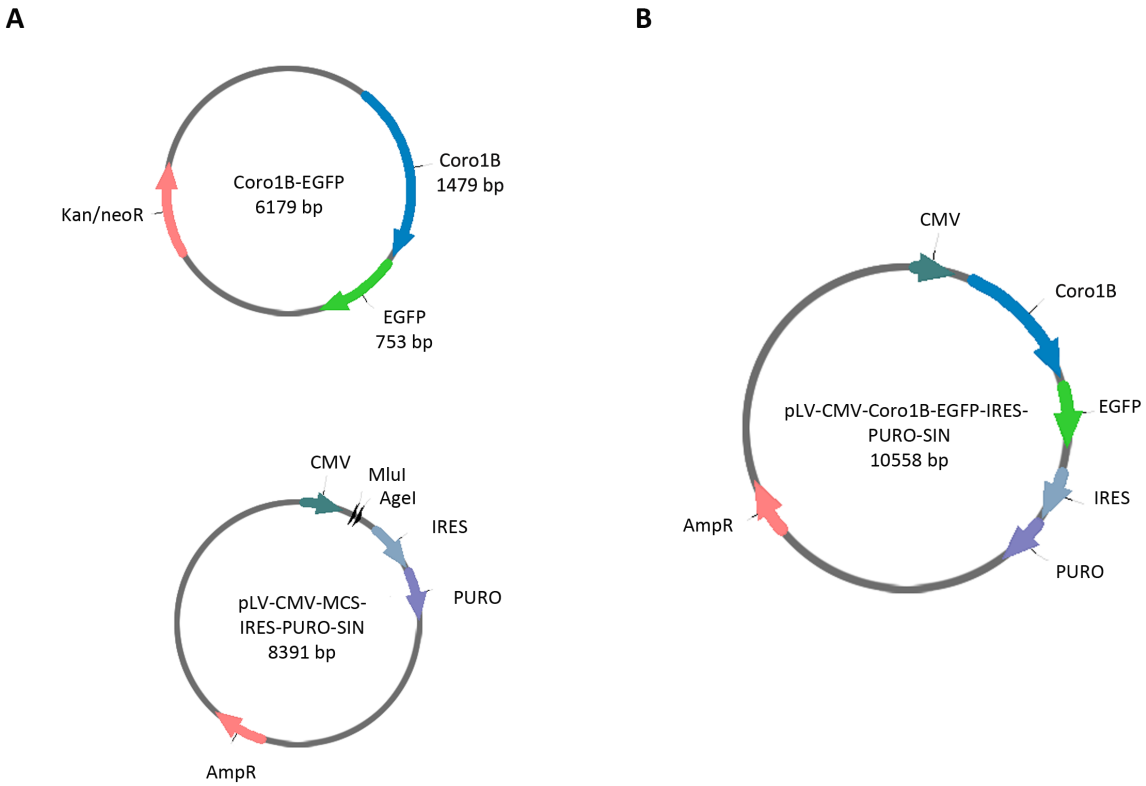

Figure 10. Generation of pLV-CMV-Coro1B-EGFP-IRES-PURO-SIN

(A) Structure of initial Coro1B-EGFP plasmid and lentiviral backbone pLV-CMV-MCS-IRES-PURO-SIN. Coro1B-EGFP plasmid containing the sequence for Coro1B-EGFP and for Kan / neoR resistance. The lentiviral backbone pLV-CMV-MCS-IRES-PURO-SIN containing the sequence for the human cytomegalovirus (CMV) promoter, recognition sites for restriction enzyme MluI and AgeI within the multiple cloning site, internal ribosomal entry site (IRES), puromycin resistance (PURO) and an ampicillin resistance (AmpR). (B) Structure of the generated pLV-CMV-Coro1B-EGFP-IRES-PURO-SIN construct containing Coro1B-EGFP from initial Coro1B-EGFP plasmid cloned into the vector pLV-CMV-MCS-IRES-PURO-SIN.

After the In-Fusion® reaction, the circular construct was transformed into Stellar competent *E. coli* cells[140]. Lentivirus encoding for Coro1B-EGFP and a puromycin resistance was established by transfecting HEK-293T cells with the generated pLV-CMV-Coro1B-EGFP-IRES-PURO-SIN vector, the envelope vector pCMV-VSV-G and the packaging vector pCMV-ΔR8.91. The envelope (pCMV-VSV-G) and the packaging vector (pCMV-ΔR8.91) were kindly provided by Prof. Dr. Barbara Walzog, Ludwig Maximilian University of Munich. Supernatant containing virus was harvested 48 hours later. HMEC-1 were transduced with virus (diluted 1:2 in culture medium) overnight. 72 hours post transduction 10 µg / ml puromycin was supplemented to the culture medium to select Coro1B-EGFP expressing cells.

4.7 Generation of EGFP expressing HMEC-1

For the generation of an EGFP expressing cell line, the sequence encoding for EGFP was cloned from pEGFP-N1 vector (compare figure 9A) into the lentiviral backbone pLV-CMV-MCS-IRES-PURO-SIN (provided by Dr. Stephan Huveneers, University of Amsterdam, compare figure 10A). Here, EGFP In-Fusion® cloning forward primer and EGFP In-Fusion® cloning reverse primer and the In-Fusion® HD cloning kit was used as described in the previous chapter[103].

4.8 Knockdown of Coro1B in HUVEC

Coro1B knockdown was performed using specific siRNA against Coro1B in a MATra system. Two different siRNAs against Coro1B and a scrambled control (see section 3.9) were used in all experiments. Before knockdown of Coro1B, HUVECs were cultured to 80% confluence in a 12-well plate. Cells were starved with reduced serum medium (Opti-MEM medium containing 0.1% FCS) 20 minutes before treatment. MATra-si reagent and siRNA were diluted in reduced serum medium (Opti-MEM medium containing 0.1% FCS) and incubated for 20 minutes, to allow association of siRNA with magnetic particles in the MATra-si reagent. Transfection mixture was supplemented to starved cells and incubated on a magnet plate for 15 minutes. The magnetic force brings the siRNA (associated with the magnetic particle) into the cells, which leads to efficient transfection. After 4 hours a medium change was performed. Cells were cultured for 72 hours before use for further experiments. In all knockdown experiments described in this study knockdown efficiency was verified by western blot[103].

4.9 Scratch-wound-assay

To analyze the migration behavior of Coro1B knockdown cells, control or knockdown HUVECs were left in the 12-well plate, where the knockdown was performed. A vertical scratch with a pipette was done in the middle of the well. Images of the closure of the scratch were taken at 0, 6, 9 and 12 hours with a 5x objective at an inverted laboratory microscope Leica DM IL LED. Labeling of the 12-well plate on the bottom site guaranteed images of the same field of view at various time frames. Per field of view 6 images were

taken. The closure of the scratch was calculated offline using ImageJ software. Therefore, in every image time point 0 was set as 100%.

4.10 Matrigel-assay

Control or knockdown HUVECs (85 x 10^3 cells per ml) were seeded on coverslips, which were coated with matrigel[22]. The matrigel matrix is laminin based and is rich of ECM proteins. After seeding of Coro1B knockdown or control cells, the tube formation was analyzed. After 15 and 20 hours images were generated using a 5x objective at an inverted laboratory microscope Leica DM IL LED. To analyze tube formation, the following vascular parameters were measured offline using ImageJ software: first, the total number of branches per field of view (whole image) was counted (figure 11A). Second, the number of connected and not connected branches was determined (figure 11B).

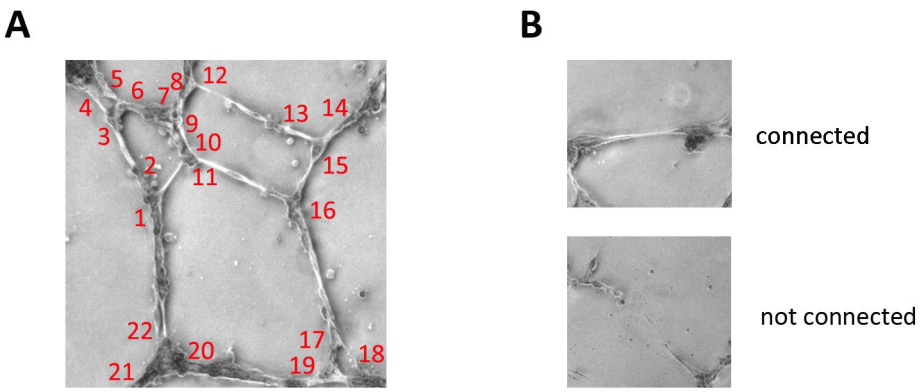

Figure 11. Representative images of tube formation analysis
(A) Representative image shows calculation of the total number of branches. Numbers indicate branches. (B) Representative images of connected and not connected branches.

ImageJ plugin angiogenesis analyzer was used to analyze the total tube length and the number of master segments[103].

4.11 Transendothelial electrical resistance (TEER)

The TEER method is used to examine monolayer formation. Control or Coro1B knockdown HUVECs (5 x 10^4 cells per ml) were plated into E-plates onto a gold electrode. E-plates were equilibrated with culture medium 30 minutes before cells were seeded. TEER was recorded by electric cell-substrate impedance sensing during monolayer formation. An XCelligence

system was used to record impedance for 24 hours. While the initial hour represented cell spreading, every additional hour (2-20 hours) displayed monolayer formation. Difference in cell spreading was analyzed after 1 hour using RTCA software 2.0. To analyze, whether Coro1B knockdown cells showed a difference in their junctional integrity and monolayer formation, impedance was compared after 2, 10, 15, and 20 hours using RTCA software 2.0.

4.12 Protein lysates from adherent cells

Cells were washed once with ice cold PBS and treated with RIPA lysis buffer (500 µL per 1 x 10^6 cells). Complete protease inhibitor (40 µl / ml) and phosphatase inhibitor (5 µl / ml sodium fluoride and 5 µl / ml sodium orthovanadate) were freshly supplemented to RIPA lysis buffer before treatment. Cells were harvested on ice using a cell scraper. Lysates were sonicated and centrifuged (10 minutes at 1600 x g and 4 °C). Supernatant was stored at -20 °C until use. The protein concentration was classified using the Qubit™ protein assay kit.

4.13 Western blot analysis

Protein lysate was mixed with the appropriate amount of 2x Lämmli-buffer. Denaturation of proteins was induced by boiling 10 minutes at 95 °C and separated due to their molecular weight and charged by SDS-polyacrylamide-gel electrophoresis (SDS-PAGE) following the method of Lämmli[141]. Protein lysates and PageRuler™ prestained protein ladder were applied to polyacrylamide gels with 10% separating and 4% stacking gels. Electrophoresis was performed using SDS-PAGE running buffer at 100 - 120 volts. For immunological identification separated proteins were transferred onto nitrocellulose transfer membranes by semi-dry blotting (7 minutes, 13 amperes, 25 volts) using Trans-Blot Turbo ™ 5x transfer buffer. After blocking the membrane for 1 hour in 1:1 TBS-T / Odyssey® blocking buffer, the membrane was incubated with specific primary antibody (diluted in Odyssey® blocking buffer with 1:500 Triton X 100) at 4 °C overnight. Membrane was washed three times for 10 minutes with TBS-T before 1 hour incubation with near-infrared labeled secondary antibodies (diluted in Odyssey® blocking buffer with 1:500 Triton X 100 and 1:100 SDS) at room temperature. After three times washing with TBS-T for 10 minutes, detection was performed using the Odyssey® CLx imaging system.

4.14 Protein pull-down assay

To identify molecular interacting partners of Coro1B, a pull-down assay with GFP-trap agarose beads was performed. This technology is based on a 13 kDa GFP binding fragment derived from the heavy chain of llama antibody, which allows a very specific and efficient precipitation of GFP fusion proteins (Coro1B-EGFP or EGFP) and their interacting partners (figure 12).

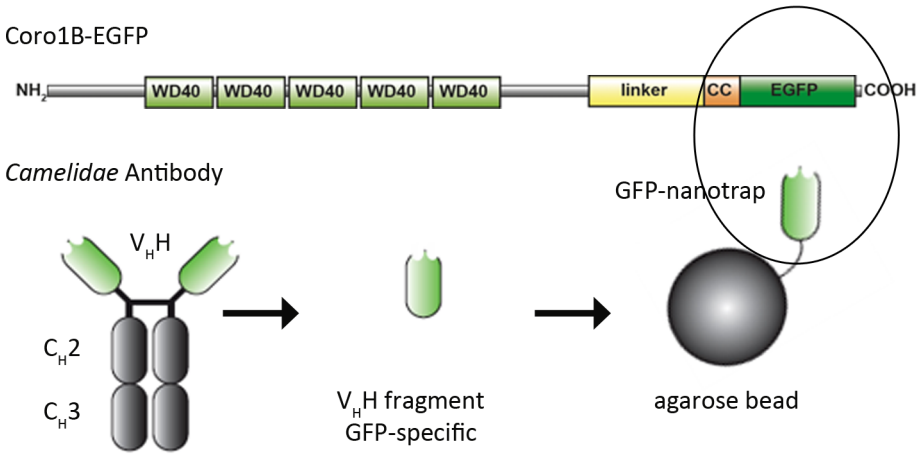

Figure 12. Schematic representation of pull-down with GFP-nanotrap technology
Modified from Rothbauer et al.[142].

HMEC-1 were cultured to 90-100% confluence. After washing with ice cold PBS, cells were treated with lysis buffer Berton II. Protease inhibitor (protease inhibitor cocktail 1:800 and 1 mM DFP 1:500) and phosphatase inhibitor (10 mM sodium fluoride 1:100 and 250 µm sodium orthovanadate 1:400) were freshly added to lysis buffer Berton II before treatment. Protein lysates were shaken for 30 minutes at 4 °C. Subsequently, protein lysates were sonicated and centrifuged for 10 minutes at 1600 x g and 4 °C. For input lysates 5% of the supernatant was used. GFP-trap agarose beads were equilibrated with dilution buffer and 2500 µg protein lysate was added to GFP-trap agarose beads and incubated for 2 hours at 4 °C. GFP-trap agarose beads were washed three times with 1 ml dilution buffer for 10 minutes before adding 100 µl 2x Lämmli-buffer. The appropriate amount of 2x Lämmli-buffer was also added to input samples before both samples (input and GFP-trap agarose beads) were boiled 10 minutes at 95 °C. In this step the GFP fusion protein and the

interacting proteins were separated from the GFP-trap agarose beads. Supernatant was used for western blot (12% separating and 4% stacking gel)[103].

To analyze samples with mass spectrometry, GFP-trap agarose beads were not suspended in 2x Lämmli-buffer. The iST sample preparation kit was used to prepare samples for mass spectrometry. Large scale proteomic analysis was conducted by the Core Facility Proteomics at the Biomedical Center, LMU Munich (Proteinanalytics (CF) Molecular Biology, head: Prof. Dr. Axel Imhof) using the mass spectrometer Q Exactive™ HF[103].

4.15 Immunofluorescence staining of cells

Immunofluorescence staining was performed on glass coverslips coated with 0.15% gelatine for 1 hour at 37 °C. Cells were seeded in various concentrations on coverslips and fixed after different time points. Before fixation, cells were washed once with PBS. Fixation was done using freshly diluted 4% formaldehyde in PBS for 10 minutes. Cells were permeabilized with 0.1% Triton X 100 in PBS for 30 minutes and incubated with blocking solution (1% bovine serum albumin (BSA), 0.1% Triton X 100 in PBS) for 1 hour at room temperature. Cells were incubated with primary antibodies diluted in blocking solution overnight at 4 °C. After three washes with PBS for 10 minutes, cells were incubated with appropriate secondary antibodies (diluted in blocking solution) for 2 hours at room temperature protected from light. Before mounting, cells were washed three times with PBS for 10 minutes. Coverslips were mounted with Fluoromount-G. Images were taken at the Core Facility Bioimaging of the Biomedical Center, LMU Munich (head: Dr. Steffen Dietzel) using a Leica SP8X WLL upright confocal microscope and lasers with an excitation wavelength of 405 nm, 488 nm and 561 nm[103].

4.16 Cell shape analysis

To analyze the shape of adherent cells, control or Coro1B knockdown HUVECs were seeded on coverslips coated with 0.15% gelatine and fixed after 6 hours with 4% formaldehyde (in PBS). Control or Coro1B knockdown cells were stained with the primary antibodies rabbit anti-human Coro1B and mouse anti-human Paxillin or with rabbit anti-human Coro1B and mouse anti-human VEcad as described in chapter 4.15. The secondary antibodies rabbit Alexa Fluor 488 and mouse Alexa Fluor 546 were used. F-actin was visualized with Phalloidin

Alexa Fluor 633. Images of 6 different fields of view of control or Coro1B knockdown cells were taken using the Leica SP8X WLL upright confocal microscope. The area of 50 cells per field of view was measured offline using ImageJ software. Additionally, the length and width of 50 control or Coro1B knockdown cells were determined. The cell elongation index was calculated by dividing cell length by cell width.

4.17 Cell proliferation assay

Coro1B knockdown or control cells were seeded on coverslips coated with 0.15% gelatine. Cells were fixed with 4% formaldehyde in PBS after 24 hours and stained for the proliferation marker rabbit anti-human phospho-Histone H3 and secondary antibody Alexa Fluor 488. The total number of cells was determined by immunofluorescence staining using DNA marker DAPI visualizing the cell nuclei. Images of 10 fields of view were taken with a 10x objective at a Leica DM2500 upright fluorescence microscope. The percentage of proliferating cells was calculated by dividing the total number of cells by the number of proliferating cells.

4.18 Cell apoptosis assay

Control or Coro1B knockdown HUVECs were seeded on coverslips coated with 0.15% gelatine and fixed with 4% formaldehyde (in PBS) after 12 hours. To detect apoptotic cells, cells with DNA strand breaks were visualized by using the APO-BrdU™ TUNEL assay kit following manufacturer's instruction. The total number of cells was determined as described in chapter 4.17. Images of 10 fields of view were taken with a 10x objective at a Leica DM2500 upright fluorescence microscope and percentage of apoptotic cells was calculated by dividing the total number of cells by the number of apoptotic cells.

4.19 Zebrafish husbandry and handling of embryos

Zebrafish husbandry and handling of embryos was conducted according to standard description by Mullins et al.[143]. All zebrafishes were bred in the Zebrafish Core Facility of the German Center for Neurodegenerative Diseases, LMU Munich (Zebrafish Models, head: Dr. Bettina Schmid). Embryos were kept at 28.5 °C in E3 medium. Developmental stages were identified according to Kimmel et al.[144].

4.20 Generation of a Coro1B knockout zebrafish by CRISPR / Cas9 genome editing

Coro1B knockout fishes were produced using the clustered regularly interspaced short palindromic repeats (CRISPR) / CRISPR-associated 9 (Cas9) technology. The CRISPR / Cas9 technology is characterized by induction of a double strand break through injection of a specific designed guideRNA (gRNA) together with the messengerRNA (mRNA) of the enzyme Cas9. The target sequence of the gRNA was designed in exon 3 of the *coro1B* gene using the ChopChop design tool (http://chopchop.cbu.uib.no/) (figure 13). Additionally, a proto-spacer adjacent motif (PAM) adjacent to the target site in the genome was added at the end, which allows a specific identification of the sequence required for Cas9 recruitment. The gRNA template was ordered from Integrated DNA technologies (IDT) as a single-strand oligonucleotide with a T7 polymerase binding site for *in vitro* transcription.

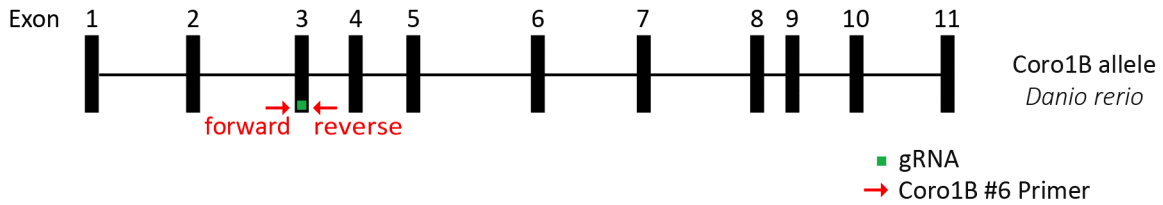

Figure 13. Genomic organization of the Coro1B gene with localization of gRNA and analytical primers
The red arrows show the specific Coro1B #6 forward and reverse primer. The green box shows the gRNA (Coro1B #6) in exon3.

To analyze whether the double strand break in exon 3 of the *coro1B* gene was successful, specific primers were designed flanking the target sequence of the gRNA (Coro1B #6 forward and Coro1B #6 reverse). The restriction enzyme (BtsCI) cutting within this sequence was chosen for restriction fragment length polymorphism (RFLP) analysis (figure 14).

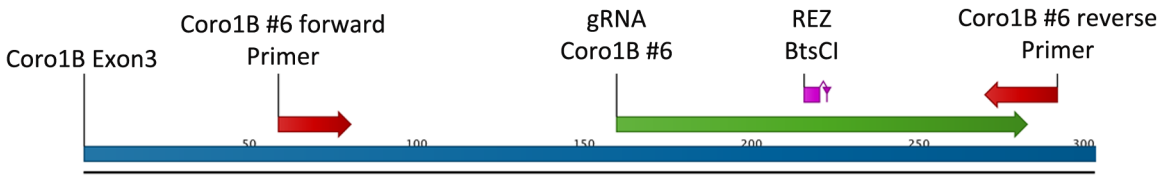

Figure 14. Schematic representation of exon 3 of the *coro1B* gene
The red arrows show the specific Coro1B #6 forward and reverse primer. The gRNA Coro1B #6 is shown in green. Recognition site of the enzyme BtsCI used for RFLP analysis is depicted in magenta.

4.21 Mating of adult zebrafishes

Female and male zebrafishes were placed in pairs in mating boxes in the afternoon. To control the mating, a separator was positioned between them and removed the following morning. The controlled mating was necessary, so that freshly spawned eggs at one cell stage could be used for microinjection.

4.22 Microinjection into zebrafish eggs

For microinjection eggs were transferred to a plate with specific molds containing 1.5% agar with E3 medium. These molds allowed to place and fix the eggs in the right position for injection. The crRNA was obtained by *in vitro* transcription using MEGAshortscript T7 Transcription Kit according to manufacturer's protocol. To prepare the single gRNA, the designed short crRNA sequence was fused to the scaffold trans-activating crRNA (tracrRNA) by diluting 2 µg / µl crRNA and 600 ng / µl tracrRNA in nuclease free duplex buffer. Additionally, Cas9 mRNA was diluted 1:20 in Cas9 reaction buffer containing 200 mM HEPES, 1000 mM NaCl, 50 mM $MgCl_2$, 1 mM EDTA in nuclease free water. The formed crRNA:tracrRNA complex (single-gRNA) was mixed 1:1 with the Cas9 mRNA and injected directly into the cell during early 1-cell stage. After injection, the eggs were stored at 28.5 °C in E3 medium. After 6 hours, normal development of the egg were screened and unfertilized eggs were eliminated.

4.23 Lysis of zebrafish embryos for sequence analysis

For sequence analysis, 20 injected fish were fixed 1 day post fertilization (dpf) in 100% methanol. Single embryos were transferred to PCR tubes. Methanol was completely removed and fully evaporated before lysis buffer containing 45 µl tris-EDTA buffer and 5 µl proteinase-K was added. Embryos were lysed for 2 hours at 55 °C. Subsequently, proteinase-K was deactivated for 10 minutes at 95 °C.

4.24 PCR and restriction fragment length polymorphism analysis

To determine genomic modifications upon CRIPSR / Cas9 genome editing, lysates were analyzed by RFLP analysis[145]. First, PCR was performed by using GoTaq G2 polymerase (table 2) and specially designed primers Coro1B #6 forward and Coro1B #6 reverse. The PCR

protocol included an initial denaturation step at 94 °C for 2 minutes, followed by 35 cycles of 30 seconds at 94 °C (denaturation), 30 seconds at the annealing temperature of the primers (hybridization), 30 seconds at 72 °C (extension) and a final extension step of 10 minutes 72 °C. In all performed PCR reactions, an annealing temperature of 69 °C was used. For RFLP analysis 10 µl of the PCR product was used. The digest with the restriction enzyme BtsCI was performed for 2 hours at the temperature of 55 °C, which was recommended by the manufacturer's instruction. To evaluate the success of the genomic modification, digested DNA fragments were separated by size utilizing agarose gel electrophoresis and visualized with midori green and UV light. As a size standard, a 100 bp DNA ladder was run on the same gel. Successful genome editing modified the restriction enzyme recognition site. Thereby, a part of the PCR product remains undigested upon gRNA / Cas9 injection due to a mutated target site. To further identify the different modifications, PCR products were Sanger sequenced by Eurofins Genomics.

Table 2. PCR components to genotype injected zebrafish

Components	**Final concentration**
GoTaq G2 Polymerase	0.2 µl
PCR Mix	15 µl
Forward primer (10 µm)	0.5 µl
Reverse primer (10 µm)	0.5 µl
Template DNA	2 µl of lysate

4.25 Bleaching of fertilized zebrafish eggs

To avoid contamination in the zebrafish facility, remaining injected fish were bleached with hydrogen peroxide (H_2O_2) diluted 1:2500 in tap water at 1 dpf. Fish were exposed to bleaching solution for 5 minutes, followed by washing in tap water for 5 minutes. Bleaching and washing steps were repeated one more time prior transferring the embryos to a new petri dish with 10 ml E3 medium. To remove denatured chorion 10 µl pronase (stock solution) was supplemented.

4.26 Fin biopsies from adult zebrafish

The genotyping of single adult fish was performed by taking fin biopsies. Adult fish were anesthetized in water containing 5-10% tricaine stock solution. A small biopsy from the tail fin (2-3 mm) was taken by resection with a scalpel, tissue was fixed in methanol and lysed as described for the eggs at 1 dpf.

4.27 Screen for inherited genome modifications

To generate a Coro1B knockout fish strain, embryos tested for genome editing were raised to adulthood (P0). Genome modified fish were identified by fin biopsies and crossed to wild type fish. The offspring (F1) was checked for germ line transmission by RFLP analysis. Siblings of positively tested offspring were raised to adulthood. Different mutations were identified by fin biopsies in the F1 fish. Fish with single type of mutation were crossed to wild type fish to generate a stable heterozygous fish strain (F2). To generate a stable homozygous fish line, heterozygous F2 fish were crossed to heterozygous fish with the same mutation. Offspring (F3) was analyzed for homozygous mutations by Sanger sequence analysis (figure 15).

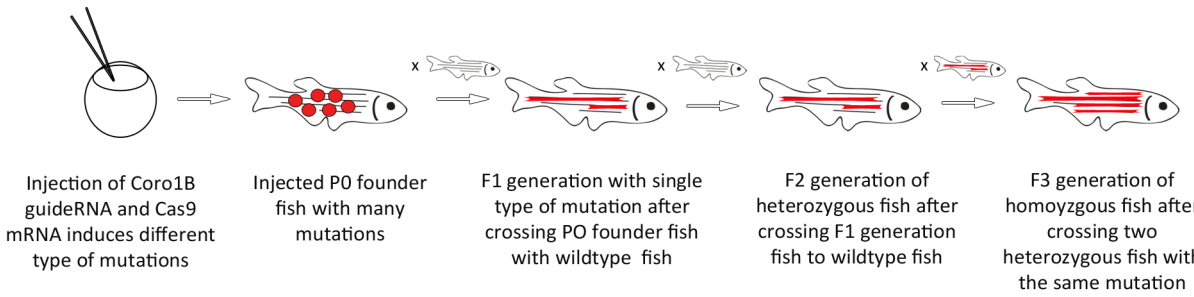

Figure 15. Schematic representation of generation of homozygous knockout fish

4.28 Lysis of zebrafish samples for western blot analysis

Fish at 4 dpf were euthanized with tricaine and shock frozen in liquid nitrogen for protein analysis. Single fish were transferred to a fresh micro centrifuge tube and medium was completely removed before 40 µl of 2x Lämmli-buffer were added. A tissue homogenizer was used to homogenize the embryos. Samples were used immediately or stored at -20 °C. Then, the samples were boiled for 5 minutes at 95 °C and centrifuged at 1600 x g for 10

minutes and finally loaded. The equivalent volume of one embryo of the supernatant was used per lane for SDS-PAGE.

4.29 Statistical analysis

Data represent mean ± standard deviation (SD). A minimum of three independent experiments was performed. Statistical analysis was conducted using GraphPad Prism 6. For pairwise comparison, the Student t-test, and for multiple comparisons, one-way ANOVA with the Dunnett's method was applied. P-values lower than 0.05 (*), 0.01 (**), 0.001 (***) or 0.0001 (****) were considered significant[103].

To statistically analyze the data of the mass spectrometry, iBAQ values as reported by MaxQuant were processed using the bio conductor DEP library (version 1.6.0) as follows: control proteins and contaminates were removed[146]. Intensity values were normalized using variance-stabilizing transformation. Missing values were imputed using the manual method in DEP function 'impute' with shift = 1.8 and scale = 0.3. Protein-wise robust enrichment was estimated using linear models and empirical Bayes statistics using limma implemented in the 'test_diff' function of DEP. The model formula included the experimental batch (replicate number) as random effect. Significant enrichment was determined by a false discovery rate (FDR) < 5%. The statistical analysis of the mass spectrometry data was done with help of the Core Facility Bioinformatics at the Biomedical Center, LMU Munich (Bioinformatics Core Unit, head: Dr. Tobias Straub).

5. Results

5.1 ECs expressed Coro1B and Coro1C

Mammalian cells express three isoforms of type I coronins namely Coro1A, Coro1B and Coro1C. Whereas Coro1A is predominantly expressed in hematopoietic cells and not present in ECs, Coro1B and Coro1C are expressed in ECs[107,128]. The expression of type I coronins in ECs was proved by western blot analysis utilizing specific antibodies against Coro1B and GAPDH as loading control. To show that Coro1B is expressed in different type of ECs, protein lysates of primary ECs (HUVECs) and a stable EC line (HMEC-1) were used. As expected, Coro1A (figure 16A) was not expressed in ECs. To verify the functionality of the Coro1A antibody, a protein lysate of differentiated neutrophil-like Hoxb8 cells was used as a positive control. However, Coro1B and Coro1C were detectable in both types of ECs (figure 16B and 16C).

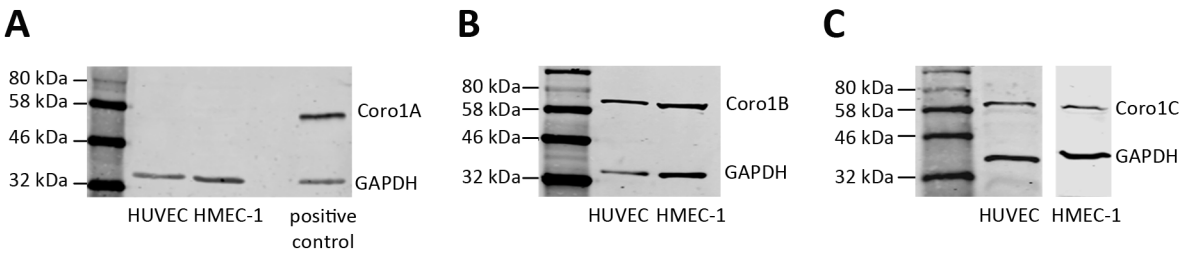

Figure 16. ECs express Coro1B and Coro1C
Western blot analysis of protein lysates from HUVECs and HMEC-1 showed no Coro1A (A) expression. As a positive control a protein lysate of differentiated neutrophil-like Hoxb8 cells was used. Western blot analysis of protein lysates from HUVECs and HMEC-1 revealed Coro1B (B) and Coro1C (C) expression. GAPDH was utilized as loading control. Shown western blots are representative images of three independent experiments.

5.2 Coro1B localized at lamellipodia and cell-cell junctions in ECs

Next, the subcellular localization of Coro1B was analyzed in different types of ECs including HUVECs, HMEC-1 and mECs. To this end, ECs were cultured on gelatine-coated coverslips and exposed to specific primary antibodies for Coro1B and for the cell-cell junction marker VEcad and afterwards to secondary antibodies labeled with fluorophores. It is known that Coro1B localized at the periphery of ECs under confluent conditions[128,129]. As expected, Coro1B was demonstrated to be at the leading edge of lamellipodia in human and in mECs using confocal microscopy (figure 17). Unexpectedly and similar to VEcad, Coro1B was localized at cell-cell junctions in all types of used ECs (figure 17)[103].

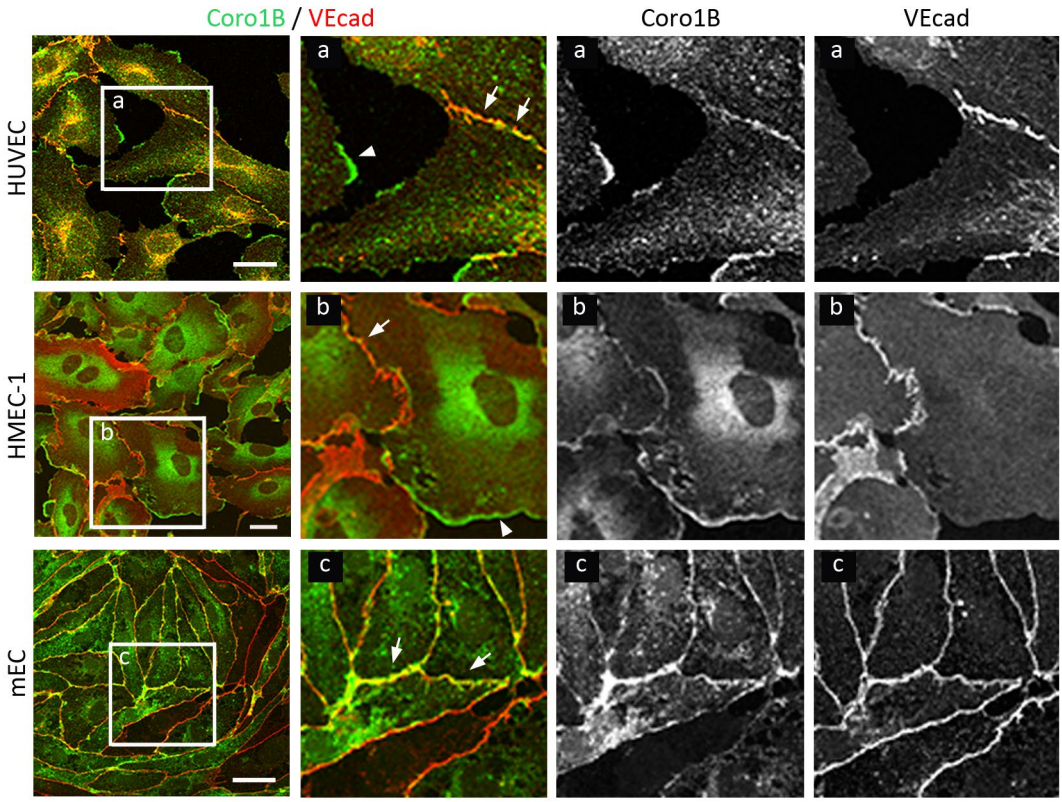

Figure 17. Coro1B localized at lamellipodia and cell-cell junctions in ECs
HUVECs, HMEC-1 and mECs were stained for Coro1B (green) and VEcad (red). First column and second column show merged images. Second to fourth columns show magnification of section a, b and c. In the third and fourth columns single color images are displayed. Coro1B localized to lamellipodia (arrowheads) and cell-cell junctions (arrows). Scale bar = 25 µm (modified from Werner et al.[103]).

5.2.1 Coro1B localized at the leading edge of JAIL together with F-actin

To examine if Coro1B associates with F-actin at cell-cell junctions, subconfluent HUVEC monolayers were immunostained for Coro1B and VEcad using specific primary antibodies. F-actin was visualized using Phalloidin[103]. Under physiological conditions *in vivo* or in confluent cells VEcad is enriched at cell-cell junctions and show a linear distribution, whereas a discontinuous pattern predominantly occurs in subconfluent cells[81,147]. Using confocal microscopy, immunofluorescence staining of HUVECs for VEcad showed a discontinuous cell-cell junction with locally reduced VEcad, which is characteristic for a JAIL (figure 18, magnification a). JAIL is part of the dynamic regulation of cell–cell junctions by regulating local VEcad dynamics[102,103]. Thereby they form new VEcad adhesion sites to establish new AJs[81]. At VEcad free gaps, JAIL appear from branched actin filament formation and protrude over a small region of the apical membrane of the neighboring cell[102]. In regions where

HUVECs grow subconfluent, JAIL with a large area were reported[148]. Immunofluorescence staining showed the presence of JAIL and Coro1B localization at the leading edge of a JAIL where it colocalized with F-actin (figure 18)[103].

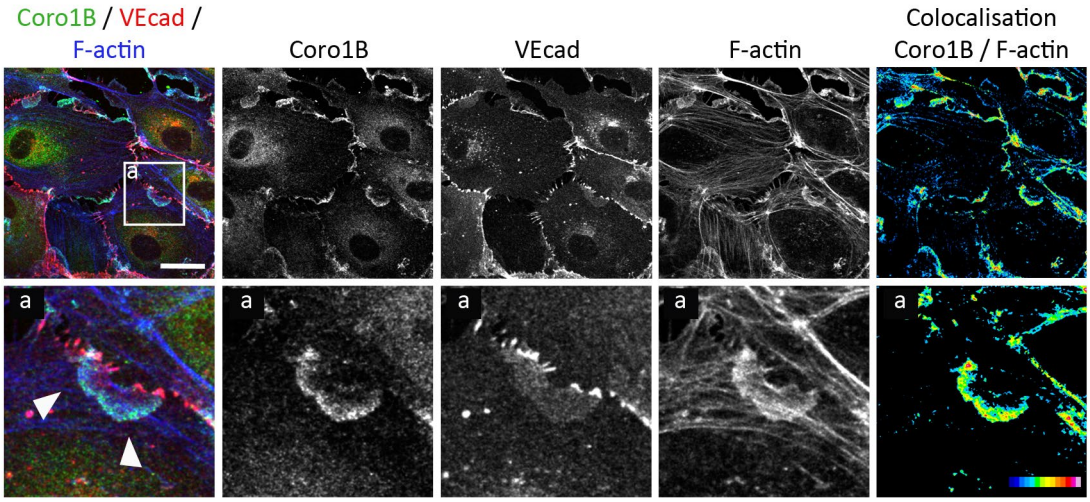

Figure 18. Coro1B localized at the leading edge of JAIL together with F-actin
Subconfluent HUVECs were stained for Coro1B (green) and VEcad (red). F-actin was visualized with Phalloidin (blue). Overview images are shown in the upper panel. Lower panel shows magnification of section a. First column shows merged images. Columns 2-4 show split channels. Colocalization between Coro1B and F-actin is demonstrated as a heat map (fifth column). Black indicates no colocalization, white indicates the highest amount of colocalization. Arrowheads point to colocalization of Coro1B and F-actin at the leading edge of JAIL. Scale bar = 25 µm (modified from Werner et al.[103]).

Similar to subconfluent monolayers the presence of JAIL has been reported in confluent cells as the natural state of ECs *in vivo* is that of a confluent resting monolayer[86]. HUVECs were grown to confluence and JAIL were visualized by immunofluorescence staining with specific primary antibodies against Coro1B and VEcad. To visualize F-actin Phalloidin was used. In contrast to subconfluent cells, the size of a JAIL in confluent cells is smaller[148]. Confocal images of confluent HUVECs showed that Coro1B also colocalized with F-actin at the leading edge of JAIL (figure 19).

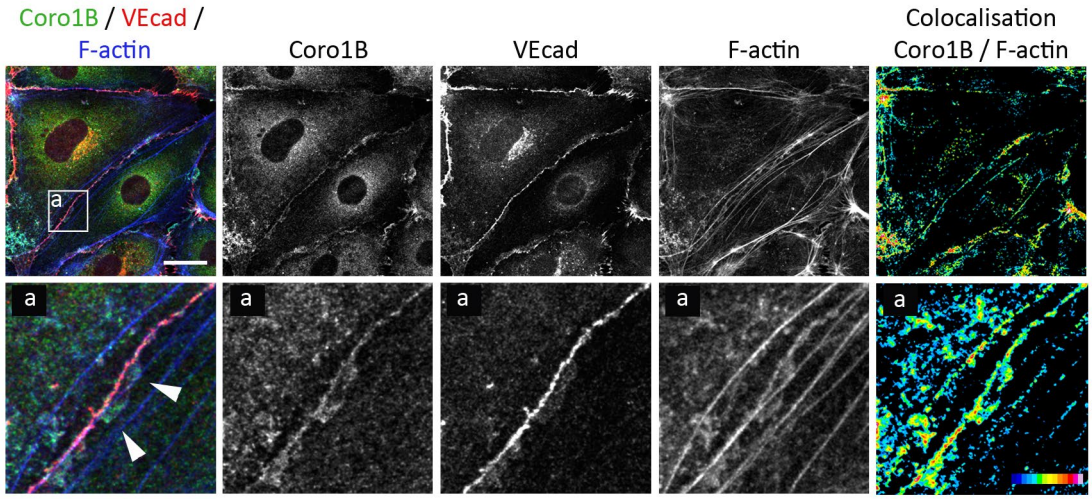

Figure 19. Coro1B localized at the leading edge of JAIL in confluent cells
Confluent HUVECs were stained for Coro1B (green) and VEcad (red). F-actin was visualized with Phalloidin (blue). Overview images are shown in the upper panel. Lower panel displays magnification of section a. First column shows merged images. Columns 2-4 show single color images. Colocalization between Coro1B and F-actin is displayed in a heat map (fifth column). Black indicates no colocalization, white indicates the highest amount of colocalization. Coro1B and F-actin colocalized at the leading edge of JAIL (arrowheads). Scale bar = 25 µm.

5.2.2 Coro1B colocalized with F-actin at cell-cell junctions

To analyze the spatio-temporal localization of Coro1B during JAIL formation, an EGFP tagged Coro1B was generated. To evaluate whether the EGFP tagged Coro1B localizes properly, the Coro1B-EGFP construct was transfected into HUVECs, HMEC-1 and fibroblasts. Immunofluorescence staining with a primary antibody against Coro1B was performed. Analysis of confocal images revealed that the Coro1B-EGFP colocalized with cell intrinsic Coro1B at lamellipodia of ECs and fibroblasts (figure 20).

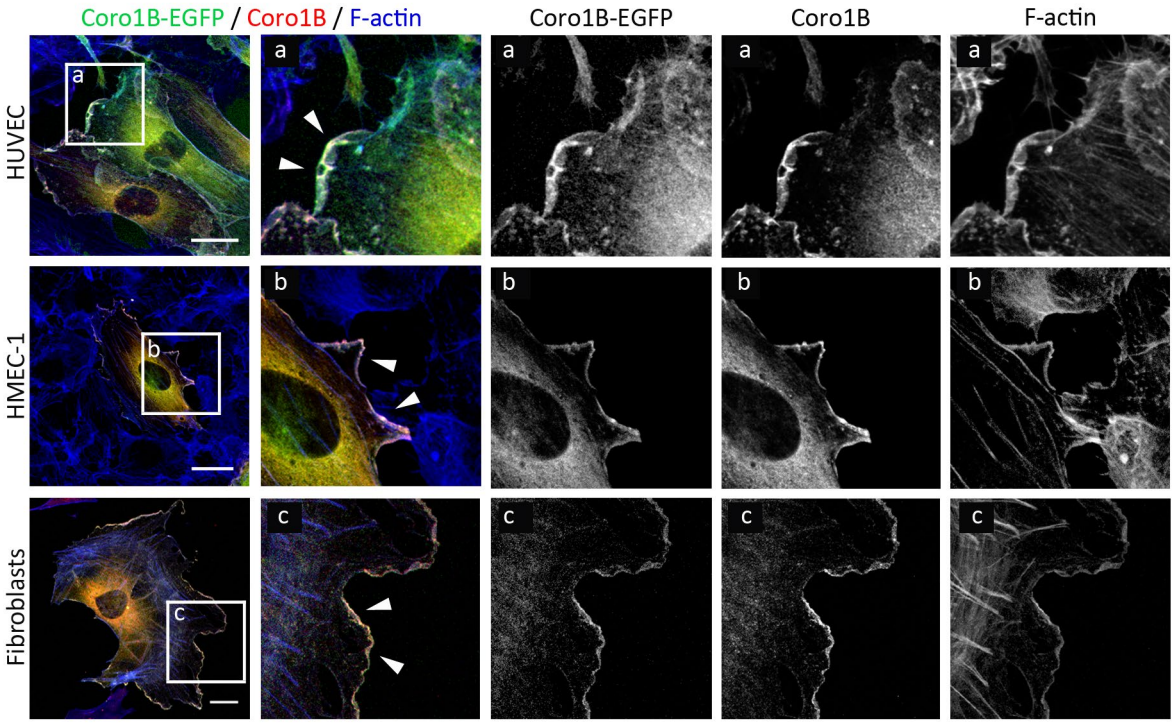

Figure 20. The generated Coro1B-EGFP construct proper colocalized with endogenous Coro1B at lamellipodia of ECs and fibroblasts

Coro1B-EGFP (green) was transfected into HUVECs, HMEC-1 and fibroblasts. Cells were stained with a specific antibody for Coro1B (red). F-actin was visualized using Phalloidin (blue). First column shows merged images. Second to fifth columns show magnification of section a, b and c. In the second column merged images of the magnification were shown. Third to fifth columns display single color images. Scale bar = 25 µm.

To assess the dynamics of Coro1B during JAIL formation, HUVECs expressing Coro1B-EGFP and VEcad-mCherry were analyzed using live-cell imaging with spinning disk confocal microscopy[103]. Live imaging was conducted in collaboration with the Institute of Anatomy and Vascular Biology, University of Münster (Director: Prof. Dr. Hans Schnittler). Still images of the video were generated to analyze the recruitment of Coro1B in relation to JAIL formation in more detail (figure 21). At the beginning of JAIL formation (time 0), VEcad-mCherry was distributed continuously between cell-cell borders of two ECs (figure 21A). After 20 seconds, a JAIL was formed and a local reduction of VEcad-mCherry combined with an enrichment of Coro1B-EGFP at the leading edge of the JAIL was observed. After 60 seconds, Coro1B-EGFP was still present at the leading edge of the JAIL and a VEcad-mCherry plaque formed as a consequence of JAIL that overlap bordering cells inducing VEcad transactions in this zone[103]. After 80 seconds, Coro1B-EGFP protrusion regressed and after 100 seconds the original continuous distribution of VEcad-mCherry along the plasma

membrane was recovered (figure 21A)[103]. Live-cell imaging demonstrated the formation and regression of JAIL within 100 seconds. This fast-live cycle showed that AJs are not static but highly dynamic structures that form JAIL. Still images in figure 21B illustrated the movement and the dynamic of the cell-cell junction within 20 minutes.

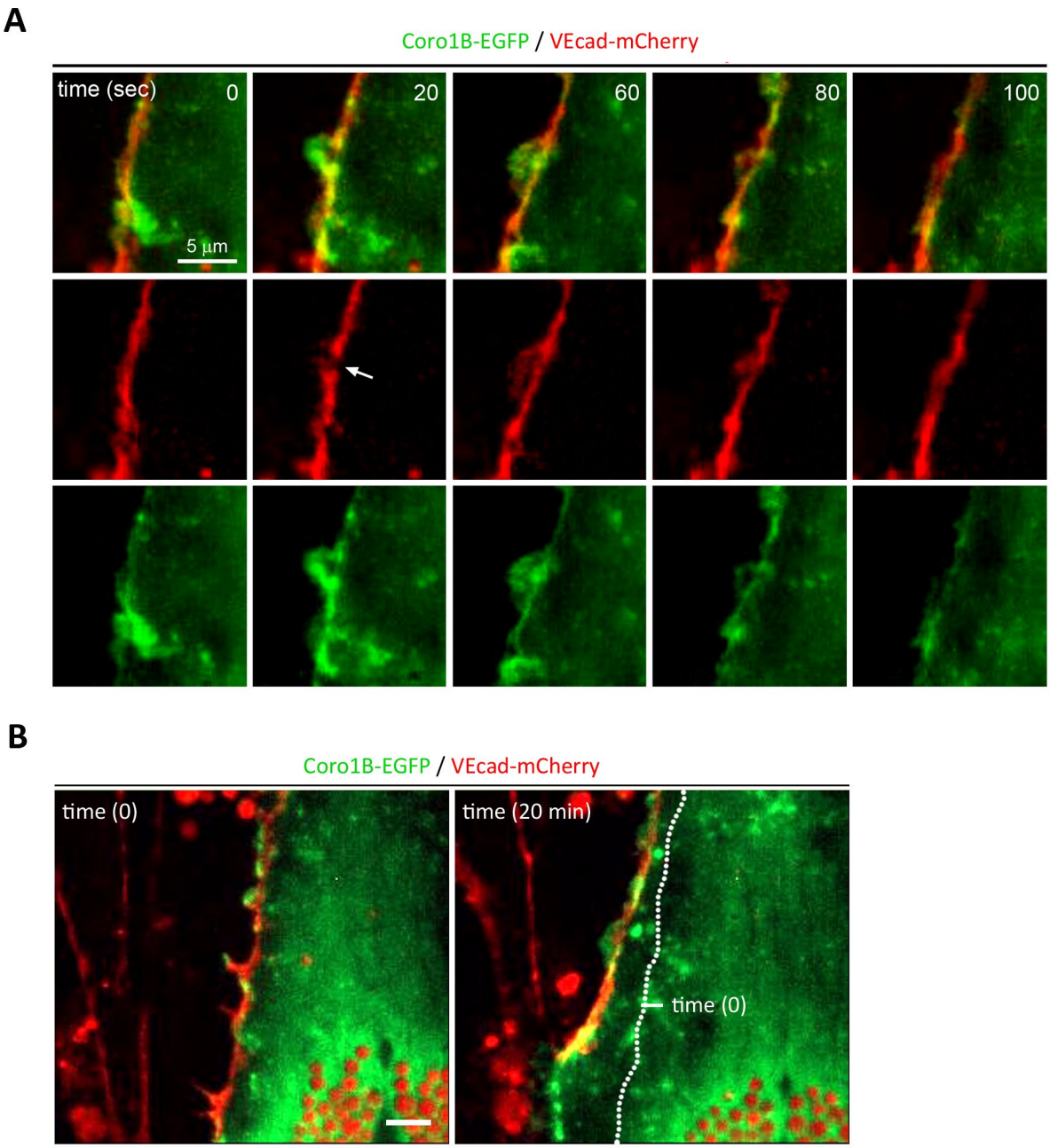

Figure 21. Coro1B-EGFP localized at the leading edge of a JAIL accompanied by local reduction of VEcad
HUVECs were transfected with Coro1B-EGFP (green) and VEcad-mCherry (red). (A) Representative still images at indicated time points. Upper panel shows merged images. Middle and lower panels show single color images. Arrow points to local reduction of VEcad at time point 20 sec. Scale bar = 5 µm. (B) Merged images show the movement of the cell-cell junction within 20 minutes. Scale bar = 10 µm (modified from Werner et al.[103]).

Since immunofluorescence staining showed a colocalization of Coro1B and F-actin at the leading edge of JAIL, the dynamic behavior of Coro1B and F-actin during JAIL formation was investigated. To this end, HUVECs that expressed Coro1B-EGFP and Lifeact-mCherry, a well-known method to visualize F-actin in living cells, were analyzed using live-cell imaging[103,149]. Spinning disc confocal microscopy images revealed a constant recruitment of Coro1B to the leading edge of lamellipodia and JAIL[103]. Still images of the generated video demonstrated the localization of Coro1B-EGFP at the leading edge of JAIL, where it colocalized with F-actin during the whole process of JAIL dynamics (figure 22)[103].

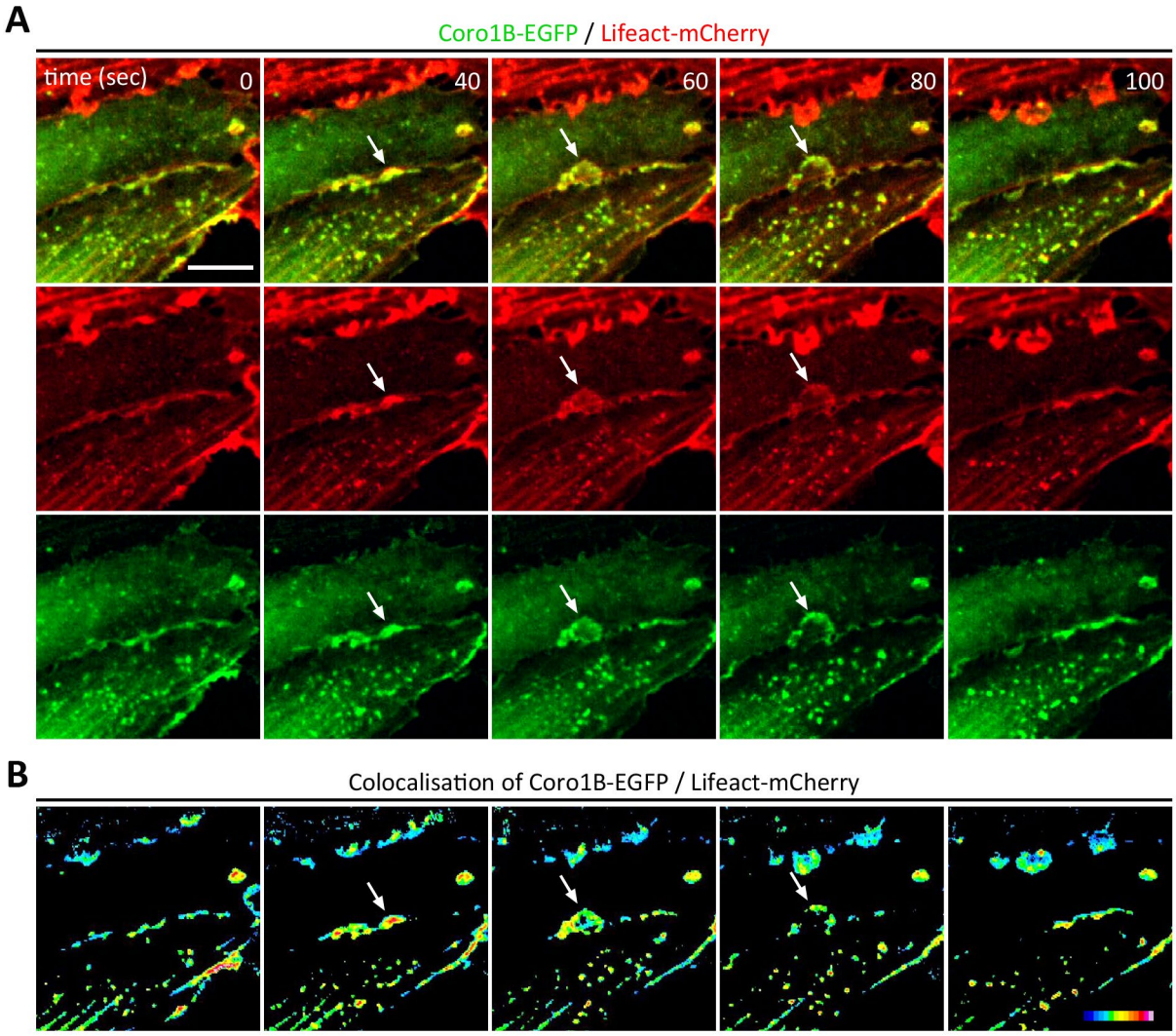

Figure 22. Colocalization of Coro1B-EGFP and F-actin at the leading edge of JAIL
Coro1B-EGFP (green) and Lifeact-mCherry (red) were transfected into HUVECs. (A) Representative still images at indicated time points. Upper panel shows merged images, two panels below show single color images. (B) Colocalization is displayed in a heat map (lowest panel). Black indicates no colocalization, white indicates the highest amount of colocalization. Arrows point to Coro1B-EGFP and F-actin at the leading edge of JAIL. Scale bar = 10 µm (modified from Werner et al.[103]).

To test whether the localization of Coro1B at cell-cell junctions is an actin-dependent process, the actin cytoskeleton was manipulated. RhoA and Rac1, two members of the group of small GTPases, antagonize each other to control cell migration and lamellipodia formation[75,78]. Whereas Rac1 stimulates actin polymerization and lamellipodia formation, activation of RhoA enhances the formation of stress fibers[79]. HUVECs were stimulated with the Rho activator thrombin, which results in the inhibition of lamellipodia formation and in an increase in stress fibers formation[78]. As expected, visualization of F-actin showed a disorganized actin cytoskeleton upon treatment with the proinflammatory mediator thrombin and the formation of stress fibers (figure 23A). Additionally, it is known that thrombin causes VEcad remodeling and thereby an increase in endothelial permeability by inducing a dissociation of p120 from VEcad[81,150]. In contrast to untreated cells, staining for VEcad revealed the described heterogeneous and partly discontinuous VEcad pattern after stimulation with thrombin. Staining revealed that the formation of JAIL was decreased in thrombin-stimulated cells. Interestingly, after stimulation with thrombin a more cytoplasmic distribution of Coro1B were observed (figure 23A). Quantitative analysis revealed that the number of JAIL per 10 µm cell-cell junction was significantly reduced after stimulation with thrombin (figure 23B)[103].

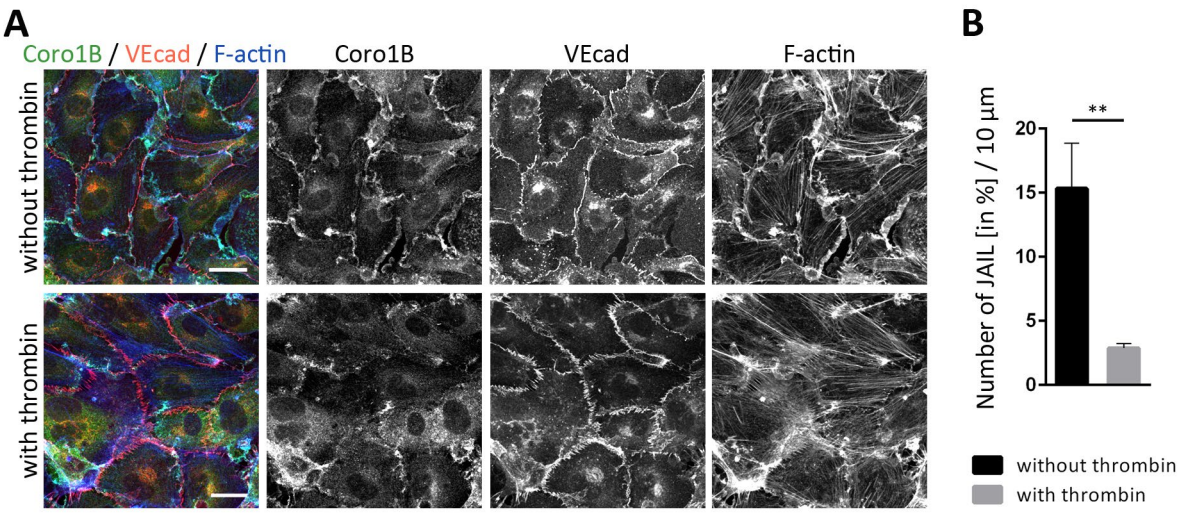

Figure 23. Thrombin stimulation revealed that Coro1B localization at cell-cell junctions was actin-dependent
(A) HUVECs were stimulated with thrombin (10 minutes, 0.2 U / ml, lower panel). As control unstimulated cells were used (upper panel). Staining for Coro1B (green) and VEcad (red) was performed. F-actin was visualized using Phalloidin. Merged images are illustrated in the first column, single color images in columns 2-4. Scale bar = 25 µm. Images are representative images of three independent experiments. (B) Quantification of number of JAIL per 10 µm in % in HUVECs without and with thrombin stimulation. Data represent mean ± SD. ** $P < 0.01$. n = 3 (10 FOV / sample) (modified from Werner et al.[103]).

To confirm that the localization of Coro1B at cell-cell junctions is actin-dependent, HUVECs were stimulated with the ROCK inhibitor Y-27632[151]. RhoA activates ROCK that inhibits cofilin activity resulting in actin cytoskeleton contraction[152]. The inhibition of ROCK leads to reduced stress fibers formation and also JAIL formation was increased in Y-27632 stimulated cells (figure 24A). Quantitative analysis showed that the number of JAIL per 10 µm cell-cell junction was significantly increased in HUVECs with Y-27632 stimulation compared to cells without Y-27632 stimulation (figure 24B)[103]. These findings suggest that actin influences Coro1B localization at the cell-cell junction.

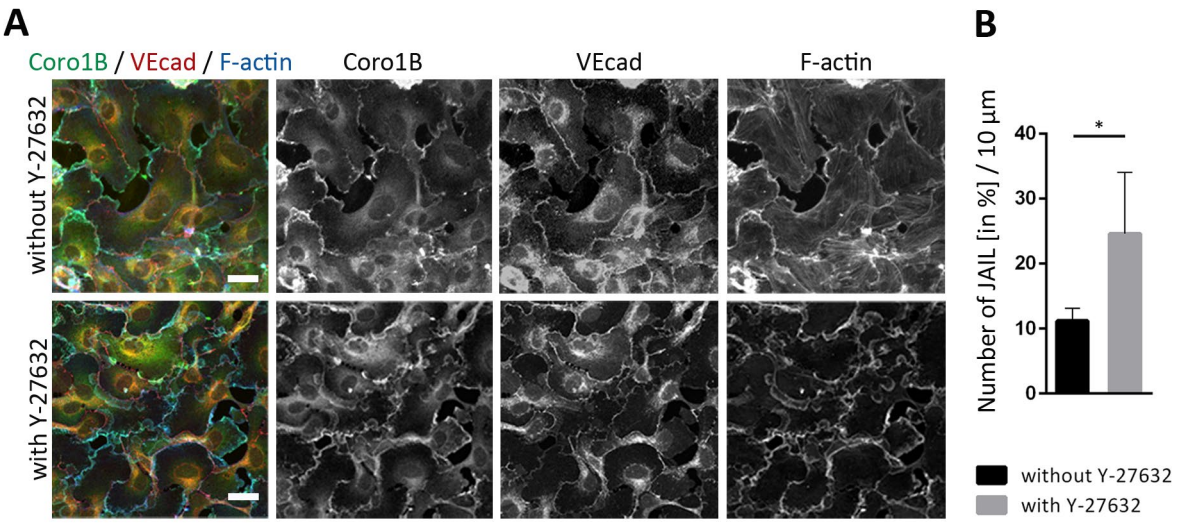

Figure 24. Y-27632 stimulation confirmed that Coro1B localization at cell-cell junctions is actin-dependent
(A) HUVECs were stimulated with Y-27632 (10 minutes, 10 µm). Unstimulated cells were used as a control. Staining for Coro1B (green) and VEcad (red) was performed. F-actin was visualized using Phalloidin. Merged images are displayed in the first column, single color images in columns 2-4. Scale bar = 25 µm. Shown images are representative images of three independent experiments. (B) Quantification of number of JAIL per 10 µm in % in HUVECs without and with Y-27632 stimulation. Data represent mean ± SD. * $P < 0.05$. n = 3 (10 FOV / sample) (modified from Werner et al.[103]).

To further verify that Coro1B localizes at sites of actin polymerization, reticular domains of AJs, which contain low levels of actin, were investigated[98]. Besides linear or discontinuous AJs, ECs have reticular AJs, which appear in areas of quiescent ECs where neighboring cells with low mechanical tension overlap. Characteristic for reticular AJs is their polygonal distribution of VEcad[100]. F-actin is absent within reticular AJs and is only enriched at their leading edges[98]. Immunofluorescence staining of HUVECs with specific primary antibodies against Coro1B and VEcad displayed the appearance of reticular AJs. F-actin was visualized using Phalloidin. The analysis showed that Coro1B localized in reticular AJs at the site of

actin polymerization, which is indicated by white arrowheads (figure 25). Coro1B is enriched at sites of F-actin dynamics and rather absent in areas where the cell is static.

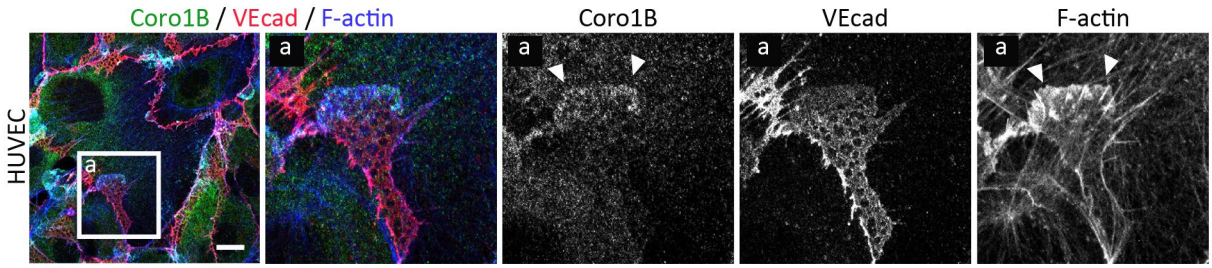

Figure 25. Coro1B localized to reticular AJs
HUVECs were stained for Coro1B (green) and VEcad (red). F-actin (blue) was visualized by using Phalloidin. First and second column show merged images. Columns 2-5 are the magnification of section a. Columns 3-5 display single stainings. Arrowheads point to enrichment of Coro1B at sites of actin polymerization. Scale bar = 25 µm. Shown images are representative images of three independent experiments.

5.3 Role of Coro1B in EC adhesion, migration, and monolayer formation *in vitro*

5.3.1 Downregulation of Coro1B in HUVECs

To analyze the role of Coro1B on EC adhesion, migration, and monolayer formation *in vitro,* Coro1B was downregulated in ECs using two different siRNAs against Coro1B. A scrambled siRNA was used as control. Downregulation of Coro1B expression was confirmed by western blot analysis 72 hours post transfection (figure 26A). Quantitative assessment showed that a reduction in Coro1B expression of 85.24% was achieved in EC in which Coro1B was downregulated by siRNA #1 and a reduction of Coro1B expression of 86.76% when treated by siRNA #2 (figure 26B)[103]. Downregulation of Coro1B was confirmed by immunofluorescence staining of HUVECs treated with scrambled siRNA (control) or treated with Coro1B siRNA #1 or #2 with specific primary antibodies against Coro1B and VEcad (figure 26C). The relative number of Coro1B expressing cells was calculated by comparing the total number of cells (visualized by VEcad) to the number of Coro1B positive cells in 10 FOV / sample (figure 26C). Quantitative analysis revealed that Coro1B expression was absent in around 84% of ECs treated with Coro1B siRNA #1 or siRNA #2 (figure 26C). The remaining 16% of transfected cells still expressed Coro1B. Thus, treatment with Coro1B siRNA did not lead to a reduction of Coro1B expression in all cells, but Coro1B expression was rather absent in the majority of transfected ECs.

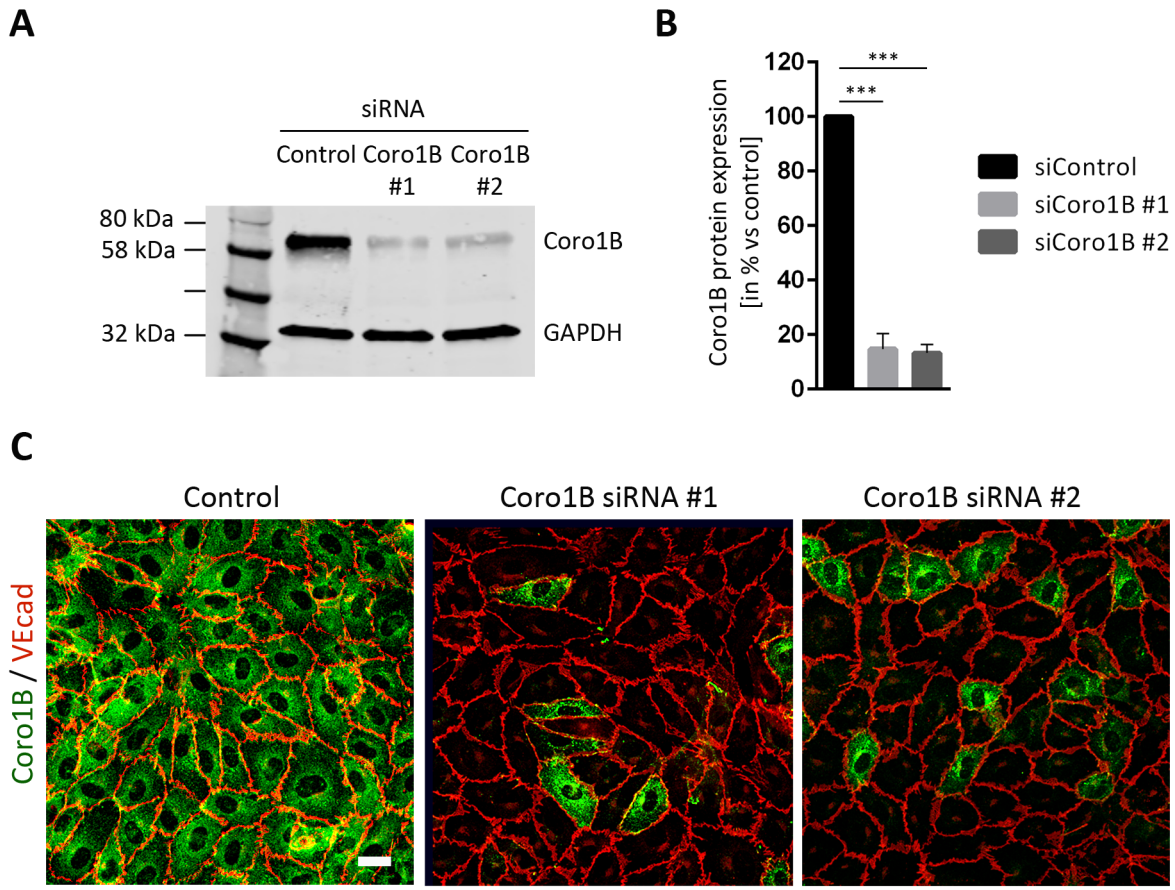

Figure 26. Knockdown of Coro1B in HUVECs using specific siRNA

(A) Western blot analysis showed reduced expression of Coro1B in cells treated with scrambled siRNA (control), Coro1B siRNA #1 or siRNA #2. GAPDH was used as a loading control. (B) Quantification of residual Coro1B protein expression normalized to control cells treated with scrambled siRNA (100%) of Coro1B siRNA #1 or #2 treated HUVECs. Data represent mean ± SD. *** $P < 0.001$. $n = 3$. (C) Representative fluorescent images of control HUVECs treated with scrambled siRNA and Coro1B knockdown cells treated with Coro1B siRNA #1 or #2 were stained for Coro1B (green) and VEcad (red). Scale bar = 25 µm. Stainings are representative images of three independent experiments (modified from Werner et al.[103]).

Western blot analysis also revealed that downregulation of Coro1B led to upregulation of Coro1C expression. Coro1C expression was increased by 2.5 fold in HUVECs treated with Coro1B siRNA #1 and increased by 2.2 fold in cells transfected with Coro1B siRNA #2 in comparison to control HUVECs treated with a scrambled siRNA (figure 27).

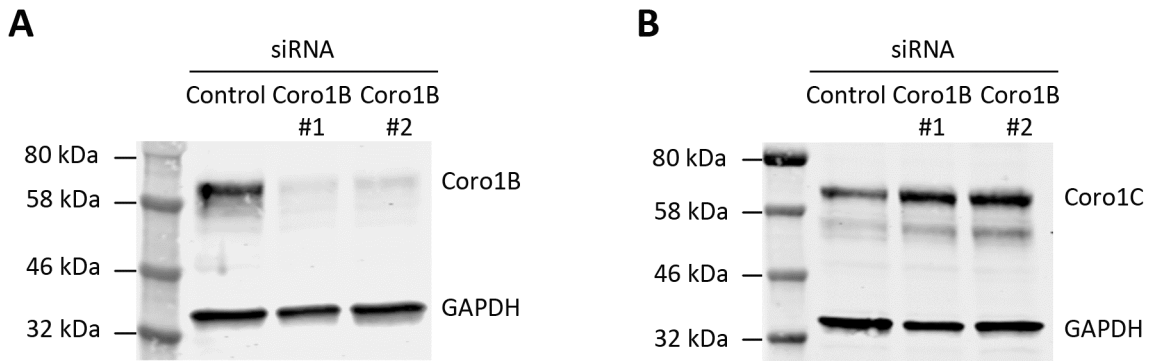

Figure 27. Knockdown of Coro1B in HUVEC resulted in upregulation of Coro1C
(A) Western blot analysis of protein lysates of control cells treated with scrambled siRNA and Coro1B knockdown cells treated with Coro1B siRNA #1 or #2 showed reduced Coro1B expression in Coro1B knockdown cells. (B) Western blot analysis with the same protein lysates demonstrated an upregulation of Coro1C expression in cells treated with Coro1B siRNA #1 or Coro1B siRNA #2 compared to cells treated with scrambled siRNA. GAPDH was used as a loading control. Shown western blots are representative images of three independent experiments.

5.3.2 Knockdown of Coro1B did not alter EC morphology

The impact of reduced Coro1B expression on the morphology of ECs was determined by analyzing the shape of control and Coro1B knockdown cells (HUVECs). 72 hours post transfection Coro1B knockdown cells (treated with Coro1B siRNA #1 or Coro1B siRNA #2) and control cells (treated with scrambled siRNA) were allowed to adhere and spread on gelatine-coated coverslips for 6 hours and subsequently stained for Coro1B and F-actin. Immunofluorescence staining showed no obvious difference in shape and morphology (figure 28A). The area and elongation index (cell length / width) of the cells were determined to measure EC morphology in detail. Quantitative analysis revealed no difference in both parameters between Coro1B knockdown and control HUVECs, indicating that Coro1B had no impact on EC morphology (figure 28B).

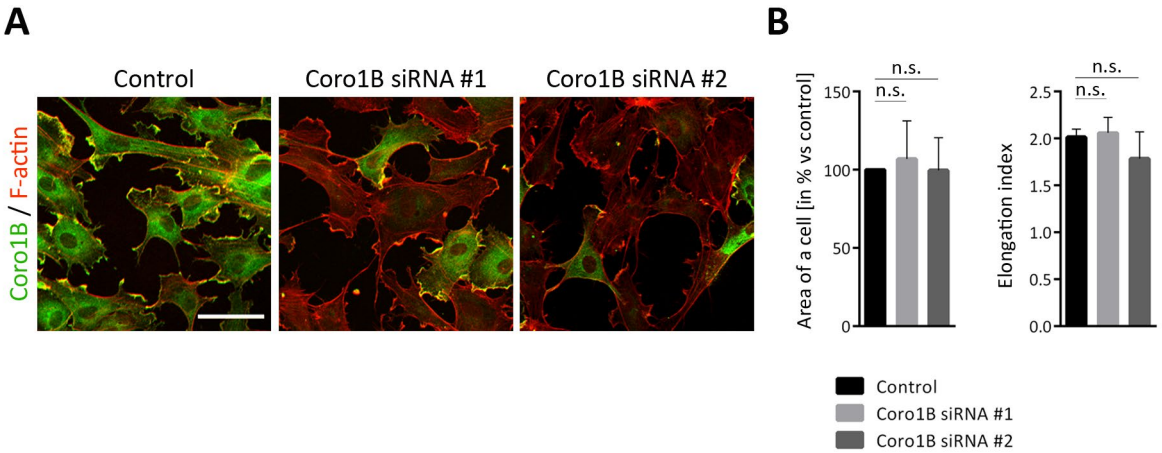

Figure 28. Cell morphology upon knockdown of Coro1B
(A) Representative immunofluorescence images of control HUVECs treated with scrambled siRNA and HUVECs treated with Coro1B siRNA #1 or siRNA #2 stained for Coro1B (green). F-actin was visualized using Phalloidin (red). Scale bar = 50 µm. (B) Quantification of the area of a cell in % normalized to control cells treated with scrambled siRNA (100%) and the elongation index (cell length / width) of a cell. Data represent mean ± SD. n.s. not significant. n = 3 (50 FOV / sample).

5.3.3 Coro1B regulated actin cytoskeleton organization and cell-cell junction morphology

To evaluate the influence of diminished Coro1B expression on actin cytoskeleton organization and cell-cell junction morphology, control HUVECs treated with scrambled siRNA or Coro1B knockdown HUVECs treated with Coro1B siRNA #1 were seeded 72 hours post transfection on gelatine-coated coverslips for 24 hours. Cells were stained with specific antibodies for Coro1B and VEcad and F-actin was visualized using Phalloidin (figure 29). Zoom-in of the F-actin immunofluorescence staining showed less stress fibers and discontinuous cortical actin when Coro1B was absent at cell-cell junctions (b, figure 29). In addition, VEcad appeared disorganized in the absence of Coro1B at the cell-cell junction (b, figure 29) compared to control cells, where Coro1B is present at the cell-cell junction (a, figure 29)[103].

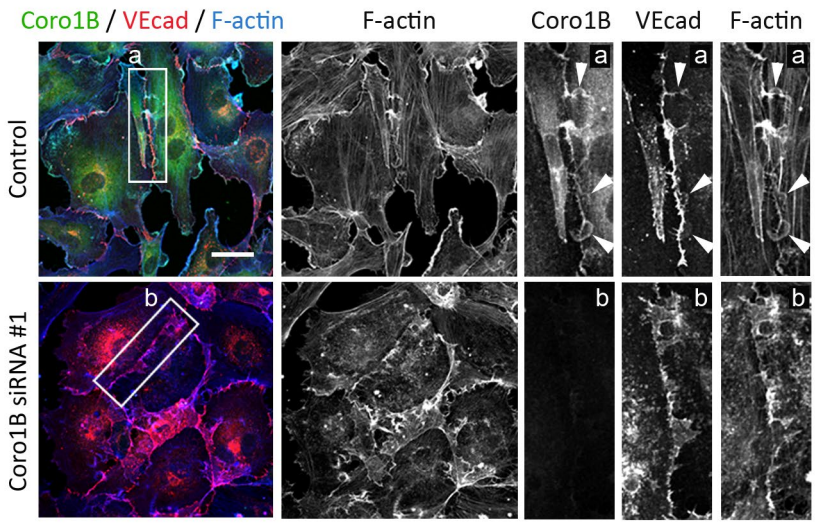

Figure 29. Downregulation of Coro1B affected VEcad and F-actin distribution
Representative immunofluorescence images of HUVECs treated with scrambled siRNA (control) or Coro1B siRNA #1 stained for Coro1B (green), VEcad (red) and F-actin (blue). Presence (a) or absence (b) of Coro1B at cell-cell junctions was shown by Zoom-in images. Arrowheads point to leading edge of JAIL. Scale bar = 25 µm. Immunofluorescent stainings are representative images of three independent experiments (modified from Werner et al.[103]).

5.3.4 Knockdown of Coro1B reduced JAIL formation but not monolayer permeability

To elucidate the role of Coro1B on monolayer integrity, TEER analysis was performed. To this end, control cells treated with scrambled siRNA or Coro1B knockdown HUVECs treated with Coro1B siRNA #1 or Coro1B siRNA #2 were seeded on a gold electrode and TEER was measured using electric cell-substrate impedance sensing[153]. The barrier integrity is measured by electrical ohmic resistance of the cell layer and was recorded for 24 hours[154]. During the first hour the impedance increased when ECs adhere to and spread over the electrode[154]. Quantitative analysis of resistance showed no significant difference between cells treated with Coro1B siRNA #1 (78.20% ± 41.23%) or Coro1B siRNA #2 (97.49% ± 21.25%) compared to control cells (100%) treated with scrambled siRNA within the first hour of recording, suggesting that Coro1B did not influence cell spreading, which is in line with previous findings (figure 30A). The seeded HUVECs continued their growth until they reach confluence. For that reason, in the following 2, 10, 15 and 20 hours monolayer formation and junctional integrity were measured. Quantitative analysis showed no significant difference in resistance after treatment of ECs with Coro1B siRNA #1 (2 hours 83.84% ± 33.17%, 10 hours 80.51% ± 24.73%, 15 hours 83.03% ± 14.47%, 20 hours 85.12% ± 8.11%) or Coro1B siRNA #2 (2 hours 104.02% ± 18.72, 10 hours 93.70% ± 16.59%, 15 hours 98.56% ±

9.66%, 20 hours 101.04% ± 10.29%) compared to control cells treated with scrambled siRNA (100%). These findings suggest that Coro1B was dispensable for monolayer integrity (figure 30A).

Next, the effect of Coro1B downregulation on the formation of JAIL was investigated. To this end, the number of JAIL per 10 µm cell-cell junction length in control and Coro1B knockdown HUVECs was quantified. Control cell treated with scrambled siRNA or cells treated with Coro1B siRNA #1 or Coro1B siRNA #2 were stained for Coro1B and VEcad. The number of JAIL was counted, and the total cell-cell junction length was measured. Quantitative analysis revealed that the number of JAIL per 10 µm cell-cell junction was significantly reduced in cells treated with Coro1B siRNA #1 to 61.66 ± 13.37% or treated with Coro1B siRNA #2 to 55.03 ± 7.17% normalized to control cells (100%) treated with scrambled siRNA (figure 30B)[103].

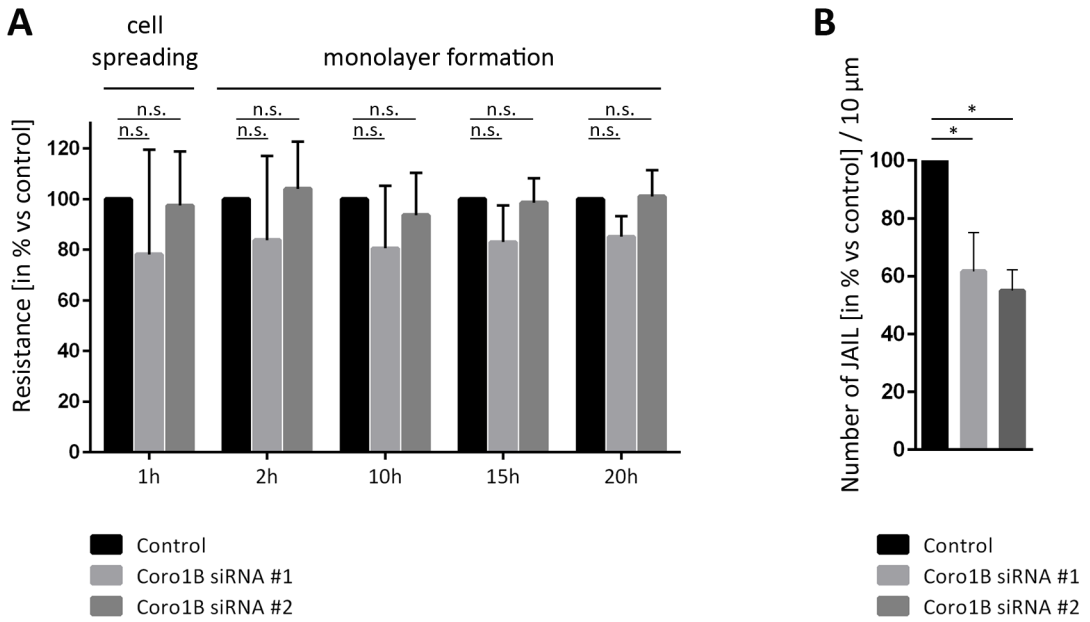

Figure 30. Coro1B had no impact on monolayer integrity but on JAIL formation

(A) Quantification of resistance normalized to control cells treated with scrambled siRNA (100%) in HUVECs treated with Coro1B siRNA #1 or Coro1B siRNA #2. n = 3. (B) Quantification of number of JAIL per 10 µm cell-cell junction normalized to control cells treated with scrambled siRNA (100%) of Coro1B knockdown HUVECs. Data represent mean ± SD n.s. not significant, * $P < 0.05$. n = 4 (15 FOV / sample) (modified from Werner et al.[103]).

5.3.5 Cell migration was not impaired by downregulation of Coro1B

A previous study described that Coro1B negatively regulated VEGF-induced migration of HUVECs[128]. Therefore, the impact of Coro1B on the migration behavior of ECs was analyzed.

To this end, a scratch-wound assay with Coro1B knockdown cells treated with Coro1B siRNA #1 or #2 and control HUVECs treated with scrambled siRNA was performed. The percentage of closure of scratch was measured after 6 and 12 hours. The comparison of cells treated with scrambled siRNA (control) or with Coro1B siRNA #1 or Coro1B siRNA #2 did not show any significant differences in the ability of non-VEGF stimulated cells to migrate, indicating that Coro1B had no effect on migration in this assay (figure 31B)[103].

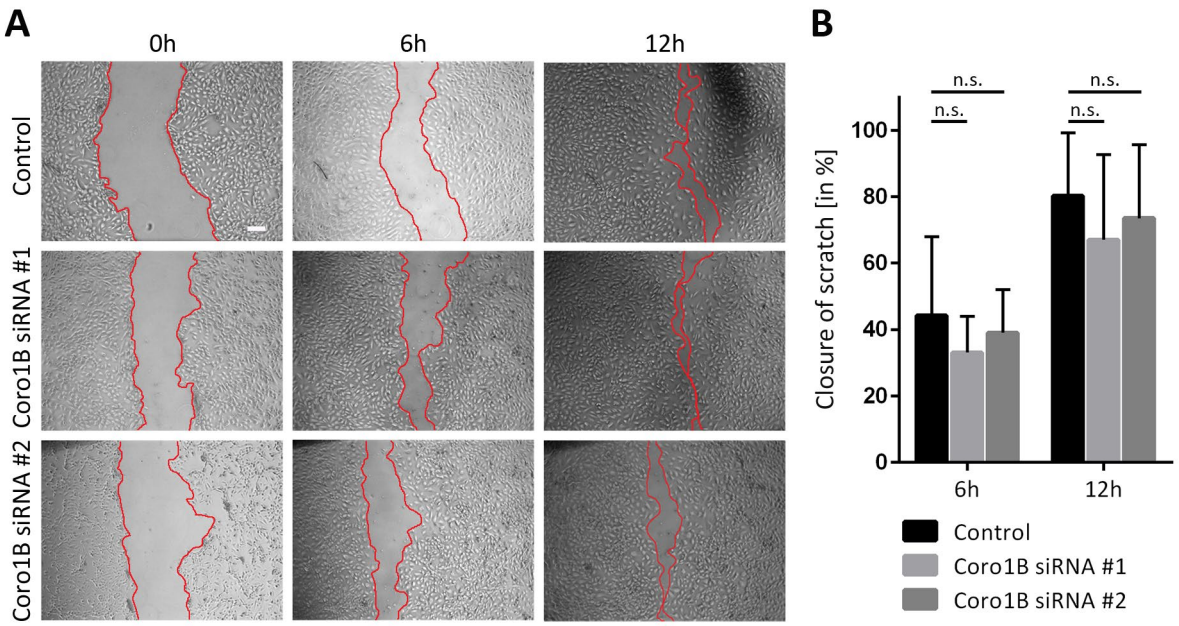

Figure 31. Migration was not impaired in Coro1B knockdown ECs
(A) Representative light microscope images after 6 and 12 hours of control cells treated with scrambled siRNA and cells treated with Coro1B siRNA #1 or Coro1B siRNA #2. Red lines indicate edges of scratch. Scale bar = 200 µm. (B) Quantification of scratch closure in % of control and Coro1B knockdown HUVECs after 6 and 12 hours. Data represent mean ± SD. n.s. not significant. n = 3 (6 FOV / sample) (modified from Werner et al.[103]).

5.3.6 Knockdown of Coro1B impaired angiogenesis *in vitro*

To determine the role of Coro1B for angiogenesis, an *in vitro* matrigel assay was performed[21]. Coro1B knockdown cells treated with Coro1B siRNA or control HUVECs treated with scrambled siRNA were seeded onto a laminin-based matrigel and were allowed to grow and form tubes for 20 hours (figure 32A)[103]. Tube formation was analyzed by counting the total number of branches. Quantitative analysis revealed that Coro1B did not affect the number of branches, indicating that Coro1B was not required for tube formation (figure 32B). Quantitative analysis of the total length of branches exhibited that in Coro1B knockdown cells the total length of tubes was significantly reduced compared to control cells

(figure 32C)[103]. Whereas in control cells the mean of the total length of branches was 10785.6 ± 1237.8 µm, Coro1B knockdown cells show a mean of the total length of branches of 8156.2 ± 2180.7 µm (Coro1B siRNA #1) or 7959 ± 1735.6 µm (Coro1B siRNA #2). Since the total length of branches is dependent of their connection, the reduced length of the branches in Coro1B knockdown cells suggests that Coro1B may have an impact on the connection of branches.

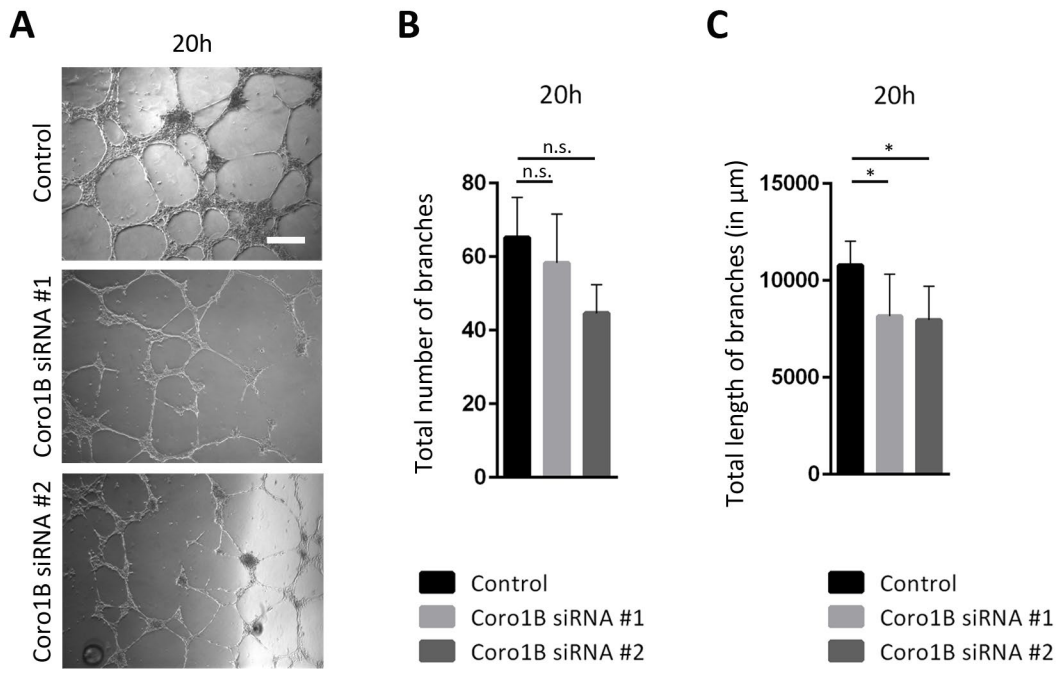

Figure 32. Knockdown of Coro1B did not affect tube formation

(A) Representative light microscope images after 20 hours of control cells and cells treated with Coro1B siRNA #1 or Coro1B siRNA #2. Scale bar = 200 µm. (B) Quantification of total number of branches in control (scrambled siRNA), Coro1B siRNA #1 or Coro1B siRNA #2 cells 20 hours post seeding. (C) Quantification of the total length of branches in control (scrambled siRNA), Coro1B siRNA #1 or Coro1B siRNA #2 cells. Data represent mean ± SD n.s. not significant, * $P < 0.05$, n = 3 (3 FOV / sample) (modified from Werner et al.[103]).

Light microscope images supported the hypothesis that knockdown of Coro1B impairs connection of branches by showing an increase of unconnected branches in Coro1B knockdown cells and compared to control cells treated with scrambled siRNA (figure 33A).

In addition, quantitative analysis of the master segments showed significantly less master segments in Coro1B knockdown cells compared to control cells after 15 hours. While control cells have 54.1 ± 4.3 master segments at this time point, cells treated with Coro1B siRNA #1 exhibit only 37.6 ± 5.1 or cells treated with Coro1B siRNA #2 29.4 ± 4.2 master segments (figure 33B). Using the angiogenesis analyzer ImageJ plugin, master segments are defined as

segments that are not exclusively associated with one branch[155]. The reduction of the number of master segments significantly increased after 20 hours to 48.0 ± 4.7 master segments in control cells, 24.8 ± 3.2 master segments in Coro1B siRNA #1 or 25.7 ± 2.5 master segments in Coro1B siRNA #2 treated cells (figure 33B)[103]. Additionally, the relative number of connected and not connected branches was analyzed (for definition of connected or not connected branches see chapter 4.10, figure 11B). Quantitative analysis after 15 and 20 hours revealed that the number of not connected branches was significantly increased after 20 hours in Coro1B knockdown cells compared to control cells, that have 14.5 ± 8.13 not connected branches, whereas Coro1B siRNA #1 treated cells displayed 37.06 ± 8.52 or Coro1B siRNA #2 treated cells 33.98 ± 5.21 not connected branches (figure 33C)[103]. These results suggest that Coro1B was not necessary for the initial formation of tubes but may be critically involved in their stability.

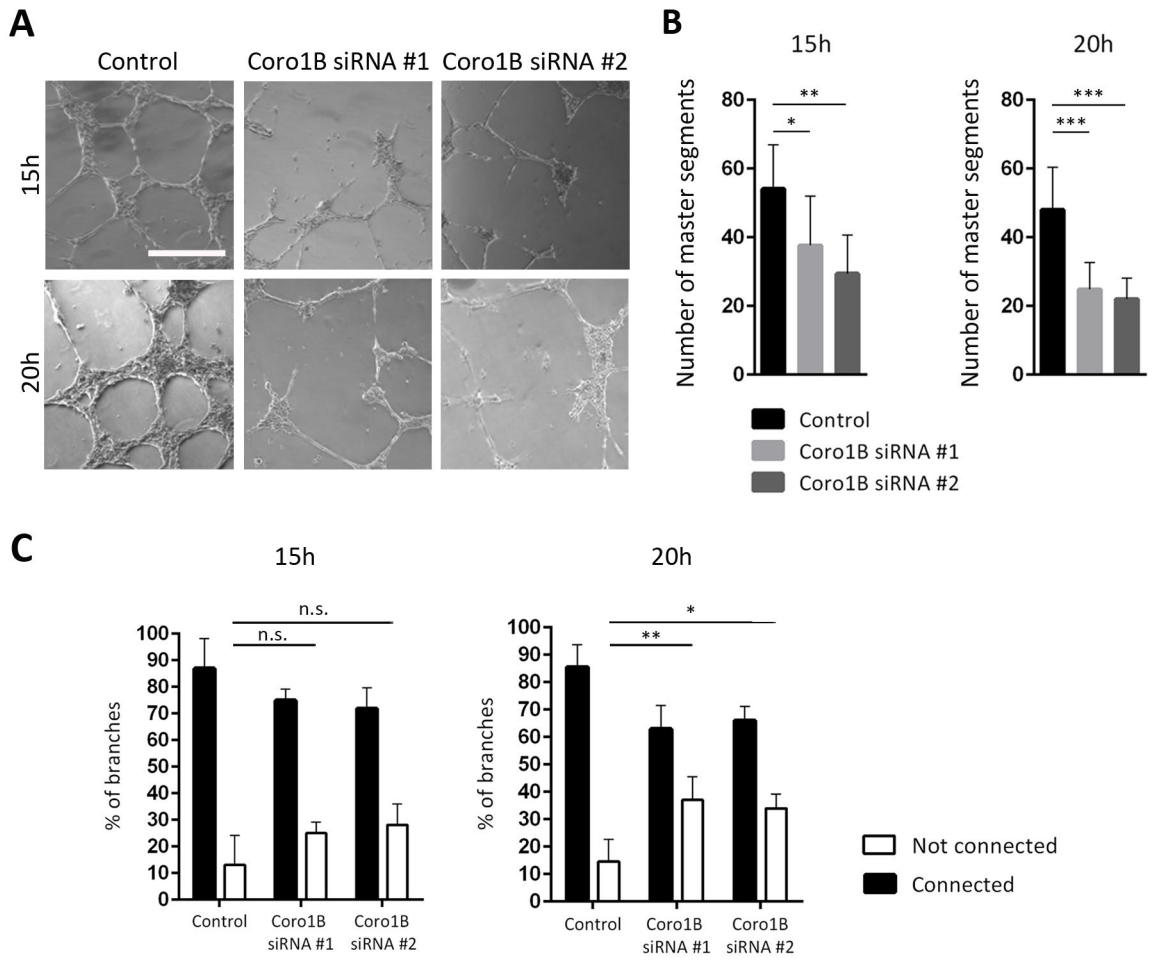

Figure 33. Reduced level of Coro1B impaired stability of branches

(A) Representative light microscope images after 15 and 20 hours of control cells treated with scrambled siRNA and cells treated with Coro1B siRNA #1 or Coro1B siRNA #2. Scale bar = 200 µm. (B) Quantification of the

number of master segments in control (scrambled siRNA), Coro1B siRNA #1 or Coro1B siRNA #2 cells after 15 and 20 hours. (C) Quantification of connected and not connected branches in control (scrambled siRNA) and Coro1B knockdown cells (Coro1B siRNA #1 or Coro1B siRNA #2) after 15 and 20 hours. Data represent mean ± SD. n.s. not significant, * P < 0.05, ** P < 0.01, *** P < 0.001. n = 3 (3 FOV / sample) (modified from Werner et al.[103]).

5.3.7 Coro1B was dispensable for proliferation and survival of ECs

To study if the stability defect in Coro1B knockdown cells was caused by altered proliferation, analysis of proliferation of control and Coro1B knockdown cells was conducted. To this end, control and Coro1B knockdown cells were stained for the proliferation marker anti-phospho-Histone H3 (pHH3) and the nuclear dye DAPI, 24 hours post seeding on coverslips coated with gelatine. The relative number of proliferating cells was calculated by comparing the number of DAPI positive cells to the number of pHiston-H3 positive cells (figure 34A). The quantitative analysis revealed a similar percentage of dividing cells in knockdown (4.00 ± 0.68% in Coro1B siRNA #1 or 4.74 ± 1.34% in Coro1B siRNA #2 treated cells) and control HUVECs (4.22 ± 1.44% in scrambled siRNA treated cells) suggesting that loss of Coro1B did not affect proliferation (figure 34B).

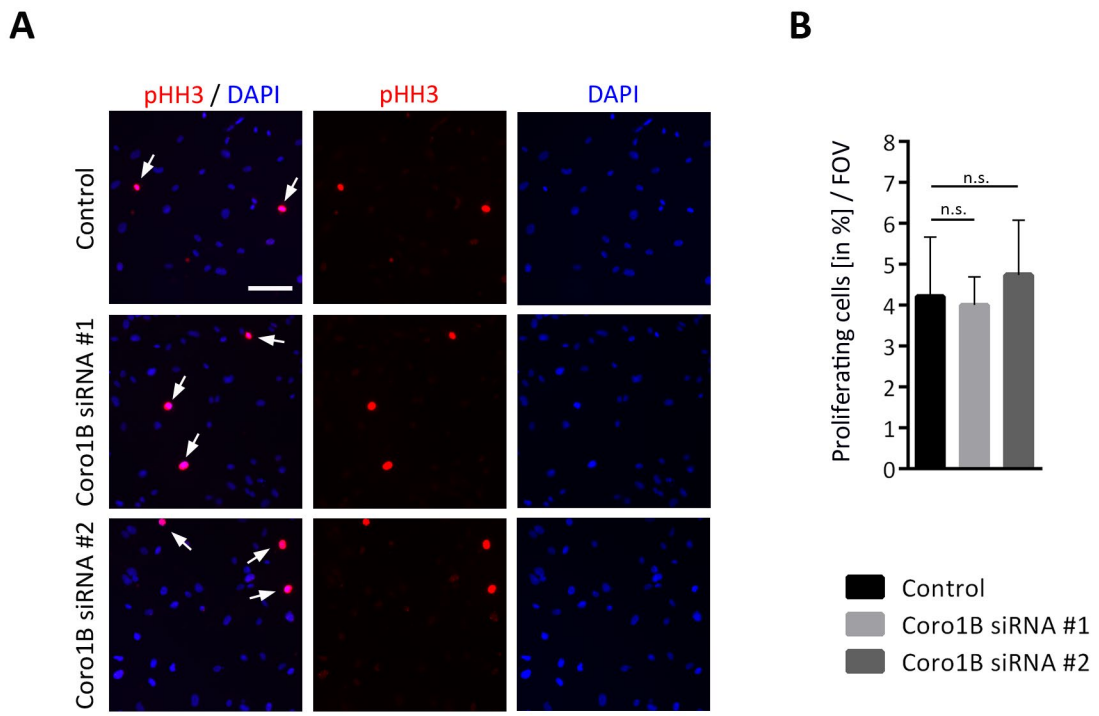

Figure 34. Knockdown of Coro1B did not influence cell proliferation

(A) Representative fluorescent images of control cells treated with scrambled siRNA and cells treated with Coro1B siRNA #1 or Coro1B siRNA #2 and stained with the nuclear dye DAPI (blue) and pHH3 (red). Arrows point to pHH3 positive cells. Scale bar = 100 µm. (B) Quantification of proliferating cells (in %) in cells treated with scrambled siRNA (control) and knockdown HUVECs (Coro1B siRNA #1 or Coro1B siRNA #2). Data represent mean ± SD. n.s. not significant. n = 3 (10 FOV / sample).

To determine whether the stability defect in Coro1B knockdown cells may result from an increased level of apoptosis in Coro1B knockdown cells, DNA strand breaks were detected using TUNEL[156]. Nuclei of cells treated with scrambled siRNA (control) or Coro1B knockdown cells were stained with DAPI. The relative number of apoptotic cells was calculated by dividing the total number of DAPI positive cells (living cells) by the number of TUNEL positive cells (apoptotic cells) (figure 35A). The percentage of apoptotic cells showed no difference between Coro1B knockdown (0.80 ± 0.67% Coro1B siRNA #1 or 0.60 ± 0.22% Coro1B #2 treated cells) and control HUVECs (0.84 ± 0.72%), suggesting that apoptosis was not influenced by Coro1B (figure 35B).

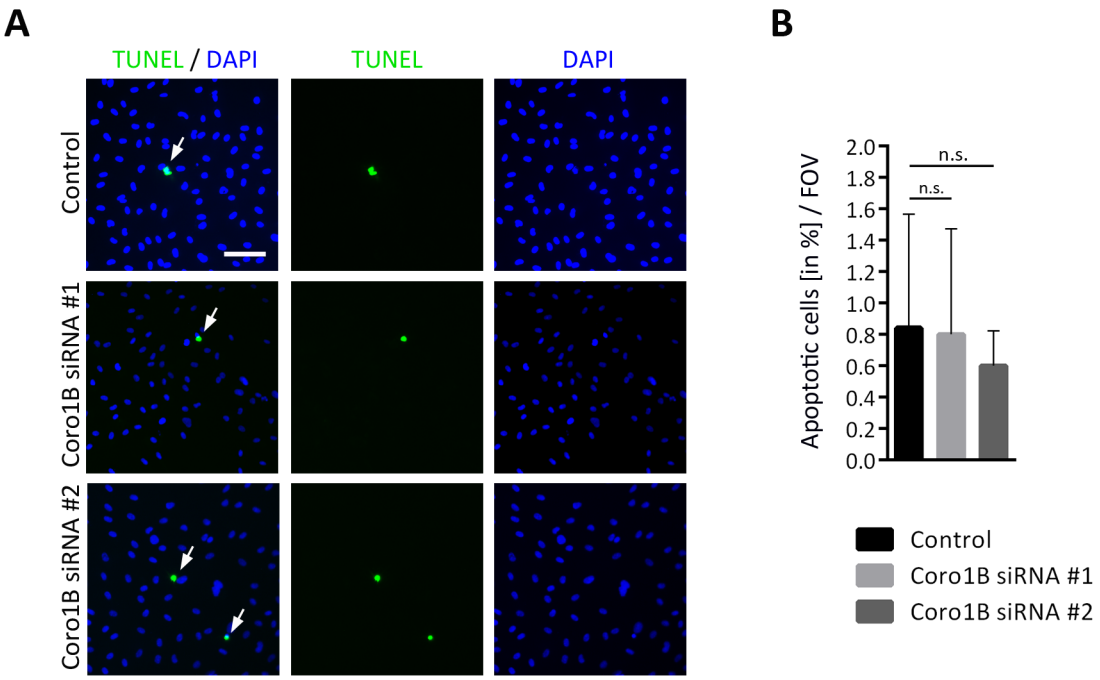

Figure 35. Knockdown of Coro1B did not induce apoptosis

(A) Representative fluorescent images of control cells treated with scrambled siRNA and cells treated with Coro1B siRNA #1 or Coro1B siRNA #2 stained with the nuclear dye DAPI (blue). Apoptotic cells were visualized by TUNEL (green). Arrows point to apoptotic cells. Scale bar = 100 µm. (B) Quantification of apoptotic cells (in %) in control cells treated with scrambled siRNA and knockdown HUVECs treated with Coro1B siRNA #1 or Coro1B siRNA #2. Data represent mean ± SD. n.s. not significant. n = 3 (10 FOV / sample).

5.4 Identification of Coro1B interacting proteins

To identify potential Coro1B interacting partners, the Coro1B interactome in ECs was investigated. According to that, immunoprecipitation (IP) of Coro1B-EGFP using the GFP Nano-Trap technology and subsequent mass spectrometry was performed. HMEC-1 stably expressing Coro1B-EGFP or EGFP alone as control were used for IP. Mass spectrometry analysis identified 118 proteins significantly interacting with Coro1B[103]. A selection of the top 75 proteins can be found in table 3.

Table 3. Selected proteins interacting with Coro1B

Coro1B interacting proteins were identified by LC-MS analysis. Resulting raw data were analyzed using MaxQuant software. Gene names of the identified proteins are based on the UniProt database. Displayed are all proteins with a log2 fold change above 2 and p-value below 0.05. n = 4.

	Uniprot	protein name	gene name	Log2 fold enrichment	p-value
1	Q8NGT1	Olfactory receptor 2K2	OR2K2	10.40	< 0.001
2	Q9BR76	Coronin-1B	CORO1B	10.25	0.002
3	Q9Y281	Cofilin-2	CFL2	8.33	< 0.001
4	Q9ULV4	Coronin-1C	CORO1C	8.22	< 0.001
5	O15145	Actin-related protein 2/3 complex subunit 3	ARPC3	6.76	< 0.001
6	P61158	Actin-related protein 3	ACTR3	6.62	< 0.001
7	Q9JHJ0	Tropomodulin-3	TMOD3	6.35	< 0.001
8	P59998	Actin-related protein 2/3 complex subunit 4	ARPC4	5.95	< 0.001
9	Q9BPX5	Actin-related protein 2/3 complex subunit 5-like protein	ARPC5L	5.70	< 0.001
10	Q9P289	Serine/threonine-protein kinase 26	STK26	5.61	< 0.001
11	O15511	Actin-related protein 2/3 complex subunit 5	ARPC5	5.57	0.001
12	O15143	Actin-related protein 2/3 complex subunit 1B	ARPC1B	5.44	< 0.001
13	P06396	Gelsolin	GSN	5.21	< 0.001
14	P62847	40S ribosomal protein S24	RPS24	5.13	< 0.001
15	P61160	Actin-related protein 2	ACTR2	4.58	0.008
16	P29419	ATP synthase subunit e, mitochondrial	ATP5ME	4.56	0.008
17	P62280	40S ribosomal protein S11	RPS11	4.54	0.001

18	P62081	40S ribosomal protein S7	RPS7	4.17	0.016
19	Q12792	Twinfilin-1	TWF1	4.16	0.002
20	P63261	Actin, cytoplasmic 2	ACTG1	4.10	< 0.001
21	D6RHI4	NAD kinase 2, mitochondrial	NADK2	4.07	0.001
22	O15144	Actin-related protein 2/3 complex subunit 2	ARPC2	4.06	0.013
23	P78371	T-complex protein 1 subunit beta	CCT2	3.99	< 0.001
24	P41731	CD63 antigen	CD63	3.98	0.032
25	P63241	Eukaryotic translation initiation factor 5A-1	EIF5A	3.95	0.005
26	G8JLA2	Myosin light polypeptide 6	MYL6	3.85	0.010
27	Q8WXX5	DnaJ homolog subfamily C member 9	DNAJC9	3.83	0.002
28	P46776	60S ribosomal protein L27a	RPL27A	3.83	0.008
29	Q5T0I0	Gelsolin	GSN	3.81	< 0.001
30	O00299	Chloride intracellular channel protein 1	CLIC1	3.78	< 0.001
31	Q99729	Heterogeneous nuclear ribonucleoprotein A/B	HNRNPAB	3.75	0.002
32	Q71UM5	40S ribosomal protein S27-like	RPS27L	3.67	0.005
33	P31146	Coronin-1A	CORO1A	3.54	0.004
34	P27635	60S ribosomal protein L10	RPL10	3.46	0.018
35	P68133	Actin, alpha skeletal muscle	ACTA1	3.45	< 0.001
37	P67870	Casein kinase II subunit beta	CSNK2B	3.29	0.012
38	P09211	Glutathione S-transferase P	GSTP1	3.28	0.001
39	P63220	40S ribosomal protein S21	RPS21	3.25	0.015
40	P52943	Cysteine-rich protein 2	CRIP2	3.22	< 0.001
41	Q02543	60S ribosomal protein L18a	RPL18A	3.20	0.009
42	P62851	40S ribosomal protein S25	RPS25	3.20	0.020
43	Q8WXH0	Nesprin-2	SYNE2	3.17	0.001
44	P49368	T-complex protein 1 subunit gamma	CCT3	3.15	0.001
45	P61254	60S ribosomal protein L26	RPL26	3.14	0.005
46	P62854	40S ribosomal protein S26	RPS26	3.14	0.018
47	O75083	WD repeat-containing protein 1	WDR1	3.11	0.032

48	0A0U1RRL7	Protein MMP24OS	MMP24OS	3.11	0.044
49	P17987	T-complex protein 1 subunit alpha	TCP1	3.05	0.001
50	Q16643	Drebrin	DBN1	3.04	< 0.001
51	Q9Y3U8	60S ribosomal protein L36	RPL36	3.03	0.107
52	Q15388	Mitochondrial import receptor subunit TOM20 homolog	TOMM20	3.01	0.041
53	P51636	Caveolin-2	CAV2	3.01	0.010
54	P62266	40S ribosomal protein S23	RPS23	3.00	0.009
55	Q13418	Integrin-linked protein kinase	ILK	2.99	0.003
56	P18124	60S ribosomal protein L7	RPL7	2.99	0.015
57	P50990	T-complex protein 1 subunit theta	CCT8	2.97	0.002
58	Q969G5	Caveolae-associated protein 3	CAVIN3	2.93	0.008
59	P26373	60S ribosomal protein L13	RPL13	2.91	0.006
60	Q6IBS0	Twinfilin-2	TWF2	2.90	0.031
61	P46779	60S ribosomal protein L28	RPL28	2.90	0.036
62	P61247	40S ribosomal protein S3a	RPS3A	2.88	0.010
63	O43175	D-3-phosphoglycerate dehydrogenase	PHGDH	2.85	< 0.001
64	P60709	Actin, cytoplasmic 1	ACTB	2.83	< 0.001
65	Q02878	60S ribosomal protein L6	RPL6	2.80	0.022
66	P61313	60S ribosomal protein L15	RPL15	2.77	0.025
67	Q99832	T-complex protein 1 subunit eta	CCT7	2.68	0.024
68	Q99623	Prohibitin-2	PHB2	2.66	0.079
69	Q8H8V7	ABC transporter G family member 5, ABC transporter ABCG.5, OsABCG5	RCN1	2.66	0.024
70	P40227	T-complex protein 1 subunit zeta	CCT6A	2.63	0.019
71	Q9BWJ5	Splicing factor 3B subunit 5	SF3B5	2.60	0.001
72	O95816	BAG family molecular chaperone regulator 2	BAG2	2.59	0.002
73	P29692	Elongation factor 1-delta	EEF1D	2.55	0.048
74	P04792	Heat shock protein beta-1	HSPB1	2.53	0.011
75	P46940	Ras GTPase-activating-like protein IQGAP1	IQGAP1	2.52	0.044

Analysis of mass spectrometry data showed the bait protein Coro1B as well as Coro1C, the other isoform expressed in ECs. The subunits of the Arp2/3 complex like actin related protein 2/3 complex subunit 5-like protein (ARPC5L), actin related protein 3 (ACTR3), actin related protein 2/3 complex subunit 4 (ARPC4) and actin related protein 2/3 complex subunit 3 (ARPC3) were identified as Coro1B interacting partners[103]. This was expected as it has been shown previously that the binding of Coro1B to the Arp2/3 complex is associated with phosphorylation[124,130]. Moreover, the already described interacting partner cofilin (CFL2) was detected[124,133]. A volcano blot of the mass spectrometry analysis showed expected and already known interacting partners indicating a specific pull-down (figure 36). Interestingly, the protein ILK was identified by mass spectrometry as a new Coro1B interacting partner (table 3 and figure 36)[103]. ILK represents together with α-parvin and PINCH a member of the IPP complex known as a main regulator of integrin-ECM interaction[14,61,157]. In contrast, no significant interaction between Coro1B and α-parvin (PARVA) was detected by mass spectrometry analysis (figure 36).

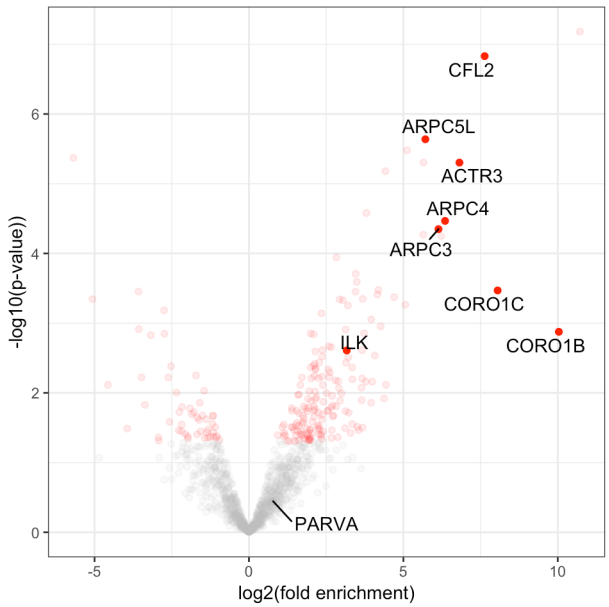

Figure 36. Mass spectrometry identified ILK as a new Coro1B interacting protein
Volcano blot showed the log2 fold enrichment of proteins (x-axis) identified by mass spectrometry and the p-value (–log10) (y-axis) of the adjusted *t-test* comparing the abundance of these proteins in immunoprecipitates from HMEC-1 Coro1B-EGFP and HMEC-1 EGFP (control). Proteins with a log2 fold enrichment of over 2.0 and a p-value below 0.05 were considered significant and are displayed in red. n = 4 (modified from Werner et al.[103]).

Next an IP of HMEC-1 Coro1B-EGFP and subsequent western blot analysis was conducted to confirm the interacting proteins identified by mass spectrometry. Protein lysates of HMEC-1 EGFP alone and HMEC-1 Coro1B-EGFP were used as positive control (input) for the IP. The Arp2/3 complex was successfully detected as an interacting partner by western blot analysis (figure 37B) since it was only expressed in the protein lysates of Coro1B-EGFP cells but absent in the protein lysates of WT and EGFP cells after IP. To verify the pull-down, western blotting for Coro1B was performed simultaneously (figure 37A). Coro1B and Coro1B-EGFP expression in protein lysates of Coro1B-EGFP after IP demonstrated that the pull-down worked.

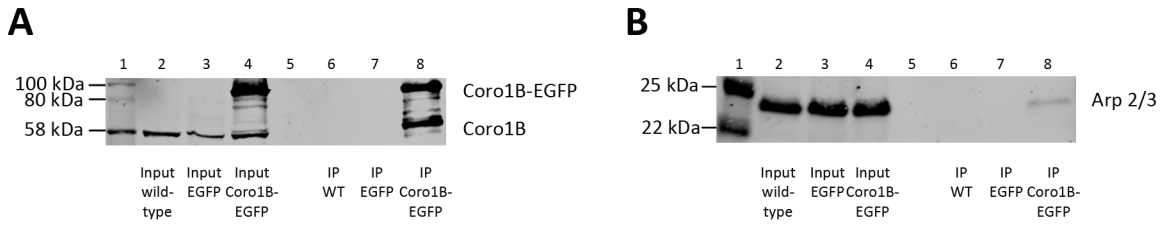

Figure 37. Western blot analysis showed the pull-down of the Arp2/3 complex
Western blot analysis of protein lysates (input) and IP samples of wild type HMEC-1 and stably HMEC-1 transfected with EGFP or Coro1B-EGFP. (A) Western blotting for Coro1B was performed with protein lysates used as input (lane 2 to 4) and protein lysates of IP experiments (lane 6 to 8) (B) Western blotting for Arp2/3 was performed with protein lysates used as input (lane 2 to 4) and protein lysates of IP experiments (lane 6 to 8). Western blots are representative of three independent experiments.

An IP of HMEC-1 expressing Coro1B-EGFP or EGFP alone as a control followed by western blot analysis was performed to verify the interaction of Coro1C and Coro1B. Western blot analyses demonstrated that Coro1C was only expressed in the protein lysates of Coro1B-EGFP cells but not in the protein lysates of EGFP cells after IP (figure 38B). Western blotting for Coro1B was performed simultaneously and validated the pull-down (figure 38A). Coro1C was confirmed as Coro1B interacting protein by western blot analysis after IP (figure 38B).

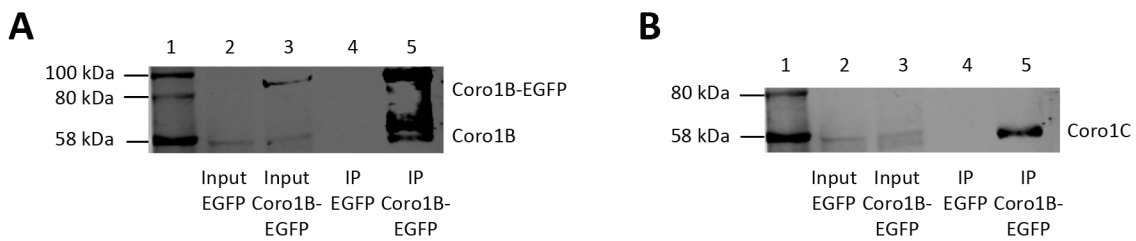

Figure 38. Western blot analysis showed the pull-down of Coro1C
Western blot analysis of protein lysates (input) and from IP samples of HMEC-1 stably transfected with EGFP or

Coro1B-EGFP. (A) Western blotting for Coro1B was performed with protein lysates used as input (lane 2 and 3) and protein lysates of IP experiments (lane 4 and 5). (B) Western blotting for Coro1C was performed with protein lysates used as input (lane 2 and 3) and protein lysates of IP experiments (lane 4 and 5). Western blots are representative of three independent experiments.

5.4.1 ILK was identified as a new interacting partner of Coro1B

Next, Coro1B interacting proteins involved in vascular development were investigated. Mass spectrometry analysis identified ILK as novel interacting partner of Coro1B as described above (table 3). The IPP complex consisting of ILK, parvin and PINCH is a main regulator of integrin-ECM interaction and thereby essential for blood vessel development[43]. ILK facilitates the interaction of the IPP complex with integrins, whereas interaction with actin is mediated via α-parvin[63]. ILK is a key regulator in EC function[135,154,155]. Therefore, the characterization of Coro1B-ILK interaction was further investigated. Western blot analysis showed the expression of ILK in protein lysates of Coro1B-EGFP expressing cells after IP (figure 39B). Pull-down of Coro1B-EGFP and subsequent western blot analysis confirmed the interaction of Coro1B and ILK (figure 39B)[103].

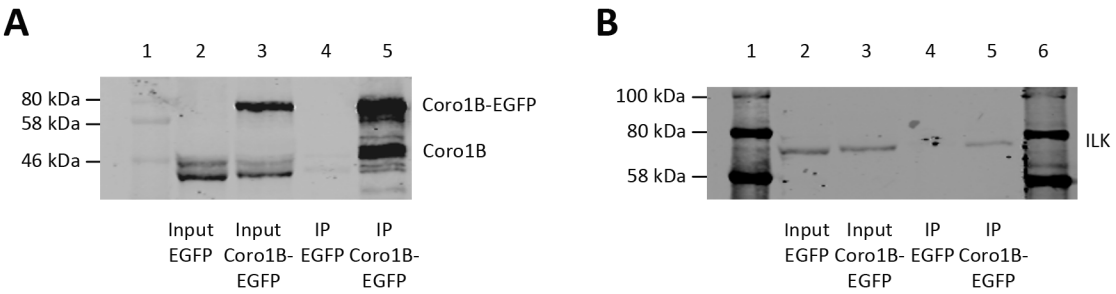

Figure 39. Western blot analysis showed the pull-down of ILK
Western blot analysis of protein lysates (input) and from IP samples of HMEC-1 stably transfected with EGFP or Coro1B-EGFP. (A) Western blotting for Coro1B was performed with protein lysates used as input (lane 2 and 3) and protein lysates of IP experiments (lane 4 and 5). (B) Western blotting for ILK was performed with protein lysates used as input (lane 2 and 3) and protein lysates of IP experiments (lane 4 and 5). Western blots are representative of three independent experiments (modified from Werner et al.[103]).

Next, another protein of the IPP complex, α-parvin was further investigated by IP and western blot analysis. Of note, α-parvin was not identified as a protein interacting with Coro1B by mass spectrometry. In line with this observation, also western blot analysis did not show α-parvin as a Coro1B interacting protein in protein lysates of Coro1B-EGFP

expressing cells after IP (figure 40B). Coro1B and Coro1B-EGFP expression in protein lysates of Coro1B-EGFP after IP demonstrated that the pull-down worked.

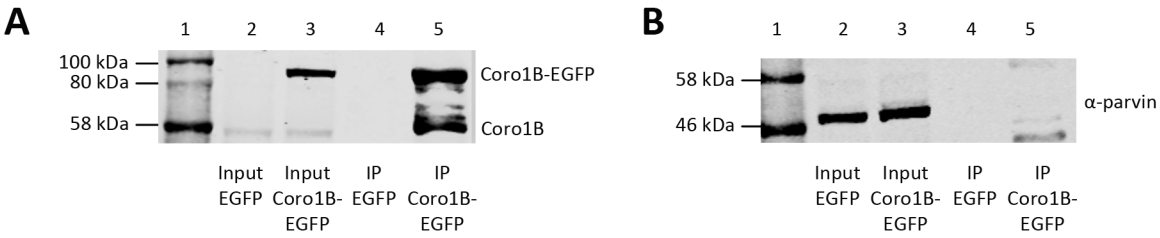

Figure 40. Western blot analysis did not show the pull-down of α-parvin
Western blot analysis of protein lysates (input) and from IP samples of HMEC-1 stably transfected with EGFP or Coro1B-EGFP. (A) Western blotting for Coro1B was performed with protein lysates used as input (lane 2 and 3) and protein lysates of IP experiments (lane 4 and 5). (B) Western blotting for α-parvin was performed with protein lysates used as input (lane 2 and 3) and protein lysates of IP experiments (lane 4 and 5). Western blots are representative of three independent experiments.

Even IP and western blot analysis did not show a direct interaction between Coro1B and α-parvin, it was further analyzed by immunofluorescence staining whether these proteins colocalize at the leading edge of lamellipodia. Since a previous study described that similar to Coro1B, α-parvin was located at the leading edge of JAIL[14]. For that reason, two types of ECs (HUVEC and HMEC-1) transfected with the Coro1B-EGFP construct, coding for Coro1B-EGFP, and were simultaneously stained for α-parvin with a specific antibody and a fluorophore-labeled secondary antibody. As expected, Coro1B was distributed along the leading edge of the lamellipodia. α-parvin localized to FA where no Coro1B was detectable. α-parvin also localized to FXs, which are nascent cell-adhesion contacts that are located near the edge of the lamellipodium. Staining of Coro1B-EGFP expressing cells for α-parvin revealed a colocalization of Coro1B and α-parvin at the leading edge of lamellipodia in both types of ECs (figure 41)[103].

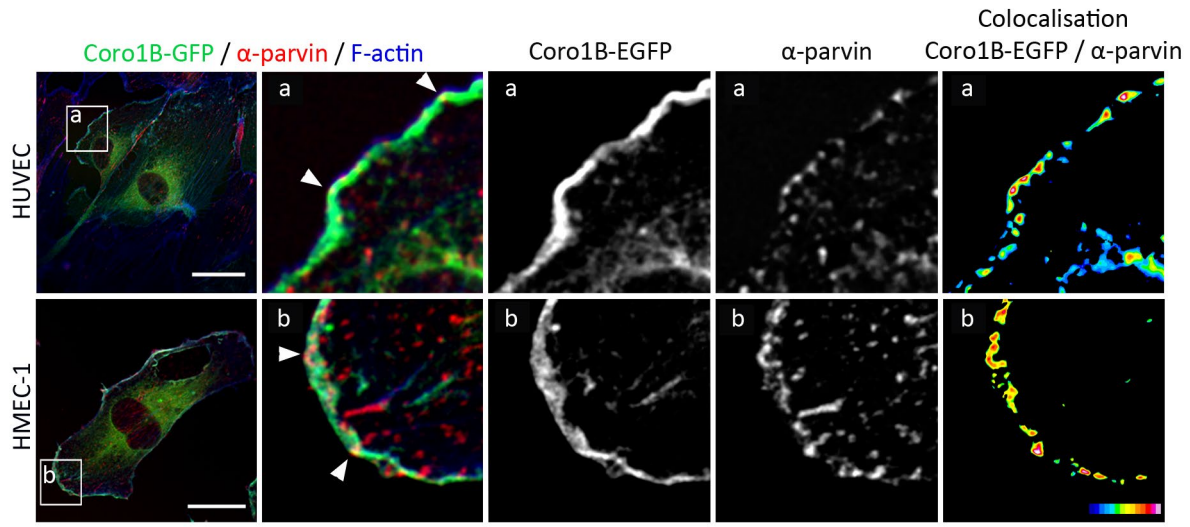

Figure 41. Colocalization of α-parvin and Coro1B at the leading edge of ECs
HUVEC and HMEC-1 were transfected with Coro1B-EGFP (green) and stained with a specific antibody for α-parvin (red). First column shows merged images. Second column displays magnification of field a (HUVECs) or b (HMEC-1). Third and fourth columns show split channels of field a and b for Coro1B-EGFP and α-parvin. Fifth column shows colocalization of Coro1B-EGFP and α-parvin. Black indicates no colocalization, white indicates the highest amount of colocalization. Arrowheads point to colocalization of Coro1B and α-parvin at the leading edge. Scale bar = 25 µm (modified from Werner et al.[103]).

To validate the observed colocalization of Coro1B and α-parvin at the leading edge, fibroblasts transfected with EGFP tagged Coro1B were stained with a specific antibody for α-parvin. Confocal images revealed that similar to its localization in EC, Coro1B was distributed at the edge of lamellipodia where it colocalized with α-parvin at FXs. Moreover, staining displayed no colocalization of α-parvin and Coro1B at FAs (figure 42).

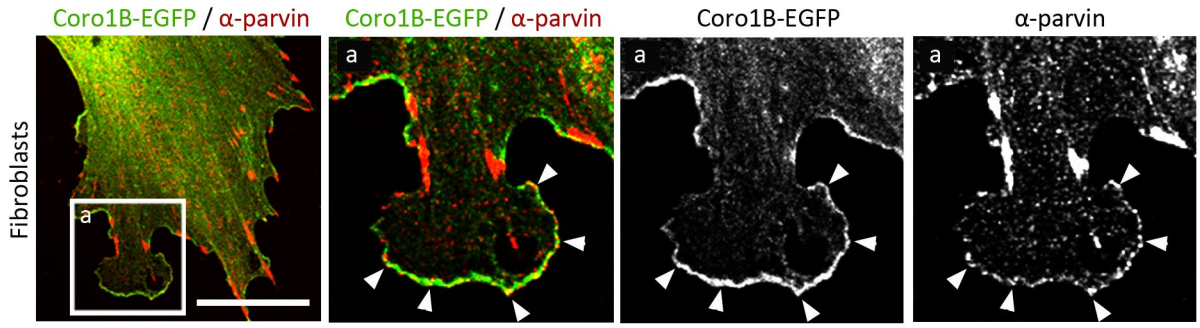

Figure 42. α-parvin colocalized with Coro1B at FX at the leading edge of fibroblasts
Fibroblasts were transfected with Coro1B-EGFP (green) and stained with a specific antibody for α-parvin (red). First and second columns show merged images. Second column shows magnification of field a. Third and fourth columns display single color pictures of field a. Arrowheads point to colocalization of Coro1B and α-parvin at the leading edge. Scale bar = 25 µm.

So far, there is no immunofluorescence staining of ECs for ILK published. In addition, it is known that Coro1B also localizes in fibroblasts to the leading edge[130]. For that reason, fibroblasts were transfected with the Coro1B-EGFP plasmid, coding for Coro1B-EGFP and stained with a specific antibody for ILK. F-actin was visualized using Phalloidin. Confocal images revealed that Coro1B was located at the leading edge, whereas ILK localized to FA and FXs. In addition, immunofluorescence staining showed that Coro1B did not localized to FA but displayed a colocalization of ILK and Coro1B at FXs at the leading edge (figure 43). These findings suggest that Coro1B interacts with ILK exclusively at FXs.

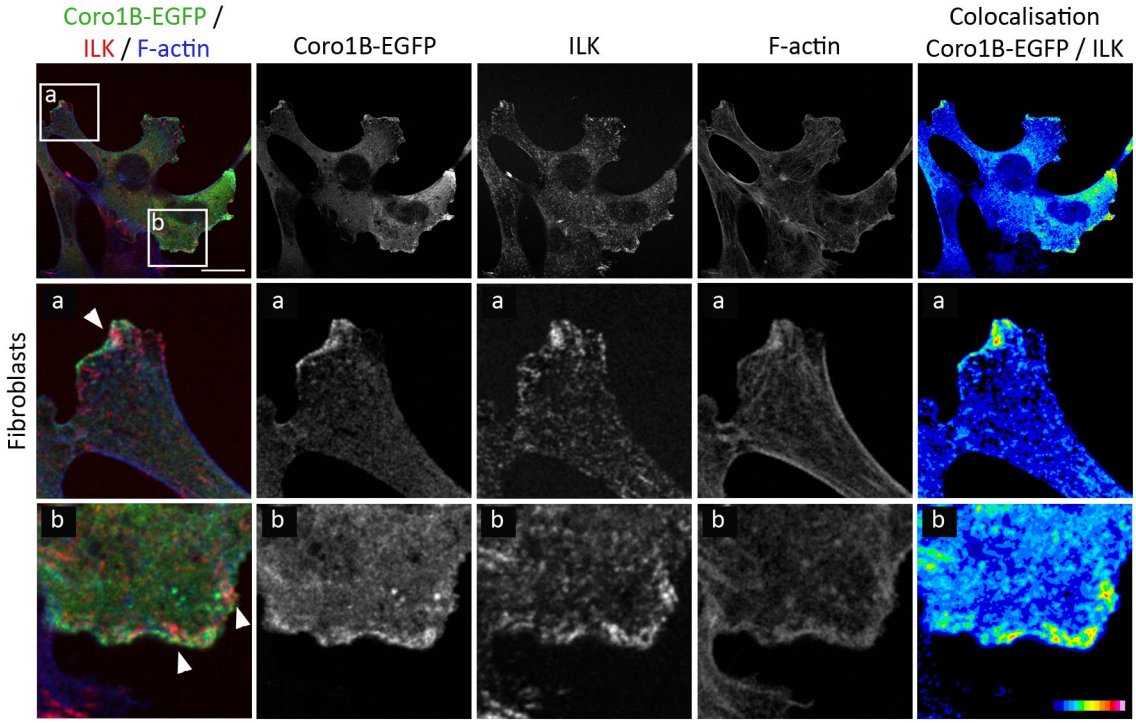

Figure 43. ILK colocalized with Coro1B at FXs in fibroblasts
Fibroblasts were transfected with Coro1B-EGFP (green) and stained with a specific antibody for ILK (red). F-actin was visualized using Phalloidin. First column shows whole merged image and magnification of two selected areas. Second to fourth columns display single color pictures of Coro1B-EGFP, ILK and F-actin. Fifth column shows colocalization of Coro1B-EGFP and ILK as heat map. Black indicates no colocalization, white indicates the highest amount of colocalization. Arrowheads point to colocalization of Coro1B and ILK at FXs. Scale bar = 25 µm.

5.5 Generation of Coro1B knockout fish

To determine the importance of Coro1B for angiogenesis and blood vessel formation *in vivo*, the zebrafish model was used**.** This model is well established to study vascular biology due to its rapid embryonic development and optical transparency[28,29]. To this end, a Coro1B knockout fish line was generated using the CRISPR / Cas9 technique. After microinjection of

Coro1B #6 gRNA / Cas9 mRNA, positive mosaic mutant fish were detected by RFLP analysis. Here, the restriction enzyme BtsCI is not able to digest a part of the PCR fragment because of the mutation in the target site, whereas the PCR fragment of the uninjected fish is completely digested (figure 44A)[158]. Heterozygous mutant fish were also identified using RFLP analysis accordingly. For further analysis, deletion of five nucleotides adjacent to the BtsCI restriction recognition site leading to an early stop codon was selected to generate a stable Coro1B knockout fish line. Next, heterozygous fish having this specific deletion of five nucleotides were bred. To identify homozygous fish, it was not possible to use RFLP, since the recognition site for the restriction enzyme was only impaired in heterozygous fish. Therefore, homozygous mutation carriers were identified by sequence analysis (figure 44B).

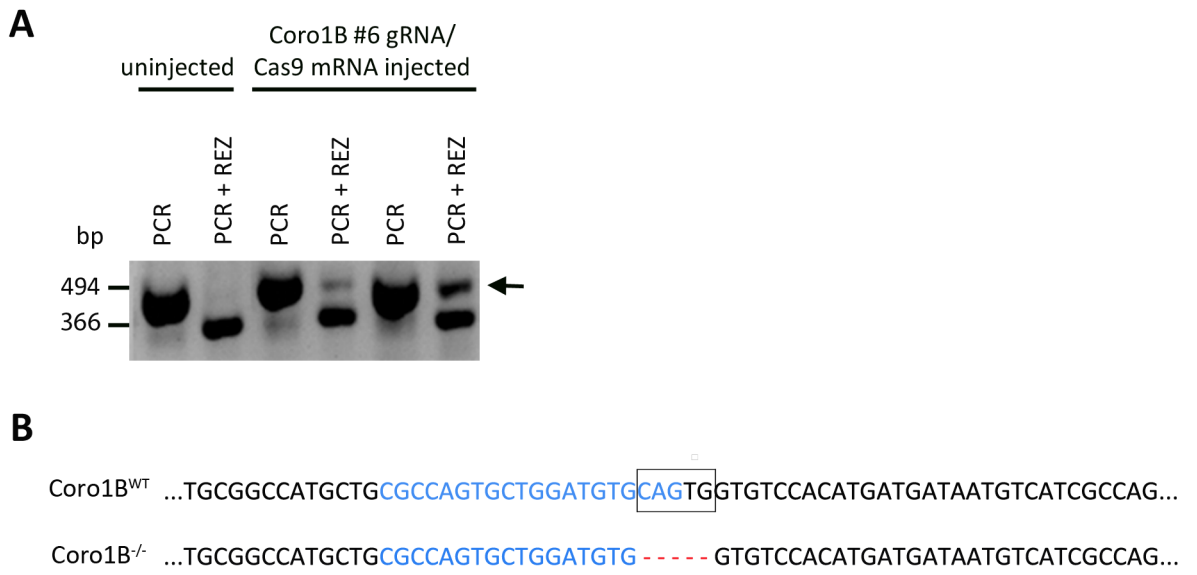

Figure 44. Identification of mutated fish
(A) PCR and RFLP analysis (PCR+ digest with a restriction enzyme) of uninjected and of two positive mosaic fish. Arrow points to an undigested PCR fragment. (B) Sequence of wild type (+ / +) and homozygous (- / -) Coro1B #6 knockout fish. Target sequence is shown in blue. Mutation is displayed in red.

To analyze whether the mutation leads to an impaired level of Coro1B protein expression, western blot analysis was conducted. Whole fish lysates of two wild type and two homozygous Coro1B knockout fish were used. Western blot analysis showed that Coro1B expression was absent in homozygous Coro1B knockout fish (figure 45).

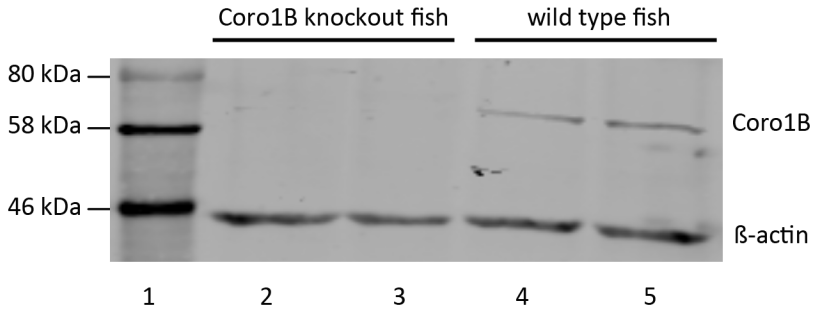

Figure 45. Western blot analysis of whole fish lysates of wild type and Coro1B knockout fish
Western blot analysis shows Coro1B expression in wild type fish (lane 4 and 5). Coro1B expression was absent in Coro1B knockout fish (lane 2 and 3). β-actin was used as loading control.

The breeding behavior of wild type and Coro1B knockout fish was compared. For that purpose, the frequency of egg spawning per mating was determined. No difference in the frequency of egg spawning between wild type and Coro1B knockout fish was observed (data not shown). The development of wild type and Coro1B knockout fish was monitored using light microscopy. The Coro1B knockout fish showed a normal development with no visible defects. The number of fish per clutch that survived up to 5 dpf was counted. No significant difference was observed between wild type (50.66 ± 15.55) and Coro1B knockout fish (53.67 ± 20.01) with regard to the survival of the offspring (figure 46B).

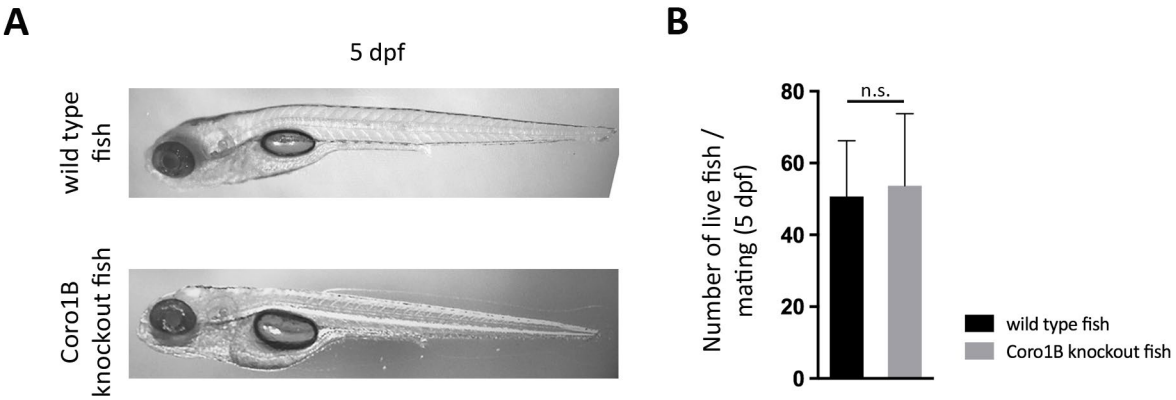

Figure 46. Breeding behaviour was not impaired in Coro1B knockout fish
(A) Representative light microscope images of wild type and Coro1B knockout fish 5 dpf. (B) Quantification of number of live fish per mating in wild type and Coro1B knockout fish 5 dpf. Data represent mean ± SD. n.s. not significant. n = 6.

6. Discussion

This study investigated the role of Coro1B in ECs, whereby Coro1B was identified as a new member of endothelial cell-cell junctions. Functional analysis revealed that Coro1B was dispensable for adhesion, spreading and migration of ECs, and had no effect on monolayer formation. Data of an *in vitro* angiogenesis assay demonstrated that Coro1B was not required for the formation of tube-like structures but for their stability[103].

6.1 Coro1B dynamically localized at cell-cell junctions in ECs

In previous studies Coro1B was found to be located at the leading edge of lamellipodia in migrating cells[103,107,124,129]. In epithelial cells, Coro1B colocalized with E-cadherin at AJ where it is involved in the reorganization of the junction supporting the integrity of cell-cell junctions[135]. In this study, immunofluorescence staining demonstrated that in embryonic mECs as well as in primary and immortalized human ECs Coro1B localized at the leading edge of lamellipodia and at cell-cell junctions where it shows a colocalization with VEcad in some parts[103]. Endothelial cell-cell junctions are highly dynamic in contrast to epithelial cells. The dynamic reorganization of the junctions is modulated by VE-PTP, VEGFR1 and angiopoietin-Tie signaling and depends on the rearrangement of the actin cytoskeleton at cell-cell contacts[81,102,159]. The interaction of the VEcad / catenin complex at cell-cell junctions with actin filaments allows a fast remodeling of the junctions and makes them highly dynamic[160]. For that reason, cell-cell junction dynamics are essential for angiogenesis, repair and regeneration of blood vessels[161]. Moreover, cell-cell junction dynamics facilitate the extravasation of leukocytes during inflammation[162].

The dynamic remodeling of cell-cell junctions is orchestrated, in part, by JAIL, which represent Arp2/3 complex-controlled actin protrusions at cell-cell junctions that appear at VEcad free gaps. JAIL protrude over a small region of the apical membrane of the bordering cell[102,103,106]. They regulate the dynamic rearrangement of VEcad and are consequently involved in the re-arrangement of cell-cell junctions[81]. Immunofluorescence staining demonstrated that Coro1B localized at the leading edge of a JAIL. In the absence of Coro1B, JAIL formation was significantly reduced. Live-cell imaging experiments revealed that Coro1B colocalizes with F-actin at the leading edge of JAIL before the VEcad plaque was formed[103]. It

is known that Coro1B binds the Arp2/3 complex and thereby regulates actin nucleation and branching at the leading edge[124,127]. The reduction in JAIL formation in Coro1B knockdown cells was associated with the disorganization of the actin cytoskeleton and distribution of VEcad at cell-cell junctions[103]. These results suggest that Coro1B regulates Arp2/3 complex-dependent actin polymerization during JAIL formation and subsequently the dynamic reorganization of VEcad and the remodeling of the cell-cell junction. That Coro1B also localized at sites of actin polymerization, which surround reticular AJs, could be another hind that it might regulate actin polymerization. Only primary ECs have reticular AJs, which localize at areas with low actomyosin-mediated tension where neighboring cells overlap[98,100]. However, the physiological function of reticular AJs is still unknown.

A main regulator involved in cytoskeletal changes necessary for cell-cell junction dynamics is the small Rho GTPase RhoA[73]. Inflammatory stimuli like thrombin or histamine activate RhoA and its target ROCK leading to actomyosin contraction and consequently to an increased permeability of the endothelial cell-cell junction facilitating extravasation of leukocytes[86,98,99]. Beside inflammation, these cytoskeletal changes at cell-cell junctions induced by Rho GTPases are also important for angiogenesis. High levels of RhoA activity induce actomyosin-mediated lamellipodia retraction, whereas another small Rho GTPase named Rac1 stimulates actin polymerization and thereby controls lamellipodia projection[76,77,163]. Additionally, activated RhoA leads to formation of stress fibers, which are actin bundles associated with non-muscle myosin II[78,79]. It has been shown that in epithelial cells Coro1B regulates cell-cell junction stability by supporting RhoA signaling at the cell junction[135,136]. Whether Coro1B regulates cell-cell junction integrity also through RhoA in ECs is not known and needs to be addressed. It is known that JAIL formation depends on actomyosin contraction[160]. In this study Coro1B knockdown cells showed impaired stress fiber formation compared to control cells suggesting that RhoA signaling was altered in the absence of Coro1B. Immunofluorescence staining showed that the linear distribution of VEcad is disturbed in Coro1B knockdown cells, which reinforce the hypothesis that in ECs Coro1B is involved in the dynamic reorganization of VEcad and thus in the regulation of cell-cell junctional remodeling.

In addition, thrombin-dependent RhoA activation led to less Coro1B expression at cell-cell junctions and an enhanced cytoplasmic distribution of Coro1B. The vice versa experiment by inhibiting ROCK confirmed that Coro1B localization at cell-cell junctions was RhoA dependent as immunofluorescence staining showed more Coro1B expression at cell-cell junction after stimulation with Y-27632[103]. The RhoA dependent localization of Coro1B supports the hypothesis that Coro1B might be involved in the regulation of cell-cell junction dynamics. Although Coro1B strongly localized to cell-cell junctions and JAIL, knockdown of Coro1B in ECs did not alter monolayer formation. A reason for that could be Coro1C, which is also expressed in ECs and which was upregulated in Coro1B knockdown cells, may have compensated for the loss of Coro1B. To test this hypothesis, Coro1C was tried to be downregulated in control and Coro1B knockdown cells using several specific siRNA. Unfortunately, preliminary experiments with siRNA against Coro1C were unsuccessful. For that reason, in the future, CRISPR / Cas9 technology or shRNA experiments could be used to knockdown Coro1C in ECs. Moreover, further experiments under physiological conditions like under flow conditions or *in vivo* experiments have to be performed to determine the role of Coro1B in the regulation of cell-cell junctions. Together, the results indicate that Coro1B localizes at endothelial cell-cell junctions in an actin-dependent manner and suggest that Coro1B might regulate actin polymerization during cell-cell junction remodeling.

6.2 Coro1B was required for *in vitro* angiogenesis

To study the role of Coro1B in ECs, a wide range of *in vitro* cell biology experiments were performed. Specifically, the impact of Coro1B on morphology, spreading, permeability and migration of ECs was analyzed.

Differences in morphology of Coro1B knockdown HUVECs compared to control HUVECs were not observed. Moreover, knockdown of Coro1B did not impair the ability of the cells to spread, as no difference in the elongation index was detectable in Coro1B knockdown cells compared to control cells. TEER analysis confirmed that spreading was unaffected after knockdown of Coro1B. These results are in contrast to observations of a previous study, which showed that Coro1B regulated the shape of HEK and T-cells, indicating that Coro1B might regulate cell morphology in a cell type specific manner[77]. Measurement of TEER showed that monolayer integrity was not impaired in Coro1B knockdown cells. These results

show that Coro1B was not necessary for the regulation of EC spreading and monolayer formation. Here, the loss of Coro1B may have been compensated by another type I coronin, which is in line with a previous report that regulatory actions in Coro1B-deficient cells could be exerted by other type I coronins[77]. A previous study supposed that Coro1A compensate for the function of Coro1B in T-lymphocytes[77]. As Coro1A was not detectable in ECs, an assumption would be that in ECs, Coro1C exerted the function of Coro1B. As mentioned above, further double knockdown experiments of Coro1B and Coro1C are necessary to address this issue.

Coro1B regulates cell migration in several cell types including fibroblasts, VSMC and ECs[124,128,130,132]. In the present study, analysis of migration behavior revealed that migration velocity was not impaired in Coro1B knockdown ECs[103]. Previous studies described that PDGF (in VSMC) and VEGF (in HUVECs) phosphorylates Coro1B at ser2, which resulted in dissociation from the Arp2/3 complex. As a consequence migration was induced[128,132]. VEGF-induced migration was increased in Coro1B-deficient HUVECs[128]. In the absence of VEGF, no effect on migration was detectable in Coro1B knockdown HUVECs in this study. A hypothesis could be that VEGF also phosphorylated Coro1C which leads to an increased migration of Coro1B-deficient HUVECs. Whereas unphosphorylated Coro1C is still able to negatively regulate Arp2/3 complex function and may compensate for the loss of Coro1B. The fact that Coro1C localized at the site of active actin dynamics and is known to negatively regulate cell migration in epithelial cells, reinforces this hypothesis[123]. Depletion of Coro1C results in an increased number of FAs, which are important for cell motility[123]. This observation suggests that Coro1C compensates for the loss of Coro1B by regulating migration through FAs, when Coro1B is not present. This could explain why no loss of function was detectable in Coro1B knockdown ECs. Previous studies showed that Coro1C mediated tumor cell migration[164]. The assembly of branched actin network by the Arp2/3 complex was required for MMP traffic[165]. Coro1C is important for tumor cell motility by regulating invadopodia formation and MMP traffic, which mediate the proteolytic degradation of the ECM[9]. Via this mechanism Coro1C promotes metastasis of breast cancer[164,165]. Moreover, Coro1C expression in diffuse gliomas and gastric cancer was found to be related to the grade of malignancy[166,167]. Based on the hypothesis that Coro1C compensated for the loss of Coro1B with overlapping functions, it would be of great interest to investigate whether Coro1B plays a role for tumor cell motility.

Although the absence of Coro1B did not affect EC migration and monolayer formation, Coro1B was critical for angiogenesis *in vitro*. The matrigel matrix is rich in ECM proteins simulating a physiologically relevant microenvironment[21,23]. Knockdown of Coro1B led to a significant reduction of the average length of branches compared to control cells[103]. The total number of branches was not affected in Coro1B knockdown cells indicating that the initial formation of branches in Coro1B knockdown cells is not impaired. Analysis demonstrated a significantly higher number of unconnected branches in Coro1B knockdown cells and a lower number of master segments compared to control cells[103]. The fact that more unconnected branches and less master segments were observed in Coro1B knockdown cells only at a later time point indicates that the branches lost their connection over time. These results suggest that Coro1B was not necessary for the initial formation of tubes but for their stability. Proliferation and apoptosis assays revealed that the observed angiogenic defects were not caused by impaired cell proliferation or cell survival. Interestingly, Coro1C was not able to compensate for the loss of Coro1B during *in vitro* angiogenesis suggesting that Coro1B and Coro1C might have distinct functions during vessel formation.

6.3 Coro1B interactome in ECs

To decipher how Coro1B mechanistically regulates *in vitro* angiogenesis, the Coro1B interactome in ECs was analyzed. Mass spectrometry analysis revealed an interaction of Coro1B with several isoforms of actin, which was expected, as Coro1B is a known to bind F-actin[103,114]. Moreover, mass spectrometry analysis confirmed the interaction of Coro1B and the Arp2/3 complex in ECs[103,130]. The identification of several subunits of the Arp2/3 complex and several isoforms of actin as Coro1B interaction partners showed that the co-immunoprecipitation with following mass spectrometry analysis was successful.

Moreover, the known Coro1B interacting partner cofilin and the new interacting partner gelsolin could be detected[124,127]. Cofilin and gelsolin limit F-actin turnover and are thereby involved in the regulation of lamellipodia dynamics[168-171]. It is well described that Coro1B interacts with cofilin and regulates its activity via SSHL at the leading edge of migrating fibroblasts[124]. The identification of cofilin and gelsolin as Coro1B interacting partners supports the assumption that Coro1B might also play a role in the regulation of lamellipodia dynamics in ECs. As cofilin has been shown to regulate remodeling and permeability of

epithelial junctions, the Coro1B / cofilin interaction might be also involved in the remodeling of endothelial cell-cell junctions[169].

In epithelial cells, it has been shown that Coro1B interacts with E-cadherin[135,172]. In ECs, cell-cell junctions are mediated by VEcad. Therefore, a potential interaction of VEcad and Coro1B was of interest[83,86]. However, we did not detect VEcad or other known cell-cell junction proteins in the mass spectrometry analysis suggesting no direct interaction with Coro1B. As immunofluorescence staining showed that Coro1B and VEcad partially colocalized at cell-cell junctions Coro1B localization at cell-cell junctions may potentially only be transient.

Mass spectrometry analysis also revealed the interaction of Coro1B and Coro1C, which showed the similar structure of type I coronins. These findings could indicate an involvement of both molecules in the same molecular networks and pathways in ECs supporting the idea that they can compensate for the loss of the other. This might be a reason why Coro1C was able to compensate for the loss of Coro1B in some processes. However, data of an *in vitro* angiogenesis model in the present study showed that knockdown of Coro1B impaired tube stability. Thus, Coro1B might regulate additional angiogenic processes where Coro1C is not involved. Although, Coro1B and Coro1C have overlapping functions there are also differences.

Moreover, we identified ILK as a new interaction partner of Coro1B[103]. ILK is a key regulator of cell-cell junctions in epithelial cells[173]. Unlike AJs in ECs, AJ in epithelial cells are much less dynamic since they belong to the stable barrier[84]. As α-parvin is crucial to maintain structural junction integrity in ECs, the other two proteins of the IPP complex ILK and PINCH could also have a function in regulating endothelial cell-cell junctions[14,173]. As the central component of the IPP complex, ILK binds to parvin and PINCH and is an important mediator of integrin signaling[43,63]. ILK has been shown to be important for regulation the EC function and blood vessel homeostasis[157,174]. Therefore, ILK was of particular interest. Co-immunoprecipitation with following western blot analysis confirmed the interaction of Coro1B and ILK[103]. Unfortunately, immunofluorescence staining of ILK in ECs was never successfully published due to lack of functional ILK antibodies. Accordingly, in our study ILK staining of ECs was not

successful. In migrating fibroblasts Coro1B also localizes at the leading edge[130]. Therefore, fibroblasts were used to study the colocalization of Coro1B and ILK. Immunofluorescence staining showed that Coro1B was not present at FA but demonstrated a colocalization of Coro1B and ILK at FXs at the leading edge of lamellipodia[103]. These findings lead to the assumption that Coro1B and ILK interact at FX[103]. The role of the Coro1B / ILK interaction on EC migration and its relevance for the formation and rearrangement of endothelial cell-cell junctions needs to be investigated in further experiments. Previous studies showed that ILK is important for blood vessel homeostasis[174]. Loss of ILK leads to impaired blood vessel formation[175]. For this reason, the interaction of Coro1B and ILK during sprouting angiogenesis would be of major interest. Moreover, a potential involvement of Coro1B / ILK interaction in tumor growth would be of future interest, as increased levels of ILK are found in various tumors[176].

Immunofluorescence staining exhibited a colocalization of Coro1B-EGFP and α-parvin in ECs as well as in fibroblasts at FXs[103]. However, α-parvin was not identified as a Coro1B interacting partner in the mass spectrometry analysis suggesting that Coro1B and α-parvin might interact through ILK. Based on the fact that ILK as the central component of the IPP-complex is bound to parvin and PINCH and mass spectrometry analysis exhibits ILK as a Coro1B interacting partner[61,103]. However, Coro1B did not localize at FAs whereas the IPP complex is mainly found at FAs. Therefore, we conclude Coro1B and the IPP complex interact exclusively at FXs before FAs are formed.

Additionally, mass spectrometry identified the actin binding protein tropomodulin-3 (TMOD3) and the cysteine-rich intestinal protein 2 (CRIP2) as Coro1B interacting partners. Both proteins play a role during angiogenesis. In ECs, TMOD3 is present at the leading edge of lamellipodia but unlike the Arp2/3 complex, TMOD3 is a negative regulator of cell migration in ECs[177,178]. Moreover, TMOD3 is involved in vessel formation as the inhibition of TMOD3 promotes angiogenesis[179]. CRIP2 is also known to regulate angiogenesis during tumor growth[180]. The data showed that Coro1B was required for blood vessel formation/maintenance as well[103]. For that reason, further knockdown experiments would be of interest to elucidate how Coro1B interacts with TMOD3 or CRIP2 during vessel formation.

Mass spectrometry analysis identified potential Coro1B interacting partners in ECs but gives only indirect information about their interaction during tube formation or cell-cell junction remodeling. To understand the role of Coro1B in the formation and maintenance of blood vessels and its interaction with potential binding partners, further experiments are required. Western blot analysis of Coro1B knockdown cells could show if expression of the identified protein is impaired by the downregulation of Coro1B. Additionally, immunofluorescence staining would demonstrate if the absence of Coro1B affects the localization of the potential interacting protein. Further knockdown experiments are needed to address if the downregulation of the protein has an effect on tube formation or cell-cell junction remodeling.

6.4 The zebrafish as an angiogenesis model

As the zebrafish is well-established model to study angiogenesis, a Coro1B KO fish was generated[181]. In contrast to Coro1B KO animals, Coro1A knockout mice have been comprehensively characterized. As Coro1A is mainly expressed in hematopoietic cells, it has been investigated in neutrophils, lymphocytes, macrophages and mast cells[120-122]. The only described Coro1B knockout mouse is a Coro1A / Coro1B double knockout. A mast cell degranulation defect was found in these particular animals[122].

The zebrafish represents a powerful model to study *in vivo* angiogenesis. Its rapid embryonic development and the optical transparency of zebrafish embryos allow to analyze the mechanisms of vascular development[28,29,182]. Therefore, a constitutive knockout of the Coro1B protein in zebrafish was generated using the CRISPR / Cas9 technology[145]. In contrast to morpholinos, the advantage of the CRISPR / Cas9 technology for loss of function studies is complete and heritable genome modifications. Thereby, CRISPR / Cas9 technology allows analysis in later stages of development, whereas a morpholinos induced knockdown would be transient[183]. Western blot analysis confirmed that the generated fish line did not express the Coro1B protein. No obvious defects in breeding behavior and development were detectable between KO and control animals. This could be explained by a potential compensation for the loss of Coro1B by Coro1C. Whether Coro1C can take over Coro1B functions in Coro1B knockout fish, could be studied by targeting Coro1C using morpholino antisense oligomers in Coro1B knockout fish. However, the presence of two orthologous of

Coro1C in zebrafish makes targeting Coro1C challenging. A tool to gain further insights into the role of Coro1B and Coro1C during vascular development could be the generation of a Coro1B / Coro1C double knockout zebrafish.

Generated Coro1B knockout fish were crossed with a flk1:mCherry zebrafish line, which allows live imaging of the developing vasculature due to constitutive expression of a red fluorescent protein in the endothelium. In preliminary data the area of different vessels and the number of connected and unconnected branches was analyzed in images of Coro1B$^{-/-}$-flk1:mCherry$^{+/+}$ and Coro1B^{wt}-flk1:mCherry$^{+/+}$ fish 30 hpf. No defects were observed in the developing vasculature of homozygous Coro1B KO fish until 30 hpf compared to wild type fish. These findings need to be verified by analyzing a greater amount of fish. If Coro1B knockout zebrafish expressing flk1:mCherry show similar defects in vessel stability as observed *in vitro* will need to be analyzed in further experiments.

In summary, the present study showed that Coro1B is dispensable for EC migration. However, the findings of this study suggest that Coro1B plays an important role in the regulation of endothelial cell–cell junction and also for the formation and maintenance of blood vessels[103]. Further experiments are necessary to address the function of Coro1B during sprouting angiogenesis, endothelial barrier function and blood vessel permeability *in vivo*[103].

7. References

1. Potente M, Mäkinen T. Vascular heterogeneity and specialization in development and disease. Nature reviews. Molecular cell biology. 2017;18:477-494.

2. Eelen G, de Zeeuw P, Simons M, Carmeliet P. Endothelial cell metabolism in normal and diseased vasculature. Circ. Res. 2015;116:1231-1244.

3. Herbert SP, Stainier DY. Molecular control of endothelial cell behaviour during blood vessel morphogenesis. Nat. Rev. Mol. Cell Biol. 2011;12:551-564.

4. Carmeliet P, Jain RK. Molecular mechanisms and clinical applications of angiogenesis. Nature. 2011;473:298-307.

5. Phng LK, Gerhardt H. Angiogenesis: a team effort coordinated by notch. Dev. Cell. 2009;16:196-208.

6. Aspelund A, Robciuc MR, Karaman S, Makinen T, Alitalo K. Lymphatic System in Cardiovascular Medicine. Circulation research. 2016;118:515-530.

7. Adams RH, Alitalo K. Molecular regulation of angiogenesis and lymphangiogenesis. Nat. Rev. Mol. Cell Biol. 2007;8:464-478.

8. Gaengel K, Genove G, Armulik A, Betsholtz C. Endothelial-mural cell signaling in vascular development and angiogenesis. Arterioscler. Thromb. Vasc. Biol. 2009;29:630-638.

9. Potente M, Gerhardt H, Carmeliet P. Basic and therapeutic aspects of angiogenesis. Cell. 2011;146:873-887.

10. Carmeliet P. Angiogenesis in health and disease. Nat. Med. 2003;9:653-660.

11. Swift MR, Weinstein BM. Arterial-venous specification during development. Circ. Res. 2009;104:576-588.

12. Gerhardt H, Golding M, Fruttiger M, Ruhrberg C, Lundkvist A, Abramsson A, Jeltsch M, Mitchell C, Alitalo K, Shima D, Betsholtz C. VEGF guides angiogenic sprouting utilizing endothelial tip cell filopodia. J. Cell Biol. 2003;161:1163-1177.

13. Blanco R, Gerhardt H. VEGF and Notch in tip and stalk cell selection. Cold Spring Harb. Perspect. Med. 2013;3:a006569.

14. Fraccaroli A, Pitter B, Taha AA, Seebach J, Huveneers S, Kirsch J, Casaroli-Marano RP, Zahler S, Pohl U, Gerhardt H, Schnittler H-J, Montanez E. Endothelial alpha-parvin controls integrity of developing vasculature and is required for maintenance of cell-cell junctions. Circulation research. 2015;117:29-40.

15. Seano G, Chiaverina G, Gagliardi PA, di Blasio L, Puliafito A, Bouvard C, Sessa R, Tarone G, Sorokin L, Helley D, Jain RK, Serini G, Bussolino F, Primo L. Endothelial

podosome rosettes regulate vascular branching in tumour angiogenesis. Nat Cell Biol. 2014;16:931-941, 931-938.

16. Dufraine J, Funahashi Y, Kitajewski J. Notch signaling regulates tumor angiogenesis by diverse mechanisms. Oncogene. 2008;27:5132-5137.

17. Claxton S, Fruttiger M. Periodic Delta-like 4 expression in developing retinal arteries. Gene Expr Patterns. 2004;5:123-127.

18. Jakobsson L, Franco CA, Bentley K, Collins RT, Ponsioen B, Aspalter IM, Rosewell I, Busse M, Thurston G, Medvinsky A, Schulte-Merker S, Gerhardt H. Endothelial cells dynamically compete for the tip cell position during angiogenic sprouting. Nat. Cell Biol. 2010;12:943-953.

19. Harrington LS, Sainson RC, Williams CK, Taylor JM, Shi W, Li JL, Harris AL. Regulation of multiple angiogenic pathways by Dll4 and Notch in human umbilical vein endothelial cells. Microvasc. Res. 2008;75:144-154.

20. Weinmaster G. Notch signaling: direct or what? Curr. Opin. Genet. Dev. 1998;8:436-442.

21. Fang Y, Eglen RM. Three-Dimensional Cell Cultures in Drug Discovery and Development. SLAS discovery : advancing life sciences R & D. 2017;22:456-472.

22. Montanez E, Casaroli-Marano RP, Vilaro S, Pagan R. Comparative study of tube assembly in three-dimensional collagen matrix and on Matrigel coats. Angiogenesis. 2002;5:167-172.

23. Staton CA, Stribbling SM, Tazzyman S, Hughes R, Brown NJ, Lewis CE. Current methods for assaying angiogenesis in vitro and in vivo. Int. J. Exp. Pathol. 2004;85:233-248.

24. Lawley TJ, Kubota Y. Induction of morphologic differentiation of endothelial cells in culture. J Invest Dermatol. 1989;93:59s-61s.

25. Eilken HM, Adams RH. Dynamics of endothelial cell behavior in sprouting angiogenesis. Curr. Opin. Cell Biol. 2010;22:617-625.

26. Uemura A, Kusuhara S, Katsuta H, Nishikawa S. Angiogenesis in the mouse retina: a model system for experimental manipulation. Exp. Cell Res. 2006;312:676-683.

27. Fruttiger M. Development of the retinal vasculature. Angiogenesis. 2007;10:77-88.

28. Geudens I, Gerhardt H. Coordinating cell behaviour during blood vessel formation. Development. 2011;138:4569-4583.

29. Vogel AM, Weinstein BM. Studying vascular development in the zebrafish. Trends Cardiovasc. Med. 2000;10:352-360.

30. Lawson ND, Weinstein BM. In vivo imaging of embryonic vascular development using transgenic zebrafish. Dev. Biol. 2002;248:307-318.

31. Jin SW, Beis D, Mitchell T, Chen JN, Stainier DY. Cellular and molecular analyses of vascular tube and lumen formation in zebrafish. Development. 2005;132:5199-5209.

32. Torres-Vazquez J, Kamei M, Weinstein BM. Molecular distinction between arteries and veins. Cell Tissue Res. 2003;314:43-59.

33. Quinn TP, Peters KG, De Vries C, Ferrara N, Williams LT. Fetal liver kinase 1 is a receptor for vascular endothelial growth factor and is selectively expressed in vascular endothelium. Proc. Natl. Acad. Sci. U. S. A. 1993;90:7533-7537.

34. Liang D, Chang JR, Chin AJ, Smith A, Kelly C, Weinberg ES, Ge R. The role of vascular endothelial growth factor (VEGF) in vasculogenesis, angiogenesis, and hematopoiesis in zebrafish development. Mech. Dev. 2001;108:29-43.

35. Siekmann AF, Covassin L, Lawson ND. Modulation of VEGF signalling output by the Notch pathway. Bioessays. 2008;30:303-313.

36. Senger DR, Davis GE. Angiogenesis. Cold Spring Harb Perspect Biol. 2011;3:a005090.

37. Schwarz US, Gardel ML. United we stand: integrating the actin cytoskeleton and cell-matrix adhesions in cellular mechanotransduction. J Cell Sci. 2012;125:3051-3060.

38. Hynes RO. Cell-matrix adhesion in vascular development. Journal of thrombosis and haemostasis : JTH. 2007;5 Suppl 1:32-40.

39. Anderson LR, Owens TW, Naylor MJ. Structural and mechanical functions of integrins. Biophys Rev. 2014;6:203-213.

40. Saharinen P, Ivaska J. Blocking integrin inactivation as an anti-angiogenic therapy. EMBO J. 2015;34:1293-1295.

41. Takada Y, Ye X, Simon S. The integrins. Genome Biol. 2007;8:215.

42. Hynes RO. Integrins: bidirectional, allosteric signaling machines. Cell. 2002;110:673-687.

43. Legate KR, Montanez E, Kudlacek O, Fässler R. ILK, PINCH and parvin: the tIPP of integrin signalling. Nat. Rev. Mol. Cell Biol. 2006;7:20-31.

44. Luo BH, Carman CV, Springer TA. Structural basis of integrin regulation and signaling. Annu. Rev. Immunol. 2007;25:619-647.

45. Fan Z, McArdle S, Marki A, Mikulski Z, Gutierrez E, Engelhardt B, Deutsch U, Ginsberg M, Groisman A, Ley K. Neutrophil recruitment limited by high-affinity bent beta2 integrin binding ligand in cis. Nature communications. 2016;7:12658.

46. Hu P,Luo BH. Integrin bi-directional signaling across the plasma membrane. J. Cell. Physiol. 2013;228:306-312.

47. Takagi J, Petre BM, Walz T, Springer TA. Global conformational rearrangements in integrin extracellular domains in outside-in and inside-out signaling. Cell. 2002;110:599-511.

48. Xiong JP, Stehle T, Diefenbach B, Zhang R, Dunker R, Scott DL, Joachimiak A, Goodman SL, Arnaout MA. Crystal structure of the extracellular segment of integrin alpha Vbeta3. Science. 2001;294:339-345.

49. Moser M, Legate KR, Zent R, Fässler R. The tail of integrins, talin, and kindlins. Science. 2009;324:895-899.

50. Brakebusch C, Fässler R. The integrin-actin connection, an eternal love affair. EMBO J. 2003;22:2324-2333.

51. Hotulainen P, Lappalainen P. Stress fibers are generated by two distinct actin assembly mechanisms in motile cells. J. Cell Biol. 2006;173:383-394.

52. Hirata H, Tatsumi H, Sokabe M. Dynamics of actin filaments during tension-dependent formation of actin bundles. Biochim. Biophys. Acta. 2007;1770:1115-1127.

53. Pankov R, Cukierman E, Katz BZ, Matsumoto K, Lin DC, Lin S, Hahn C, Yamada KM. Integrin dynamics and matrix assembly: tensin-dependent translocation of alpha(5)beta(1) integrins promotes early fibronectin fibrillogenesis. J. Cell Biol. 2000;148:1075-1090.

54. Geiger B, Yamada KM. Molecular architecture and function of matrix adhesions. Cold Spring Harb. Perspect. Biol. 2011;3:

55. Murphy DA, Courtneidge SA. The 'ins' and 'outs' of podosomes and invadopodia: characteristics, formation and function. Nat Rev Mol Cell Biol. 2011;12:413-426.

56. Calle Y, Chou HC, Thrasher AJ, Jones GE. Wiskott-Aldrich syndrome protein and the cytoskeletal dynamics of dendritic cells. J. Pathol. 2004;204:460-469.

57. Moreau V, Tatin F, Varon C, Genot E. Actin can reorganize into podosomes in aortic endothelial cells, a process controlled by Cdc42 and RhoA. Mol. Cell. Biol. 2003;23:6809-6822.

58. Osiak AE, Zenner G, Linder S. Subconfluent endothelial cells form podosomes downstream of cytokine and RhoGTPase signaling. Exp. Cell Res. 2005;307:342-353.

59. Buccione R, Orth JD, McNiven MA. Foot and mouth: podosomes, invadopodia and circular dorsal ruffles. Nat. Rev. Mol. Cell Biol. 2004;5:647-657.

60. Pitter B, Werner AC, Montanez E. Parvins Are Required for Endothelial Cell-Cell Junctions and Cell Polarity During Embryonic Blood Vessel Formation. Arterioscler. Thromb. Vasc. Biol. 2018;38:1147-1158.

61. Montanez E, Wickstrom SA, Altstatter J, Chu H, Fässler R. Alpha-parvin controls vascular mural cell recruitment to vessel wall by regulating RhoA/ROCK signalling. EMBO J. 2009;28:3132-3144.

62. Xu H, Cao H, Xiao G. Signaling via PINCH: Functions, binding partners and implications in human diseases. Gene. 2016;594:10-15.

63. Wickstrom SA, Lange A, Montanez E, Fässler R. The ILK/PINCH/parvin complex: the kinase is dead, long live the pseudokinase! EMBO J. 2010;29:281-291.

64. Edwards M, Zwolak A, Schafer DA, Sept D, Dominguez R, Cooper JA. Capping protein regulators fine-tune actin assembly dynamics. Nat. Rev. Mol. Cell Biol. 2014;15:677-689.

65. Phng LK, Gebala V, Bentley K, Philippides A, Wacker A, Mathivet T, Sauteur L, Stanchi F, Belting HG, Affolter M, Gerhardt H. Formin-mediated actin polymerization at endothelial junctions is required for vessel lumen formation and stabilization. Dev. Cell. 2015;32:123-132.

66. Pollard TD, Borisy GG. Cellular motility driven by assembly and disassembly of actin filaments. Cell. 2003;112:453-465.

67. Mattila PK, Lappalainen P. Filopodia: molecular architecture and cellular functions. Nat. Rev. Mol. Cell Biol. 2008;9:446-454.

68. Huber AB, Kolodkin AL, Ginty DD, Cloutier JF. Signaling at the growth cone: ligand-receptor complexes and the control of axon growth and guidance. Annu. Rev. Neurosci. 2003;26:509-563.

69. Heasman SJ, Ridley AJ. Mammalian Rho GTPases: new insights into their functions from in vivo studies. Nat. Rev. Mol. Cell Biol. 2008;9:690-701.

70. Ridley AJ. Rho GTPases and cell migration. J. Cell Sci. 2001;114:2713-2722.

71. Lundquist EA. Small GTPases. WormBook. 2006;1-18.

72. Sit ST, Manser E. Rho GTPases and their role in organizing the actin cytoskeleton. J. Cell Sci. 2011;124:679-683.

73. van Nieuw Amerongen GP, van Hinsbergh VW. Cytoskeletal effects of rho-like small guanine nucleotide-binding proteins in the vascular system. Arterioscler. Thromb. Vasc. Biol. 2001;21:300-311.

74. Fryer BH, Field J. Rho, Rac, Pak and angiogenesis: old roles and newly identified responsibilities in endothelial cells. Cancer Lett. 2005;229:13-23.

75. Small JV, Stradal T, Vignal E, Rottner K. The lamellipodium: where motility begins. Trends Cell Biol. 2002;12:112-120.

76. Ridley AJ. Rho GTPase signalling in cell migration. Curr. Opin. Cell Biol. 2015;36:103-112.

77. Ojeda V, Castro-Castro A, Bustelo XR. Coronin1 proteins dictate rac1 intracellular dynamics and cytoskeletal output. Mol. Cell. Biol. 2014;34:3388-3406.

78. Wojciak-Stothard B, Ridley AJ. Rho GTPases and the regulation of endothelial permeability. Vascul. Pharmacol. 2002;39:187-199.

79. Sander EE, ten Klooster JP, van Delft S, van der Kammen RA, Collard JG. Rac downregulates Rho activity: reciprocal balance between both GTPases determines cellular morphology and migratory behavior. J. Cell Biol. 1999;147:1009-1022.

80. Ridley AJ, Hall A. The small GTP-binding protein rho regulates the assembly of focal adhesions and actin stress fibers in response to growth factors. Cell. 1992;70:389-399.

81. Cao J, Schnittler H. Putting VE-cadherin into JAIL for junction remodeling. J. Cell Sci. 2019;132:

82. Bazzoni G, Dejana E. Endothelial cell-to-cell junctions: molecular organization and role in vascular homeostasis. Physiol. Rev. 2004;84:869-901.

83. Dejana E, Tournier-Lasserve E, Weinstein BM. The control of vascular integrity by endothelial cell junctions: molecular basis and pathological implications. Dev. Cell. 2009;16:209-221.

84. Dejana E. Endothelial cell-cell junctions: happy together. Nat. Rev. Mol. Cell Biol. 2004;5:261-270.

85. Suzuki S, Sano K, Tanihara H. Diversity of the cadherin family: evidence for eight new cadherins in nervous tissue. Cell Regul. 1991;2:261-270.

86. Giannotta M, Trani M, Dejana E. VE-cadherin and endothelial adherens junctions: active guardians of vascular integrity. Dev. Cell. 2013;26:441-454.

87. Ghitescu L, Robert M. Diversity in unity: the biochemical composition of the endothelial cell surface varies between the vascular beds. Microsc Res Tech. 2002;57:381-389.

88. Breier G, Breviario F, Caveda L, Berthier R, Schnurch H, Gotsch U, Vestweber D, Risau W, Dejana E. Molecular cloning and expression of murine vascular endothelial-cadherin in early stage development of cardiovascular system. Blood. 1996;87:630-641.

89. Dejana E, Vestweber D. The role of VE-cadherin in vascular morphogenesis and permeability control. Prog. Mol. Biol. Transl. Sci. 2013;116:119-144.

90. Xiao K, Garner J, Buckley KM, Vincent PA, Chiasson CM, Dejana E, Faundez V, Kowalczyk AP. p120-Catenin regulates clathrin-dependent endocytosis of VE-cadherin. Mol. Biol. Cell. 2005;16:5141-5151.

91. Hartsock A, Nelson WJ. Adherens and tight junctions: structure, function and connections to the actin cytoskeleton. Biochim. Biophys. Acta. 2008;1778:660-669.

92. Beckers CM, van Hinsbergh VW,van Nieuw Amerongen GP. Driving Rho GTPase activity in endothelial cells regulates barrier integrity. Thromb. Haemost. 2010;103:40-55.

93. Sidibe A, Imhof BA. VE-cadherin phosphorylation decides: vascular permeability or diapedesis. Nat. Immunol. 2014;15:215-217.

94. Grazia Lampugnani M, Zanetti A, Corada M, Takahashi T, Balconi G, Breviario F, Orsenigo F, Cattelino A, Kemler R, Daniel TO, Dejana E. Contact inhibition of VEGF-induced proliferation requires vascular endothelial cadherin, beta-catenin, and the phosphatase DEP-1/CD148. J Cell Biol. 2003;161:793-804.

95. Hayashi M, Majumdar A, Li X, Adler J, Sun Z, Vertuani S, Hellberg C, Mellberg S, Koch S, Dimberg A, Koh GY, Dejana E, Belting HG, Affolter M, Thurston G, Holmgren L, Vestweber D, Claesson-Welsh L. VE-PTP regulates VEGFR2 activity in stalk cells to establish endothelial cell polarity and lumen formation. Nat Commun. 2013;4:1672.

96. Millan J, Cain RJ, Reglero-Real N, Bigarella C, Marcos-Ramiro B, Fernandez-Martin L, Correas I, Ridley AJ. Adherens junctions connect stress fibres between adjacent endothelial cells. BMC Biol. 2010;8:11.

97. Muller WA. Leukocyte-endothelial-cell interactions in leukocyte transmigration and the inflammatory response. Trends Immunol. 2003;24:327-334.

98. Fernandez-Martin L, Marcos-Ramiro B, Bigarella CL, Graupera M, Cain RJ, Reglero-Real N, Jimenez A, Cernuda-Morollon E, Correas I, Cox S, Ridley AJ, Millan J. Crosstalk between reticular adherens junctions and platelet endothelial cell adhesion molecule-1 regulates endothelial barrier function. Arterioscler. Thromb. Vasc. Biol. 2012;32:e90-102.

99. Vestweber D, Winderlich M, Cagna G,Nottebaum AF. Cell adhesion dynamics at endothelial junctions: VE-cadherin as a major player. Trends Cell Biol. 2009;19:8-15.

100. Seebach J, Taha AA, Lenk J, Lindemann N, Jiang X, Brinkmann K, Bogdan S, Schnittler HJ. The CellBorderTracker, a novel tool to quantitatively analyze spatiotemporal endothelial junction dynamics at the subcellular level. Histochem. Cell Biol. 2015;144:517-532.

101. Efimova N, Svitkina TM. Branched actin networks push against each other at adherens junctions to maintain cell-cell adhesion. J. Cell Biol. 2018;217:1827-1845.

102. Abu Taha A, Taha M, Seebach J, Schnittler HJ. ARP2/3-mediated junction-associated lamellipodia control VE-cadherin-based cell junction dynamics and maintain monolayer integrity. Mol. Biol. Cell. 2014;25:245-256.

103. Werner A-C, Weckbach LT, Salvermoser M, Pitter B, Cao J, Maier-Begandt D, Forné I, Schnittler H-J, Walzog B, Montanez E. Coronin 1B Controls Endothelial Actin Dynamics at Cell–Cell Junctions and Is Required for Endothelial Network Assembly. Frontiers in Cell and Developmental Biology. 2020;8:

104. Abu Taha A, Schnittler HJ. Dynamics between actin and the VE-cadherin/catenin complex: novel aspects of the ARP2/3 complex in regulation of endothelial junctions. Cell adhesion & migration. 2014;8:125-135.

105. Taha M, Aldirawi M, Marz S, Seebach J, Odenthal-Schnittler M, Bondareva O, Bojovic V, Schmandra T, Wirth B, Mietkowska M, Rottner K, Schnittler H. EPLIN-alpha and -beta Isoforms Modulate Endothelial Cell Dynamics through a Spatiotemporally Differentiated Interaction with Actin. Cell Rep. 2019;29:1010-1026.e1016.

106. Cao J, Ehling M, Marz S, Seebach J, Tarbashevich K, Sixta T, Pitulescu ME, Werner AC, Flach B, Montanez E, Raz E, Adams RH, Schnittler H. Polarized actin and VE-cadherin dynamics regulate junctional remodelling and cell migration during sprouting angiogenesis. Nature communications. 2017;8:2210.

107. Chan KT, Creed SJ, Bear JE. Unraveling the enigma: progress towards understanding the coronin family of actin regulators. Trends in cell biology. 2011;21:481-488.

108. Nakamura T, Takeuchi K, Muraoka S, Takezoe H, Takahashi N, Mori N. A neurally enriched coronin-like protein, ClipinC, is a novel candidate for an actin cytoskeleton-cortical membrane-linking protein. J. Biol. Chem. 1999;274:13322-13327.

109. de Hostos EL, Bradtke B, Lottspeich F, Guggenheim R, Gerisch G. Coronin, an actin binding protein of Dictyostelium discoideum localized to cell surface projections, has sequence similarities to G protein beta subunits. EMBO J. 1991;10:4097-4104.

110. Mishima M, Nishida E. Coronin localizes to leading edges and is involved in cell spreading and lamellipodium extension in vertebrate cells. J. Cell Sci. 1999;112 (Pt 17):2833-2842.

111. Appleton BA, Wu P, Wiesmann C. The crystal structure of murine coronin-1: a regulator of actin cytoskeletal dynamics in lymphocytes. Structure. 2006;14:87-96.

112. Goode BL, Wong JJ, Butty AC, Peter M, McCormack AL, Yates JR, Drubin DG, Barnes G. Coronin promotes the rapid assembly and cross-linking of actin filaments and may link the actin and microtubule cytoskeletons in yeast. J. Cell Biol. 1999;144:83-98.

113. Martorella M, Barford K, Winkler B, Deppmann CD. Emergent Role of Coronin-1a in Neuronal Signaling. Vitam Horm. 2017;104:113-131.

114. Cai L, Makhov AM, Bear JE. F-actin binding is essential for coronin 1B function in vivo. J. Cell Sci. 2007;120:1779-1790.

115. Uetrecht AC, Bear JE. Coronins: the return of the crown. Trends Cell Biol. 2006;16:421-426.

116. Chen Y, Ip FC, Shi L, Zhang Z, Tang H, Ng YP, Ye WC, Fu AK, Ip NY. Coronin 6 regulates acetylcholine receptor clustering through modulating receptor anchorage to actin cytoskeleton. J. Neurosci. 2014;34:2413-2421.

117. Marshall TW, Aloor HL, Bear JE. Coronin 2A regulates a subset of focal-adhesion-turnover events through the cofilin pathway. J. Cell Sci. 2009;122:3061-3069.

118. Huang W, Ghisletti S, Saijo K, Gandhi M, Aouadi M, Tesz GJ, Zhang DX, Yao J, Czech MP, Goode BL, Rosenfeld MG, Glass CK. Coronin 2A mediates actin-dependent de-repression of inflammatory response genes. Nature. 2011;470:414-418.

119. Rybakin V, Stumpf M, Schulze A, Majoul IV, Noegel AA, Hasse A. Coronin 7, the mammalian POD-1 homologue, localizes to the Golgi apparatus. FEBS Lett. 2004;573:161-167.

120. Pick R, Begandt D, Stocker TJ, Salvermoser M, Thome S, Bottcher RT, Montanez E, Harrison U, Forne I, Khandoga AG, Coletti R, Weckbach LT, Brechtefeld D, Haas R, Imhof A, Massberg S, Sperandio M, Walzog B. Coronin 1A, a novel player in integrin biology, controls neutrophil trafficking in innate immunity. Blood. 2017;130:847-858.

121. Foger N, Rangell L, Danilenko DM, Chan AC. Requirement for coronin 1 in T lymphocyte trafficking and cellular homeostasis. Science. 2006;313:839-842.

122. Foger N, Jenckel A, Orinska Z, Lee KH, Chan AC, Bulfone-Paus S. Differential regulation of mast cell degranulation versus cytokine secretion by the actin regulatory proteins Coronin1a and Coronin1b. J. Exp. Med. 2011;208:1777-1787.

123. Samarin SN, Koch S, Ivanov AI, Parkos CA, Nusrat A. Coronin 1C negatively regulates cell-matrix adhesion and motility of intestinal epithelial cells. Biochem. Biophys. Res. Commun. 2010;391:394-400.

124. Cai L, Marshall TW, Uetrecht AC, Schafer DA, Bear JE. Coronin 1B coordinates Arp2/3 complex and cofilin activities at the leading edge. Cell. 2007;128:915-929.

125. Spoerl Z, Stumpf M, Noegel AA, Hasse A. Oligomerization, F-actin interaction, and membrane association of the ubiquitous mammalian coronin 3 are mediated by its carboxyl terminus. J. Biol. Chem. 2002;277:48858-48867.

126. Rosentreter A, Hofmann A, Xavier CP, Stumpf M, Noegel AA, Clemen CS. Coronin 3 involvement in F-actin-dependent processes at the cell cortex. Exp. Cell Res. 2007;313:878-895.

127. Howell M, Brickner H, Delorme-Walker VD, Choi J, Saffin JM, Miller D, Panopoulos A, DerMardirossian C, Fotedar A, Margolis RL, Fotedar R. WISp39 binds phosphorylated Coronin 1B to regulate Arp2/3 localization and Cofilin-dependent motility. J. Cell Biol. 2015;208:961-974.

128. Kim GY, Park JH, Kim H, Lim HJ, Park HY. Coronin 1B serine 2 phosphorylation by p38alpha is critical for vascular endothelial growth factor-induced migration of human umbilical vein endothelial cells. Cell. Signal. 2016;28:1817-1825.

129. Usatyuk PV, Burns M, Mohan V, Pendyala S, He D, Ebenezer DL, Harijith A, Fu P, Huang LS, Bear JE, Garcia JG, Natarajan V. Coronin 1B regulates S1P-induced human lung endothelial cell chemotaxis: role of PLD2, protein kinase C and Rac1 signal transduction. PLoS One. 2013;8:e63007.

130. Cai L, Holoweckyj N, Schaller MD, Bear JE. Phosphorylation of coronin 1B by protein kinase C regulates interaction with Arp2/3 and cell motility. J. Biol. Chem. 2005;280:31913-31923.

131. Cai L, Makhov AM, Schafer DA, Bear JE. Coronin 1B antagonizes cortactin and remodels Arp2/3-containing actin branches in lamellipodia. Cell. 2008;134:828-842.

132. Williams HC, San Martin A, Adamo CM, Seidel-Rogol B, Pounkova L, Datla SR, Lassegue B, Bear JE, Griendling K. Role of coronin 1B in PDGF-induced migration of vascular smooth muscle cells. Circ. Res. 2012;111:56-65.

133. Agnew BJ, Minamide LS, Bamburg JR. Reactivation of phosphorylated actin depolymerizing factor and identification of the regulatory site. J. Biol. Chem. 1995;270:17582-17587.

134. Bamburg JR, McGough A, Ono S. Putting a new twist on actin: ADF/cofilins modulate actin dynamics. Trends Cell Biol. 1999;9:364-370.

135. Michael M, Meiring JCM, Acharya BR, Matthews DR, Verma S, Han SP, Hill MM, Parton RG, Gomez GA, Yap AS. Coronin 1B Reorganizes the Architecture of F-Actin Networks for Contractility at Steady-State and Apoptotic Adherens Junctions. Dev. Cell. 2016;37:58-71.

136. Priya R, Wee K, Budnar S, Gomez GA, Yap AS, Michael M. Coronin 1B supports RhoA signaling at cell-cell junctions through Myosin II. Cell cycle (Georgetown, Tex.). 2016;15:3033-3041.

137. Rana MK, Worthylake RA. Novel mechanism for negatively regulating Rho-kinase (ROCK) signaling through Coronin1B protein in neuregulin 1 (NRG-1)-induced tumor cell motility. J. Biol. Chem. 2012;287:21836-21845.

138. Kawano Y, Fukata Y, Oshiro N, Amano M, Nakamura T, Ito M, Matsumura F, Inagaki M, Kaibuchi K. Phosphorylation of myosin-binding subunit (MBS) of myosin phosphatase by Rho-kinase in vivo. J. Cell Biol. 1999;147:1023-1038.

139. Montanez E, Piwko-Czuchra A, Bauer M, Li S, Yurchenco P, Fässler R. Analysis of integrin functions in peri-implantation embryos, hematopoietic system, and skin. Methods in enzymology. 2007;426:239-289.

140. Park J, Throop AL, LaBaer J. Site-specific recombinational cloning using gateway and in-fusion cloning schemes. Curr. Protoc. Mol. Biol. 2015;110:3.20.21-23.

141. Laemmli UK. Cleavage of structural proteins during the assembly of the head of bacteriophage T4. Nature. 1970;227:680-685.

142. Rothbauer U, Zolghadr K, Muyldermans S, Schepers A, Cardoso MC, Leonhardt H. A versatile nanotrap for biochemical and functional studies with fluorescent fusion proteins. Molecular & cellular proteomics : MCP. 2008;7:282-289.

143. Mullins MC, Hammerschmidt M, Haffter P, Nusslein-Volhard C. Large-scale mutagenesis in the zebrafish: in search of genes controlling development in a vertebrate. Current biology : CB. 1994;4:189-202.

144. Kimmel CB, Ballard WW, Kimmel SR, Ullmann B, Schilling TF. Stages of embryonic development of the zebrafish. Dev Dyn. 1995;203:253-310.

145. Hruscha A, Schmid B. Generation of zebrafish models by CRISPR /Cas9 genome editing. Methods in molecular biology (Clifton, N.J.). 2015;1254:341-350.

146. Cox J,Mann M. MaxQuant enables high peptide identification rates, individualized p.p.b.-range mass accuracies and proteome-wide protein quantification. Nat. Biotechnol. 2008;26:1367-1372.

147. Lampugnani MG, Corada M, Caveda L, Breviario F, Ayalon O, Geiger B, Dejana E. The molecular organization of endothelial cell to cell junctions: differential association of plakoglobin, beta-catenin, and alpha-catenin with vascular endothelial cadherin (VE-cadherin). J Cell Biol. 1995;129:203-217.

148. Seebach J, Cao J, Schnittler H. Quantitative dynamics of VE-cadherin at endothelial cell junctions at a glance: basic requirements and current concepts. Discoveries. 2016;4:e63.

149. Riedl J, Crevenna AH, Kessenbrock K, Yu JH, Neukirchen D, Bista M, Bradke F, Jenne D, Holak TA, Werb Z, Sixt M, Wedlich-Soldner R. Lifeact: a versatile marker to visualize F-actin. Nature methods. 2008;5:605-607.

150. Garrett JP, Lowery AM, Adam AP, Kowalczyk AP, Vincent PA. Regulation of endothelial barrier function by p120-cateninVE-cadherin interaction. Mol. Biol. Cell. 2017;28:85-97.

151. Uehata M, Ishizaki T, Satoh H, Ono T, Kawahara T, Morishita T, Tamakawa H, Yamagami K, Inui J, Maekawa M, Narumiya S. Calcium sensitization of smooth muscle mediated by a Rho-associated protein kinase in hypertension. Nature. 1997;389:990-994.

152. Pober JS, Sessa WC. Evolving functions of endothelial cells in inflammation. Nat. Rev. Immunol. 2007;7:803-815.

153. Mitra P, Keese CR, Giaever I. Electric measurements can be used to monitor the attachment and spreading of cells in tissue culture. Biotechniques. 1991;11:504-510.

154. Benson K, Cramer S, Galla HJ. Impedance-based cell monitoring: barrier properties and beyond. Fluids Barriers CNS. 2013;10:5.

155. Steinle H, Golombek S, Behring A, Schlensak C, Wendel HP, Avci-Adali M. Improving the Angiogenic Potential of EPCs via Engineering with Synthetic Modified mRNAs. Mol Ther Nucleic Acids. 2018;13:387-398.

156. Kim S, Han JH, Nam DH, Kim GY, Lim JH, Kim JR, Woo CH. PAR-1 is a novel mechano-sensor transducing laminar flow-mediated endothelial signaling. Sci. Rep. 2018;8:15172.

157. Friedrich EB, Liu E, Sinha S, Cook S, Milstone DS, MacRae CA, Mariotti M, Kuhlencordt PJ, Force T, Rosenzweig A, St-Arnaud R, Dedhar S, Gerszten RE. Integrin-linked kinase regulates endothelial cell survival and vascular development. Mol. Cell. Biol. 2004;24:8134-8144.

158. Hruscha A, Krawitz P, Rechenberg A, Heinrich V, Hecht J, Haass C, Schmid B. Efficient CRISPR/Cas9 genome editing with low off-target effects in zebrafish. Development. 2013;140:4982-4987.

159. Wang Y, Jin G, Miao H, Li JY, Usami S, Chien S. Integrins regulate VE-cadherin and catenins: dependence of this regulation on Src, but not on Ras. Proc. Natl. Acad. Sci. U. S. A. 2006;103:1774-1779.

160. Schnittler H. Contraction of endothelial cells: 40 years of research, but the debate still lives. Histochem. Cell Biol. 2016;146:651-656.

161. Paatero I, Sauteur L, Lee M, Lagendijk AK, Heutschi D, Wiesner C, Guzman C, Bieli D, Hogan BM, Affolter M, Belting HG. Junction-based lamellipodia drive endothelial cell rearrangements in vivo via a VE-cadherin-F-actin based oscillatory cell-cell interaction. Nature communications. 2018;9:3545.

162. Vestweber D. How leukocytes cross the vascular endothelium. Nat. Rev. Immunol. 2015;15:692-704.

163. Hall A. Rho GTPases and the control of cell behaviour. Biochem. Soc. Trans. 2005;33:891-895.

164. Shao J, Zhang H, Wang Z. Coronin 1c and F-actin Promote Metastasis of Breast Cancer. Med. Sci. Monit. 2018;24:5980-5987.

165. Castagnino A, Castro-Castro A, Irondelle M, Guichard A, Lodillinsky C, Fuhrmann L, Vacher S, Aguera-Gonzalez S, Zagryazhskaya-Masson A, Romao M, El Kesrouani C, Noegel AA, Dubois T, Raposo G, Bear JE, Clemen CS, Vincent-Salomon A, Bieche I, Chavrier P. Coronin 1C promotes triple-negative breast cancer invasiveness through regulation of MT1-MMP traffic and invadopodia function. Oncogene. 2018;37:6425-6441.

166. Thal D, Xavier CP, Rosentreter A, Linder S, Friedrichs B, Waha A, Pietsch T, Stumpf M, Noegel A, Clemen C. Expression of coronin-3 (coronin-1C) in diffuse gliomas is related to malignancy. J. Pathol. 2008;214:415-424.

167. Cheng X, Wang X, Wu Z, Tan S, Zhu T, Ding K. CORO1C expression is associated with poor survival rates in gastric cancer and promotes metastasis in vitro. FEBS open bio. 2019;9:1097-1108.

168. Dawe HR, Minamide LS, Bamburg JR, Cramer LP. ADF/cofilin controls cell polarity during fibroblast migration. Current biology : CB. 2003;13:252-257.

169. Wang D, Naydenov NG, Feygin A, Baranwal S, Kuemmerle JF, Ivanov AI. Actin-Depolymerizing Factor and Cofilin-1 Have Unique and Overlapping Functions in Regulating Intestinal Epithelial Junctions and Mucosal Inflammation. Am. J. Pathol. 2016;186:844-858.

170. Gremm D, Wegner A. Gelsolin as a calcium-regulated actin filament-capping protein. Eur. J. Biochem. 2000;267:4339-4345.

171. Mazur AJ, Gremm D, Dansranjavin T, Litwin M, Jockusch BM, Wegner A, Weeds AG, Mannherz HG. Modulation of actin filament dynamics by actin-binding proteins residing in lamellipodia. Eur. J. Cell Biol. 2010;89:402-413.

172. Guo Z, Neilson LJ, Zhong H, Murray PS, Zanivan S, Zaidel-Bar R. E-cadherin interactome complexity and robustness resolved by quantitative proteomics. Science signaling. 2014;7:rs7.

173. Vespa A, D'Souza SJ, Dagnino L. A novel role for integrin-linked kinase in epithelial sheet morphogenesis. Mol. Biol. Cell. 2005;16:4084-4095.

174. Park H, Yamamoto H, Mohn L, Ambuhl L, Kanai K, Schmidt I, Kim KP, Fraccaroli A, Feil S, Junge HJ, Montanez E, Berger W, Adams RH. Integrin-linked kinase controls retinal angiogenesis and is linked to Wnt signaling and exudative vitreoretinopathy. Nature communications. 2019;10:5243.

175. Tan C, Cruet-Hennequart S, Troussard A, Fazli L, Costello P, Sutton K, Wheeler J, Gleave M, Sanghera J, Dedhar S. Regulation of tumor angiogenesis by integrin-linked kinase (ILK). Cancer Cell. 2004;5:79-90.

176. Hannigan G, Troussard AA, Dedhar S. Integrin-linked kinase: a cancer therapeutic target unique among its ILK. Nat. Rev. Cancer. 2005;5:51-63.

177. Fischer RS, Fritz-Six KL, Fowler VM. Pointed-end capping by tropomodulin3 negatively regulates endothelial cell motility. J. Cell Biol. 2003;161:371-380.

178. Yamashiro S, Gokhin DS, Kimura S, Nowak RB, Fowler VM. Tropomodulins: pointed-end capping proteins that regulate actin filament architecture in diverse cell types. Cytoskeleton (Hoboken, N.J.). 2012;69:337-370.

179. Liu CH, Wang Z, Huang S, Sun Y, Chen J. MicroRNA-145 Regulates Pathological Retinal Angiogenesis by Suppression of TMOD3. Molecular therapy. Nucleic acids. 2019;16:335-347.

180. Cheung AK, Ko JM, Lung HL, Chan KW, Stanbridge EJ, Zabarovsky E, Tokino T, Kashima L, Suzuki T, Kwong DL, Chua D, Tsao SW, Lung ML. Cysteine-rich intestinal protein 2 (CRIP2) acts as a repressor of NF-kappaB-mediated proangiogenic cytokine transcription to suppress tumorigenesis and angiogenesis. Proc. Natl. Acad. Sci. U. S. A. 2011;108:8390-8395.

181. Gore AV, Monzo K, Cha YR, Pan W, Weinstein BM. Vascular development in the zebrafish. Cold Spring Harb Perspect Med. 2012;2:a006684.

182. Schmid B, Haass C. Genomic editing opens new avenues for zebrafish as a model for neurodegeneration. J Neurochem. 2013;127:461-470.

183. Ablain J, Durand EM, Yang S, Zhou Y, Zon LI. A CRISPR/Cas9 vector system for tissue-specific gene disruption in zebrafish. Dev. Cell. 2015;32:756-764.

8. Acknowledgments

This work could not have been completed without the support from several people.

I would like to especially thank Prof. Dr. Jörg Renkawitz for his support, time and advice.
I would also like to express my special appreciation and thanks to my advisor Prof. Dr. Eloi Montañez for his excellent supervision and support. Even from abroad, he always had time for my questions and scientific discussions. Thanks Eloi, for your motivation, advise and support over the whole time of my PhD.

Furthermore, I would like to acknowledge Prof. Barbara Walzog for her support and to enable excellent working conditions. I appreciate the help of her and Dr. Ludwig Weckbach through which I was able to stay at the institute for a year after my PhD.

I am grateful to Prof. Dr. Christoph Scheiermann and Dr. Bettina Schmid for inspiring scientific TAC meeting discussions. Additionally, I would like to thank Dr. Bettina Schmid for providing help in all zebrafish terms and always having time for discussions. Furthermore, I would like to thank Prof. Dr. Stefan Zahler and Dr. Christina Orgler for their help with the TEER experiments. I am also grateful to Dr. Tobias Straub for his support with the statistical analysis and to Dr. Ignasi Forné for his help with the large-scale proteomic analysis.

I would like to acknowledge the SFB 914 and the associated IRTG for financial support and excellent professional training possibilities. A special thank you to Dr. Verena Kochan.

I am grateful for the generous help of all current and former members of the Montanez and Walzog group providing constructive criticism, advice on experimental techniques, and a great working atmosphere. In this respect I would like to mention Dr. Melanie Salvermoser, Dr. Annette Zehrer, Dr. Bettina Pitter, Jennifer Truong, Anna-Karina Becker, Felicitas Böhm, Marina Majaj and Brigitte Bergner for their unlimited support, on both professional and personal levels. Without them my time as a doctoral student would have been much harder to endure. I am also thankful to all the members of the Walter Brendel Center and the zebrafish group of Dr. Bettina Schmid for a great working atmosphere.

This phase of my life would not have been possible without the love and support of my family. Their education, enthusiasm, advice, support and generosity in any situation of my life have made me the person I am. Mama, Papa and Leni, thank you for listening, motivating, strengthening and your unlimited support.

I would also like to thank all my friends for their patience, support, trust and inspiration during this phase of my life, especially towards the end of my PhD.

Finally, I would like to thank Julian. Thank you for your unlimited support, your encouragement, and most of all, your patience.

9. Appendix

9.1 Affidavit

Werner, Ann-Cathrin
……..
Surname, first name

……..
Street

……..
Zip code, town

……..
Country

I hereby declare, that the submitted thesis entitled

Role of Coronin 1B on the regulation of endothelial cell function and angiogenesis

is my own work. I have only used the sources indicated and have not made unauthorized use of services of a third party. Where the work of others has been quoted or reproduced, the source is always given.

I further declare that the submitted thesis or parts thereof have not been presented as part of an examination degree to any other university.

München, 11.07.2022	Ann-Cathrin Werner
……..	……..
Place, Date	Signature

9.2 Publications

Major parts of the present work have been published in Frontiers in Cell and Developmental Biology:

Werner AC*, Weckbach LT*, Salvermoser M, Pitter B, Cao J, Maier-Begandt D., Forné I, Schnittler H, Walzog B, Montanez E (2020): Coronin 1B controls endothelial actin dynamics at cell-cell junctions and is required for endothelial network assembly; Front. Cell Dev. Biol. (8),708. *equal contribution

Additional publications

Pitter B*, **Werner AC***, Montanez E (2018): Parvins are required for endothelial cell-cell junctions and cell polarity during embryonic blood vessel formation; Arterioscler Thromb Vasc Biol; 38(5):1147-1158. *equal contribution

Cao J, Ehling M, März S, Seebach J, Tarbashevich K, Sixta T, Pitulescu ME, **Werner AC**, Flach B, Montanez E, Raz E, Adams RH, Schnittler H (2017): Polarized actin and VE-cadherin dynamics regulate junctional remodelling and cell migration during sprouting angiogenesis; Nat Commun; 8(1):2210.

Herrmann J, Schröder B, Klinger S, Thorenz A, **Werner AC**, Abel H, Breves G (2012): Segmental diversity of electrogenic glucose transport characteristics in the small intestines of weaned pigs.; Comp.Physiol; 163(1):161-169.

Scientific presentations & Conference attendances

11.2018 Annual Retreat of the IRTG of the SFB 914, Günzburg, Germany (oral presentation)

07.2018 Vasculata 2018, St. Louis, MO, USA (poster presentation)

06.2018 20th International Vascular Biology Meeting 2018 (IVBM2018), Helsinki, Finland (poster presentation)

03.2018 2nd International Conference on Leukocyte Trafficking, Munich, Germany

10.2017 39th Annual Meeting of the German Society for Microcirculation and Vascular Biology (GfMVB), Grainau / Garmisch, Germany (poster presentation)

09.2016 Joint International Meeting Perspectives in Vascular Biology, Frankfurt, Germany

07.2016 Annual Retreat of the IRTG of the SFB 914, Schöntal, Germany (poster presentation)

04.2016 50th Annual Meeting of the European Society for Clinical Investigation (ESCI), Paris, France